MEDJ

Volume: 40 Issue: 2 June 2025

MEDENIYET MEDICAL JOURNAL

THE OFFICAL JOURNAL OF ISTANBUL MEDENIYET UNIVERSITY FACULTY OF MEDICINE

Formerly Göztepe Tıp Dergisi

ISSN 2149-2042
E-ISSN 2149-4606

www.medeniyetmedicaljournal.org

ISSN 2149-2042
E-ISSN 2149-4606

MEDENIYET MEDICAL JOURNAL

Formerly Göztepe Tıp Dergisi

Year 2025
Volume 40
Issue 2

www.medeniyetmedicaljournal.org

Administrative Office
Istanbul Medeniyet University Dumlupınar Mahallesi, D-100 Karayolu No:98, 34000 Kadıköy, Istanbul, Türkiye

Publication type: Periodical

Finance: Istanbul Medeniyet University Scientific Research Fund

Publisher
Galenos Publishing House
Address: Molla Gürani Mah. Kaçamak Sk. No: 21/1 34093 Istanbul, Türkiye
Phone: +90 (530) 177 30 97
E-mail: info@galenos.com.tr/yayin@galenos.com.tr
Web: www.galenos.com.tr

Printing at:
Son Sürat Daktilo Dijital Baskı San. Tic. Ltd. Şti.
Gayrettepe Mah. Yıldızposta Cad. Evren Sitesi A Blok No: 32 D: 1-3 34349 Beşiktaş/Istanbul
Phone: +90 212 288 45 75

Printing Date: June 2025

International scientific journal published quarterly.

Medeniyet Medical Journal is the official journal of Istanbul Medeniyet University

It is published four times a year (March, June, September, December).

MEDJ is an open Access, free and peer-reviewed journal

PubMed Abbreviation: Medeni Med J

"Please refer to the journal's webpage (**https://medeniyetmedicaljournal.org/jvis.aspx**) for "Publication Policy", "Instructions to Authors" and "Aims and Scope".

The Medeniyet Medical Journal and/or its editors are members of ICMJE, COPE, WAME, CSE and EASE, and follow their recommendations.

The Medeniyet Medical Journal is indexed in **Emerging Sources Citation Index (Web of Science), PubMed/MEDLINE, PubMed Central, Scopus, EBSCO Academic Search Complete, i-Journals, J-Gate, Türk Medline, Türkiye Atıf Dizini** and **TÜBİTAK ULAKBİM TR Index**.

The journal is printed on an acid-free paper and published electronically.

Owner: ISTANBUL MEDENİYET UNIVERSITY FACULTY OF MEDICINE

Responsible Manager: M. Tayyar KALCIOGLU

www.medeniyetmedicaljournal.org

International Advisory Board

MEDJ

International Advisory Board

Contents

Original Articles

MEDJ

Contents

Contents

DOI: 10.4274/MMJ.galenos.2025.71163
Medeni Med J 2025;40:37-45

Original Article

Explaining Uncertain Hepatoprotective Effects: When Silibinin Co-Administered with Other Drugs

Silibinin Diğer İlaçlarla Birlikte Uygulandığında Belirsiz Hepatoprotektif Etkilerin Açıklanması

Dong Pu, Qinwei SUN, Zengxiang ZHAO, Sisi WANG, Ji LI, Feng YU

China Pharmaceutical University School of Basic Medical Sciences and Clinical Pharmacy, Department of Clinical Pharmacy, Nanjing, China

ABSTRACT

Objective: This study investigated the herb-drug interaction between silibinin and carbamazepine (CBZ) and the potential risk of adverse drug reactions (ADR) when silibinin is co-administered with other drugs.

Methods: Primary fresh hepatocytes were cultured, and an methylthiazolyldiphenyl-tetrazolium bromide assay was performed after administration of different concentrations of CBZ, and silibinin. Meanwhile, a retrospective study on hepatic adverse reactions involving the combination of silibinin with other drugs was performed using the Food and Drug Administration Adverse Event Reporting System (FAERS).

Results: The protective effects of silibinin on CBZ do not appear on hepatocytes in a dose-dependent manner. When silibinin (25μM) was co-administered with CBZ (2mM), the cell viability increased from 47.8% to 75.9% ($p<0.05$), while increasing the silibinin concentration to 50μM with CBZ (2mM), the hepatocyte viability significantly declined from 47.8% to 38.7% ($p<0.05$). In the FAERS database, the risk of adverse reactions significantly increases when combined with silibinin. The silibinin co-administration was significantly associated with hepatotoxicity reports.

Conclusions: The results of the cell experiment showed that silibinin's liver protective effects were uncertain when it was combined with CBZ. FAERS database analysis revealed elevated risks of ADRs with silibinin co-administration, collectively highlighting the necessity for vigilance against unanticipated herb-drug interactions.

Keywords: Silibinin, carbamazepine, hepatotoxicity, adverse drug reactions, herb-drug interaction, Food and Drug Administration adverse event reporting system

ÖZ

Amaç: Bu çalışmada silibinin ve karbamazepin (CBZ) arasındaki bitki-ilaç etkileşimi ve silibinin diğer ilaçlarla birlikte uygulandığında potansiyel advers ilaç reaksiyonu (ADR) riski araştırılmıştır.

Yöntemler: Birincil taze hepatositler kültürlenmiş ve farklı konsantrasyonlarda CBZ ve silibinin uygulamasından sonra metiltetrazolium tetrazolyum testi deneyi yapılmıştır. Bu arada, Gıda ve İlaç Dairesi Advers Olay Raporlama Sistemi (FAERS) kullanılarak silibinin diğer ilaçlarla kombinasyonunu içeren hepatik advers reaksiyonlar hakkında retrospektif bir çalışma yapılmıştır.

Bulgular: Silibininin CBZ üzerindeki koruyucu etkileri hepatositler üzerinde doza bağlı bir şekilde görülmemektedir. Silibinin (25μM) CBZ (2mM) ile birlikte uygulandığında hücre canlılığı %47,8'den %75,9'a yükselmiştir ($p<0,05$); silibinin konsantrasyonu CBZ (2mM) ile birlikte 50μM'a eklendiğinde ise hepatosit canlılığı %47,8'den %38,7'ye düşmüştür ($p<0,05$). FAERS veri tabanında, silibinin ile kombine edildiğinde advers reaksiyon riski önemli ölçüde artmaktadır. Ve silibinin birlikte uygulanması hepatotoksisite raporları ile önemli ölçüde ilişkilendirilmiştir.

Sonuçlar: Hücre deneyinin sonuçları, silibininin CBZ ile kombine edildiğinde karaciğer koruyucu etkilerinin belirsiz olduğunu göstermiştir. FAERS veri tabanı analizi, silibinin birlikte uygulanmasıyla ADR riskinin arttığını ortaya koymuş ve beklenmedik Bitki-ilaç etkileşimine (HDI) karşı dikkatli olunması gerektiğini vurgulamıştır.

Anahtar kelimeler: Silibinin, karbamazepin, hepatotoksisite, advers ilaç reaksiyonları, bitki-ilaç etkileşimi, Gıda ve İlaç Dairesi advers olay raporlama sistemi

INTRODUCTION

Silibinin is the major active compound in silymarin, which is a mixture of flavonolignans extracted from *Silybum marianum* seeds. Milk thistle (*Silybum marianum L.*) is a medicinal plant widely used in traditional European medicine. Pharmacological studies indicate that silibinin has a strong capability to protect the liver and cure liver damage caused by various toxicants[1-3]. Silibinin is often used to treat acute and chronic hepatitis, early liver injury, and toxic liver injury.

CBZ is often prescribed as an anti-convulsant, and long-term use of it can cause liver abnormalities.

Address for Correspondence: J. Li, China Pharmaceutical University School of Basic Medical Sciences and Clinical Pharmacy, Department of Clinical Pharmacy, Nanjing, China
E-mail: Ji.Li@ubc.ca **ORCID ID:** orcid.org/0000-0002-2931-798X

Cite as: Pu D, Sun Q, Zhao Z, Wang S, Li J, Yu F. Explaining uncertain hepatoprotective effects: when silibinin co-administered with other drugs drugs. Medeni Med J. 2025;40:37-45

Received: 20 December 2024
Accepted: 18 March 2025
Epub: 22 May 2025
Published: 26 June 2025

Patients on CBZ therapy would often use alternate hepatoprotective therapies concomitantly with CBZ to prevent CBZ associated liver side effects. Silibinin is one of the compounds from hepatoprotective herbs that is commonly used in cases of drug-induced liver injury with mild to moderate hepatocellular damage[4].

The most versatile enzyme systems involved in the metabolism of xenobiotics are cytochromes P450 (CYP450) and Uridine Diphosphate (UDP)-glucuronosyltransferases (UGTs). Silibinin has been reported to have a potential inhibitory effect on CYP450, UGTs, and some efflux transporters such as P-glycoprotein (P-gp)[5-7]. These findings suggest that silibinin may modulate the pharmacokinetics and pharmacodynamics of co-administered drugs through interactions with P-gp, CYP450, UGTs. However, the clinical implications of such herb-drug interactions remain underrecognized in therapeutic settings.

In this experiment, the effect of interactions between CBZ and silibinin on the pharmacokinetics was explored in primary hepatocytes and rats. We also analyzed the data from real-world data in the Food and Drug Administration Adverse Event (AE) Reporting System (FAERS) database to explore the risk of adverse drug reactions caused by silymarin when drugs are combined. For safety reasons, it is important to evaluate the potential pharmacokinetic interaction when silibinin is combined with medication.

METHODS

Reagents

Silibinin (batch no: 130617) was provided by Tasly Pharmaceutiacal Company (Tianjin, China), and CBZ (batch no: 120502) was provided by Sine-Yellow River Pharmaceutiacal Company (Shanghai, China). All reagents were either HPLC-grade or analytical-grade.

Animals and Ethics Statement

Specific pathogen free grade male Sprague-Dawley (SD) rats, weighing 200-220 g, were housed in a controlled environment with a 12-hour light/dark cycle and had free access to food and water. All efforts were made to minimize animal suffering and to use the minimum number of animals necessary to produce reliable scientific data. All animal experiments were approved by the Experimental Animal Welfare Ethics Committee of China Pharmaceutical University (acceptance number: 2020-09-013, date: 10.03.2023).

Primary Hepatocyte Isolation and Culture

Primary hepatocytes were isolated from SD rats using a modified Seglen's two-step *in situ* perfusion method[8], which has been widely validated and applied. A total of 1.5-2 million cells were obtained at a viability greater than 80%, confirmed with the trypan blue dye exclusion test. Cells were then seeded at a density of 1.5×10^5/mL on 96-well plates and a density of 10^6/mL on 6-well plates with Williams' medium E containing 10% FBS and 1% penicillin/streptomycin. The primary hepatocytes were cultured in an incubator with a 95% oxygen/5% CO_2 gas cylinder at 37 °C.

Cell Morphology Observation and methylthiazolyldiphenyl-tetrazolium bromide Assay

The primary hepatocyte was cultured for 12 hours on 6-well plates, then treated with silibinin and CBZ. The primary hepatocytes were then cultured for another 24 hours before cell morphology was observed by a microscope.

The rat primary hepatocytes were seeded in 96-well plates at a concentration of 5000 cells/well. The cell was incubated with Williams' medium E containing different concentrations of silibinin and CBZ for 24 hours. Then, the 20μL 5 g/L methylthiazolyldiphenyl-tetrazolium bromide (MTT) solution was added to each well of the 96- well plate, followed by 4 hours of additional culturing. Every well was treated with 150 μL DMSO after removing the solution, and then shaken for 10 minutes. After this, OD490 was detected.

Statistical Analysis

All experiments were conducted with independent biological replicates. Quantitative data from the MTT assay are presented as mean±standard deviation, derived from at least three independent experiments. Normality of data distribution and homogeneity of variances were assessed using Shapiro-Wilk and Levene's tests, respectively. Dose-response relationships were evaluated by non-linear regression analysis. For multi-group comparisons, when data satisfied both normality and variance homogeneity assumptions, one-way analysis of variance with Tukey's honestly significant difference post-hoc test was employed to control family-wise error rates. For datasets violating these assumptions, non-parametric analyses were performed using the Kruskal-Wallis test followed by Dunn's post-hoc test with Bonferroni adjustment for pairwise comparisons. All statistical analyses were executed in GraphPad Prism 9.0, with $p<0.05$ considered statistically significant.

Pharmacovigilance Study

Data Processing and Exposure Definition

A retrospective, disproportionality pharmacovigilance study was performed from 2015 quarter 1 to 2022 quarter 2 using the FAERS database. Both generic and brand names were used to identify the drug silibinin. AEs in the FAERS were coded in terms of Preferred Terms (PTs) from the Medical Dictionary for Regulatory Activities and all AEs of interest were coded as PTs from the System Organ Class (SOC) of Hepatobiliary disorders. The deduplication step was performed to retain the most recent version of the report[9]. Delete the case report when a null value for either AE or drug is present. After SOC analysis, PT analysis was performed to deliver more comprehensive information.

Disproportionality Analysis

Combination analysis refers to an AE report where two or more drugs are used, and the occurrence of the target AE may be the result of their combination[10]. The reporting odds ratio (ROR) and Bayesian confidence propagation neural networks (BCPNN) of information components (ICs) were used to identify statistical associations between target drugs (combined or not combined with silibinin) and AEs of interest[11]. Target drugs here were defined as drugs that were in combination with silibinin and had developed hepatotoxicity as reported in the FAERS database.

The study takes one report as a unit, which means when silibinin occurs in the report, the report is included in the silibinin therapy group. The analysis could be performed by ROR or IC. The ROR lower limit of the 95% confidence interval ROR_{025} was greater than 1, and at least 3 cases, or the IC lower limit of the 95% confidence interval IC_{025} was greater than 0, were defined as a significant signal, indicating a significant risk of target AEs of the therapy drugs. Only ROR can be used in the comparison of different groups. In PT analysis, the method of IC is used because ROR is prone to signal score inflation when the number of reports is small[12]. Time-to-onset (TTO) (TTO= Time to event-Start of treatment)analysis was performed to evaluate the profile from the start of treatment to event occurrence.

RESULTS

Cell Morphology Observation and methylthiazolyldiphenyl-tetrazolium bromide Assay

The results showed that treating the primary hepatocyte with 25μM silibinin had no obvious effect on cell growth compared with the control group

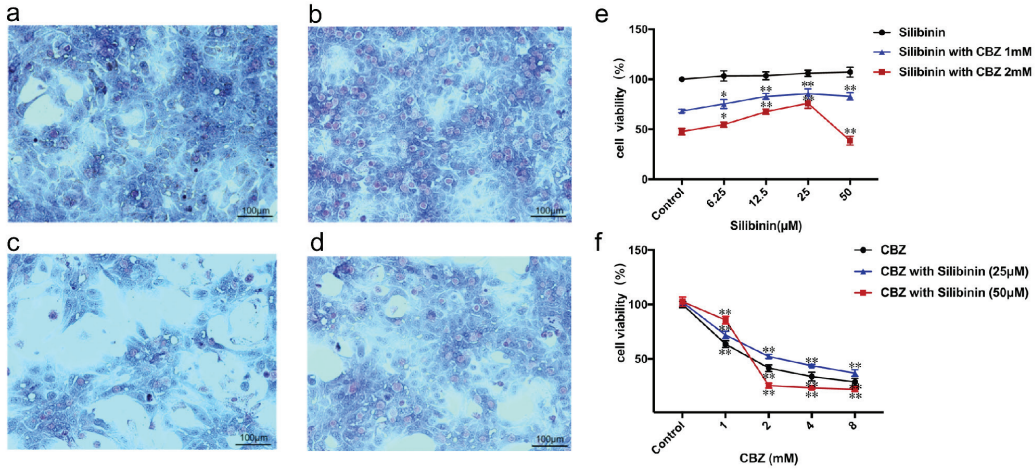

Figure 1. Cell morphology observation (a-d) and MTT assay results (e-f). (a) Treated the primary hepatocyte with neither silibinin nor CBZ (control group); (b) Treated the primary hepatocyte with 25μM Silibinin; (c) Treated the primary hepatocyte with 2mM CBZ; (d) Treated the primary hepatocyte with 2mM CBZ and 25μM silibinin. (e) Treated the primary hepatocyte with different concentration of silibinin; Treated the primary hepatocyte with different concentration of silibinin co-administrated with 1mM and 2mM CBZ. (f) Treated the primary hepatocyte with different concentration of CBZ; Treated the primary hepatocyte with different concentration of CBZ co-administrated with 25μM and 50μM silibinin. *p<0.05, **p<0.01 vs the control group.

MTT: Methylthiazolyldiphenyl-tetrazolium bromide, CBZ: Carbamazepine

(Figure 1a, b). Treating primary hepatocytes with CBZ 2mM caused severe cell damage, which was mitigated when 25μM silibinin was added (Figure 1c, d).

Treating a primary hepatocyte with 6.25μM, 12.5μM, 25μM, or 50μM silibinin had no obvious effect on cell growth. Treating primary hepatocytes with 1mM or 2mM CBZ caused cell damage, which was mitigated when different concentrations of silibinin were added. However, treating the primary hepatocyte with 2mM CBZ caused cell damage that couldn't be mitigated when 50μM silibinin was added. When silibinin (25μM) was co-administrated with CBZ (2mM), the cell viability increased from 47.8% to 75.9% ($p<0.05$); when the concentration of silibinin was increased to 50μM with CBZ (2mM), the hepatocyte viability significantly declined from 47.8% to 38.7% ($p<0.05$) (Figure 1. e).

Primary hepatocytes exhibited a concentration-dependent decrease in viability with increasing CBZ concentrations (0-4 mM). Co-administration of 25 μM silibinin significantly enhanced cell viability across all tested CBZ concentrations. Notably, while 50 μM silibinin partially restored viability in cells treated with 1 mM CBZ, it paradoxically exacerbated cytotoxicity at higher CBZ concentrations (2, 4, 8 mM), resulting in lower viability compared to CBZ treatment alone (Figure 1. f).

Disproportionality Analysis with or without Silibinin Therapy in Food and Drug Administration Adverse Event Reporting System

Reports available in the FAERS database allow the analysis of large amounts of data to detect safety signals. FAERS contains real-world results from a large population. Between the first quarter of 2015 and the second quarter of 2022, a total of 36,603 AEs associated with the combination therapy involving silibinin were documented, including 7814 drugs, of which 50.35% were known to be metabolized by CYP450 and UGTs. Among these events, 42 individual medications were reported with a frequency exceeding 100 instances (Figure 2).

When the target drug was combined with silibinin therapy, hepatotoxicity occurred in 260 reports. In the FAERS database analysis of silibinin, silibinin combined with the target drug had a higher ROR_{025} signal value for hepatotoxicity (4.49 vs 2.57) in SOC analysis in the full database than the target drug without silibinin (Figure 3).

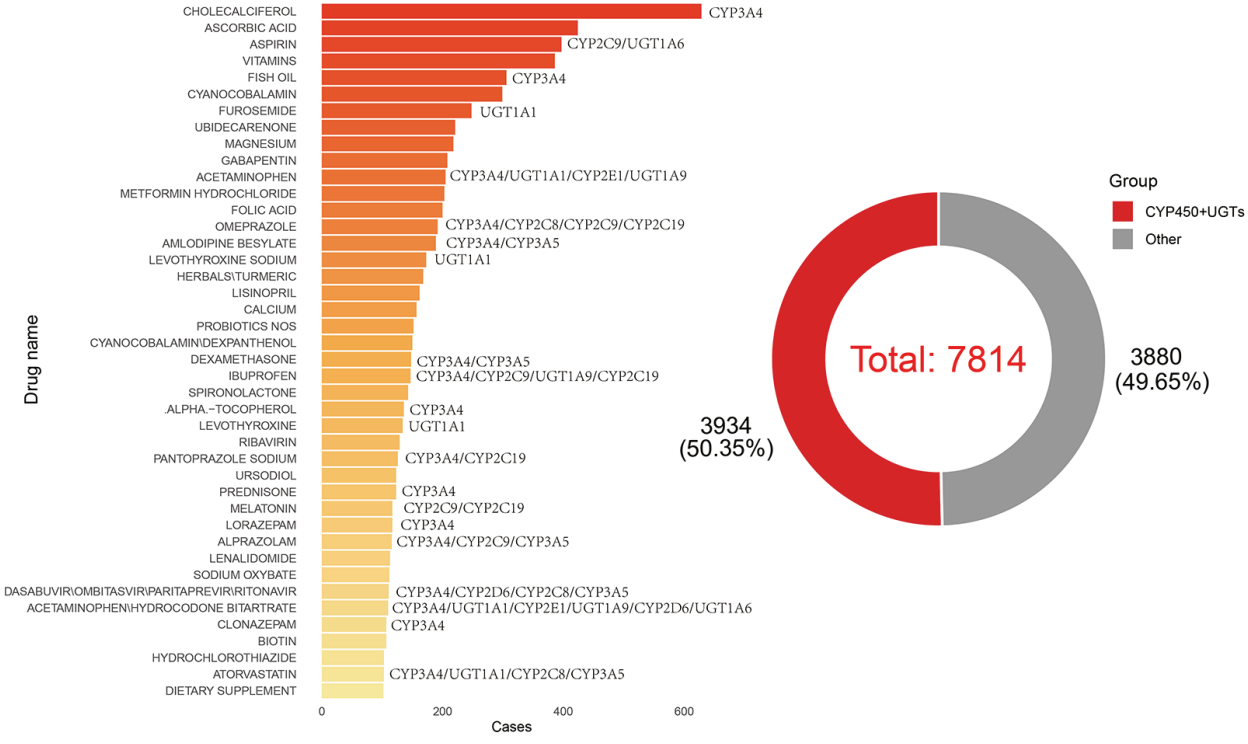

Figure 2. Forty-two drugs from the FAERS database that exhibit an adverse reaction frequency exceeding 100 instances when co-administered with silibinin.

FAERS: Food and frug administration adverse event reporting system

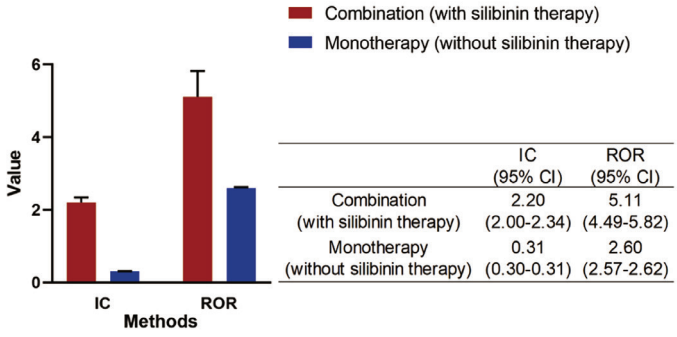

	IC (95% CI)	ROR (95% CI)
Combination (with silibinin therapy)	2.20 (2.00-2.34)	5.11 (4.49-5.82)
Monotherapy (without silibinin therapy)	0.31 (0.30-0.31)	2.60 (2.57-2.62)

Figure 3. Disproportionality analysis of target drugs (with or without silibinin) and hepatotoxicity in full FAERS database. Target drugs here were defined as drugs that were in combination with silibinin and had developed hepatotoxicity in the FAERS database. ROR: reporting odds ratio; IC: information components; CI: Confidence interval. The IC lower limit of the 95% confidence interval was greater than 0 or the ROR lower limit of the 95% confidence interval was exceeded 1, and at least 3 cases were defined as significant.

IC: information component, ROR: Reporting odds ratio, FAERS: Food and Drug Administration Adverse Event Reporting System

Preferred Terms Disproportionality Analysis, Time-to-Onset Analysis and Preferred Term Outcome Analysis with Silibinin Therapy Group

In PT analysis, the IC_{025} value of the silibinin therapy group in the full database is significant for most hepatotoxicity PTs. Ascites (n=22), hepatic cirrhosis (n=20), jaundice (n=20), liver disorder (n=20), and Drug-induced liver injury (n=19) are the top five PT frequencies in the analysis, and the IC_{025} value is 2.03, 2.41, 2.13, 1.45, and 1.62 respectively (Figure 4). The results from Figure 5 found that the median TTO in hepatotoxicity combined with silibinin is about 1 year. The most frequent serious AE in hepatotoxicity associated with silibinin therapy is ascites. The most frequent cause of death is hepatic cirrhosis. The top 5 outcomes of all serious AEs in hepatotoxicity combined with silibinin therapy are ascites, hepatic cirrhosis, liver disorder, hepatocellular carcinoma, and jaundice (Figure 6).

Based on data from the FAERS database, we found that the combination of silibinin with some prescription drugs had a higher ROR_{025} (4.49) for hepatotoxicity than that without silibinin (2.57). In PT analysis, the IC_{025} value in combination with the silibinin therapy group is significant

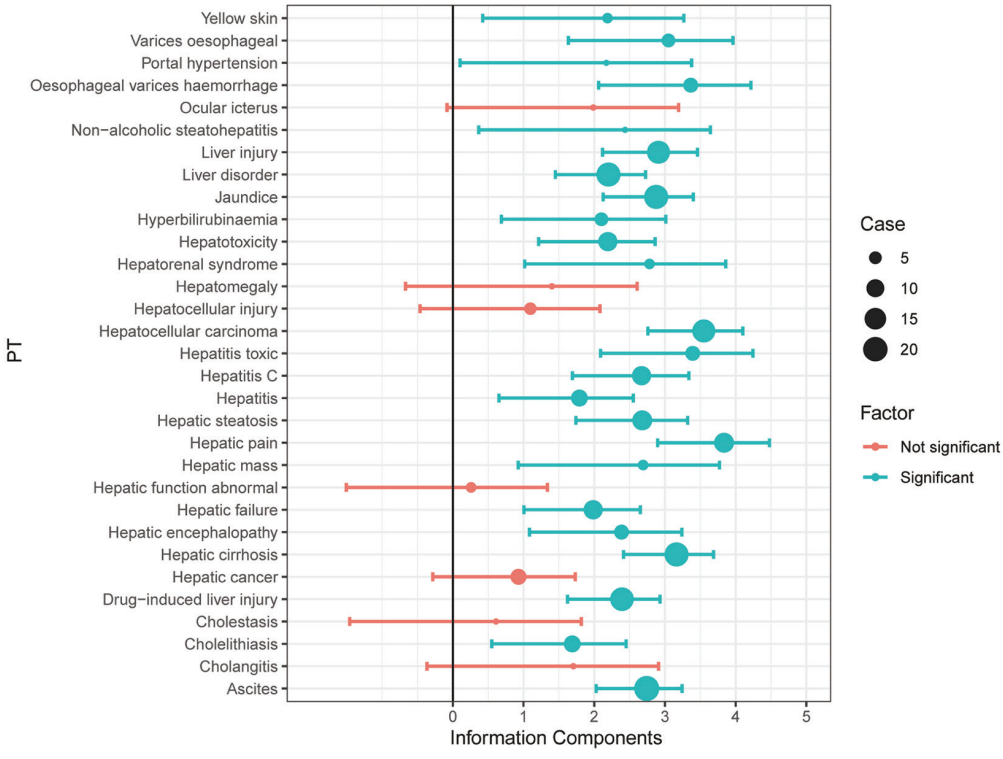

Figure 4. The information components of hepatotoxicity preferred terms associated with silibinin (case number ≥ 3) are presented in the full database. Significance is defined as an IC lower limit greater than 0 for the 95% confidence interval.

IC: Information component, PT: Preferred terms

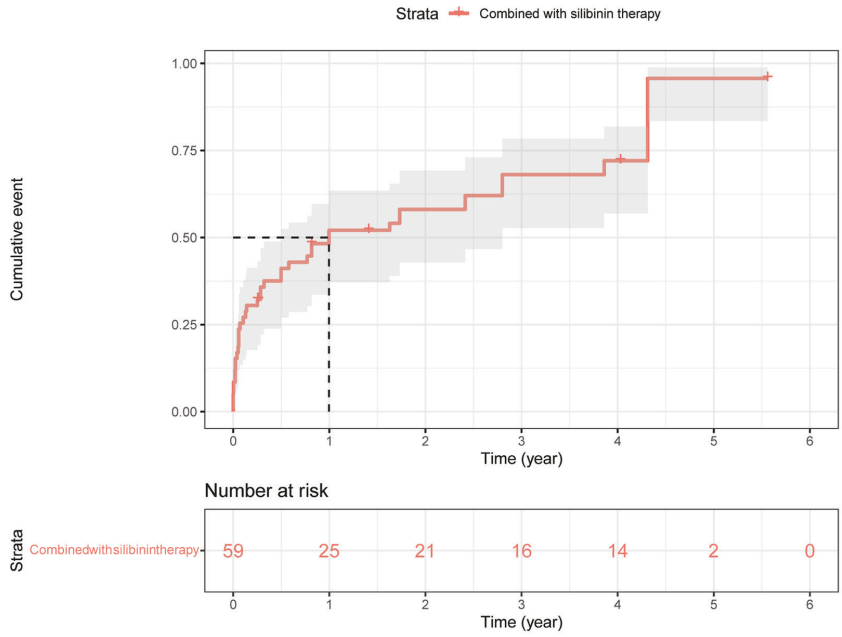

Figure 5. The Time-To-Onset of all hepatotoxicity with silibinin (year).

TTO: Time-To-Onset

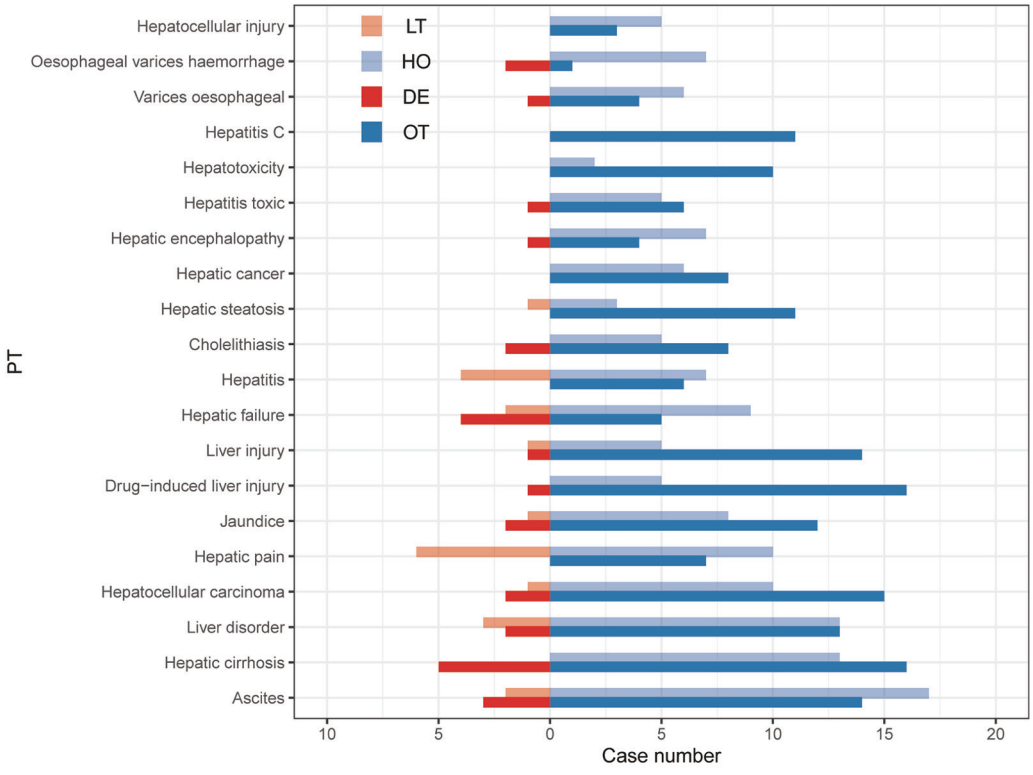

Figure 6. The top 20 preferred terms outcome of hepatotoxicity with silibinin.

LT: Life-Threatening; HO: Hospitalization-Initial or Prolonged; DE: Death; OT: Other Serious (Important Medical Event), PTs: Preferred terms

in most hepatotoxicity PTs. The IC_{025} values for the top five frequently occurring PTs, such as ascites, hepatic cirrhosis, jaundice, liver disorder, drug-induced, and liver injury, are 2.03, 2.41, 2.13, 1.45, and 1.62, respectively.

Analysis of Adverse Reaction Signals for Silibin in Combination with Amlodipine or furosemide in Food and Drug Administration Adverse Event Reporting System

Results from drawing on the FAERS database and employing the ROR method showed that the co-administration of amlodipine and silibinin significantly increases the risk of adverse reactions observed with amlodipine monotherapy. The ROR values for fatigue, nausea, and asthenia were 2.66, 2.04, and 1.91 (Figure 7a). Additionally, the concurrent use of furosemide and silibinin can notably elevate the risk of adverse reactions when compared to amlodipine monotherapy. The ROR values for headache, acute respiratory failure, and encephalopathy are 2.40, 14.79, and 20.02 (Figure 7b).

DISCUSSION

This experiment studied both the interaction of silibinin with carbamazepine and pharmacovigilance data on silibinin using the FAERS database. For the primary hepatocyte experiments, the MTT assay showed that the hepatoprotective effect of silibinin was uncertain with a higher concentration of co-administered CBZ. Our previous research in rats, suggested that CBZ increased silibinin clearance, which implies a decreased drug efficacy. This may coincide with the result of uncertain hepatoprotective effects of silibinin in primary fresh hepatocytes.

CYP450 and UGTs are essential for metabolism of many drugs, and they can be inhibited or induced by drugs causing DDIs (drug-drug interactions) that can lead to adverse effects or therapeutic failure. Faisal et al.[6] demonstrated that certain silymarin components/metabolites can inhibit CYP enzymes. 2,3-dehydrosilychristin-19-O-sulfate showed the strongest inhibitory effect on CYP3A4. D'Andrea et

(a)

Group	Cases	ROR value (95% CI)
Amlodipine besylate (Reference)		
Amlodipine besylate combined with silibinin		
Fatigue	28	2.66(1.78–3.98)
Nausea	19	2.04(1.27–3.28)
Asthenia	12	1.91(1.06–3.43)
Fall	12	1.81(1.01–3.26)
Back pain	10	3.02(1.59–5.71)
Insomnia	9	2.78(1.42–5.43)
Anaemia	8	2.23(1.09–4.53)
Neutropenia	7	6.09(2.85–12.98)
Ascites	6	12.14(5.36–27.48)
Stomatitis	6	6.72(2.97–15.19)

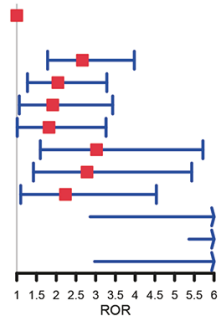

(b)

Group	Cases	ROR value (95% CI)
Furosemide (Reference)		
Furosemide combined with silibinin		
Off label use	23	2.75(1.79–4.23)
Confusional state	22	5.59(3.60–8.63)
Headache	17	2.40(1.47–3.93)
Acute respiratory failure	16	14.79(8.88–24.64)
Encephalopathy	16	20.02(12.00–33.39)
Hypertension	16	3.99(2.40–6.63)
Pulmonary oedema	16	7.01(4.21–11.66)
Hypoxia	15	10.19(6.03–17.23)
Brain oedema	14	83.06(47.40–145.56)
Cardiovascular insufficiency	14	183.27(101.99–329.31)

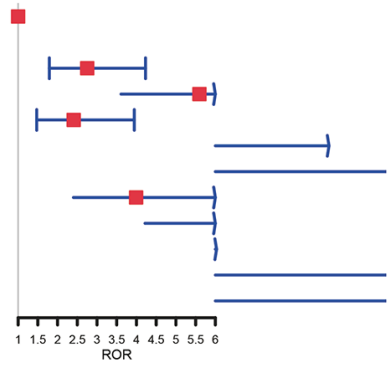

Figure 7. Comparison of adverse reaction signals of amlodipine besylate (a) or furosemide (b) combined with silibinin, based on the proportional imbalance method.

ROR: Reporting odds ratio, IC: Information component

al, showed that silibinin and the metabolite silibinin-glucuronide were also inhibitors of human UGT1A isozymes[7]. Ferreira et al.[13] found that silymarin (silibinin) significantly increased the CBZ concentrations over the 1-2 h post-dosing period compared to the negative control group. Similarly, Wang et al. identified that consecutive administration of water-soluble silymarin significantly increased the K_a of CBZ and the AUC_{0-12} and C_{max} of its metabolite[14].

Moreover, P-gp modulators have been reported as a contributor to DDI. Previous studies have demonstrated that silibinin is a CYP450 and P-gp inhibitor *in vitro*, which leads to increased accumulation of P-gp substrate within cells[15,16]. This has also been confirmed by several recent studies. Lee and Choi[17] found that silibinin significantly inhibited P-gp activity. Compared to the control group, silibinin significantly increased the area under the plasma concentration-time curve and the peak plasma concentration of paclitaxel. Nguyen et al.[18] found that silibinin reduced the efflux of two substrates of P-gp, including digoxin and vinblastine, in Panc-1 cells, indicating the inhibitory effect of silibinin on P-gp. Dobiasová et al.'s[5] research showed that silibinin exhibits the ability to modulate P-gp activity by acting as a competitive inhibitor. It is highly likely that silibinin will change how the combined drugs are processed in the body, possibly leading to ineffective treatment or even increased liver damage.

The analysis of FAERS revealed a significant association between silibinin co-administration and drug-induced hepatotoxic events. Mechanistically, this phenomenon may be attributable to silibinin-mediated inhibition of metabolic enzymes, as evidenced by a focused investigation on amlodipine (primarily metabolized by CYP3A4) and furosemide (UGT1A1-dependent metabolism). The disproportionality analysis using the ROR method demonstrated elevated risks of AEs in silibinin combination therapies. Notably, these herb-drug interactions were frequently associated with severe clinical outcomes, including mortality, hospitalization (initial/prolonged), and life-threatening complications. These findings underscore the necessity for systematic safety evaluation of phytopharmaceuticals in the case of drug combination therapy.

Study Limitations

This study has several limitations. It concentrated exclusively on silibinin's protective role against carbamazepine-induced hepatic injury, without exploring the underlying mechanisms responsible for these effects. Furthermore, the FAERS database operates as a spontaneous reporting system, inherently subject to limitations such as underreporting, duplicate entries, and incomplete case information. The absence of data regarding pre-existing conditions and concomitant medications might also confound the interpretation of the results.

Despite these constraints, the identification of ADR signals within the FAERS database in conjunction with other pharmacological agents offers valuable insights into rational pharmacotherapy. Such findings can inform clinical practice by highlighting potential safety concerns and guiding more judicious prescribing practices.

Future research should aim to address the current study's limitations through mechanistic studies and more comprehensive pharmacovigilance approaches, thereby enhancing our understanding of silibinin's therapeutic profile and its interaction with other drugs.

CONCLUSION

Despite silibinin's established clinical use in hepatic disorders and its role as an adjunct therapy to mitigate drug-induced hepatotoxicity through hepatic function enhancement or toxicity reduction, its widespread availability as an over-the-counter dietary supplement often leads to underestimation of its pharmacological complexity. This study indicates that the combination of silibinin with other prescription drugs, especially those with narrow therapeutic windows or indexes, should be used with caution because of the herb-drug interaction. With the increased popularity of herbal products, prescribers must be aware of potential herb-drug interactions.

Ethics

Ethics Committee Approval: All animal experiments were approved by the Experimental Animal Welfare Ethics Committee of China Pharmaceutical University (acceptance number: 2020-09-013, date: 10.03.2023).

Informed Consent: Since this study was conducted on animals, patient consent was not required.

Footnotes

Author Contributions

Surgical and Medical Practices: D.P., Q.S., Concept: D.P., Q.S., J.L., F.Y., Design: D.P., Q.S., J.L., F.Y., Data Collection and/or Processing: D.P., Q.S., Z.Z., Analysis

and/or Interpretation: D.P., Q.S., Z.Z., Literature Search: D.P., Q.S., S.W., Writing: D.P., Q.S., Z.Z., S.W., J.L., F.Y.

Conflict of Interest: The authors have no conflict of interest to declare.

Financial Disclosure: The authors declared that this study has received no financial support.

REFERENCES

1. Betsou A, Lambropoulou M, Georgakopoulou AE, et al. The hepatoprotective effect of silibinin after hepatic ischemia/reperfusion in a rat model is confirmed by immunohistochemistry and qRT-PCR. J Pharm Pharmacol. 2021;73:1274-84.
2. Saxena N, Dhaked RK, Nagar DP. Silibinin ameliorates abrin induced hepatotoxicity by attenuating oxidative stress, inflammation and inhibiting Fas pathway. Environ Toxicol Pharmacol. 2022;93:103868.
3. Song XY, Li RH, Liu WW, et al. Effect of silibinin on ethanol- or acetaldehyde-induced damge of mouse primary hepatocytes in vitro. Toxicol In Vitro. 2021;70:105047.
4. Federico A, Dallio M, Loguercio C. Silymarin/silybin and chronic liver disease: a marriage of many years. Molecules. 2017;22:191.
5. Dobiasová S, Řehořová K, Kučerová D, et al. Multidrug resistance modulation activity of silybin derivatives and their anti-inflammatory potential. Antioxidants (Basel). 2020;9:455.
6. Faisal Z, Mohos V, Fliszár-Nyúl E, et al. Interaction of silymarin components and their sulfate metabolites with human serum albumin and cytochrome P450 (2C9, 2C19, 2D6, and 3A4) enzymes. Biomed Pharmacother. 2021;138:111459.
7. D'Andrea V, Pérez LM, Sánchez Pozzi EJ. Inhibition of rat liver UDP-glucuronosyltransferase by silymarin and the metabolite silibinin-glucuronide. Life Sci. 2005;77:683-92.
8. Seglen PO. Preparation of isolated rat liver cells. Methods Cell Biol. 1976;13:29-83.
9. Khaleel MA, Khan AH, Ghadzi SMS, Adnan AS, Abdallah QM. A standardized dataset of a spontaneous adverse event reporting system. Healthcare (Basel). 2022;10:420.
10. Salem JE, Manouchehri A, Moey M, et al. Cardiovascular toxicities associated with immune checkpoint inhibitors: an observational, retrospective, pharmacovigilance study. Lancet Oncol. 2018;19:1579-89.
11. Norén GN, Hopstadius J, Bate A. Shrinkage observed-to-expected ratios for robust and transparent large-scale pattern discovery. Stat Methods Med Res. 2013;22:57-69.
12. Villa-Zapata L, Gómez-Lumbreras A, Horn J, Tan MS, Boyce RD, Malone DC. A disproportionality analysis of drug-drug interactions of tizanidine and CYP1A2 inhibitors from the FDA Adverse Event Reporting System (FAERS). Drug Saf. 2022;45:863-71.
13. Ferreira A, Rodrigues M, Meirinho S, Fortuna A, Falcão A, Alves G. Silymarin as a flavonoid-type P-glycoprotein inhibitor with impact on the pharmacokinetics of carbamazepine, oxcarbazepine and phenytoin in rats. Drug Chem Toxicol. 2021;44:458-69.
14. Min W, Zhen-ji J, Chang-qing Y. Effects of water-soluble silymarin on the pharmacokinetics of carbamazepine in rats. China Pharmacy. 2015;26:68-70.
15. Maitrejean M, Comte G, Barron D, El Kirat K, Conseil G, Di Pietro A. The flavanolignan silybin and its hemisynthetic derivatives, a novel series of potential modulators of P-glycoprotein. Bioorg Med Chem Lett. 2000;10:157-60.
16. Wu JW, Lin LC, Hung SC, Lin CH, Chi CW, Tsai TH. Hepatobiliary excretion of silibinin in normal and liver cirrhotic rats. Drug Metab Dispos. 2008;36:589-96.
17. Lee CK, Choi JS. Effects of silibinin, inhibitor of CYP3A4 and P-glycoprotein in vitro, on the pharmacokinetics of paclitaxel after oral and intravenous administration in rats. Pharmacology. 2010;85:350-6.
18. Nguyen H, Zhang S, Morris ME. Effect of flavonoids on MRP1-mediated transport in Panc-1 cells. J Pharm Sci. 2003;92:250-7.

DOI: 10.4274/MMJ.galenos.2025.34017
Medeni Med J 2025;40:46-52

Original Article

Comparison of Ultrasound-Based Techniques and Magnetic Resonance Imaging Proton Density Fat Fraction in Measuring the Amount of Hepatic Fat in Children with Hepatosteatosis

Hepatosteatozlu Çocuklarda Hepatik Yağ Miktarının Ölçülmesinde Ultrason Tabanlı Teknikler ile Manyetik Rezonans Görüntüleme Proton Yoğunluğu Yağ Fraksiyonunun Karşılaştırılması

Sabriye Gulcin BOZBEYOGLU, Murat ASIK

Goztepe Prof. Dr. Suleyman Yalcin City Hospital, Clinic of Radiology, Istanbul, Türkiye

ABSTRACT

Objective: The aim of this study is to demonstrate the reliability of Quantitative Ultrasound (QUS) in assessing liver fat content in children, using magnetic resonance imaging proton density fat fraction (MRI-PDFF) values as a reference, and to determine threshold values for QUS in grading hepatosteatosis.

Methods: The study group consisted of pediatric patients under 18 years of age without known liver disease who volunteered to participate. All patients underwent MRI-PDFF scanning, and QUS imaging was performed using the tissue attenuation imaging (TAI) ve tissue scatter distribution imaging (TSI) tools. The cut-off values for MRI-PDFF were set at ≥5%, ≥16.3%, and ≥21.7%, corresponding to mild, moderate, and severe steatosis, respectively. The diagnostic performance of TAI and TSI in detecting various degrees of hepatic steatosis was evaluated using the area under the ROC (AUROC) curves.

Results: The frequencies of hepatosteatosis grading were as follows: S1: 19 (37%), S2: 5 (10%), S3: 22 (43%). The AUROCs for TAI and TSI tools in detecting QUS measurements (MRI PDFF ≥5%) were 0.95 [95% confidence interval (CI): 0.91-0.99] (p< 0.001) and 0.96 (95% CI: 0.93-0.99) (p<0.001), respectively. For distinguishing different degrees of steatosis, TAI showed values of 0.75, 0.86, and 0.96 dB/cm/MHz, corresponding to sensitivities of 88%, 88%, and 100%, respectively, while TSI showed values of 92.44, 96.64, and 99.45, with sensitivities of 90%, 92%, and 91.7%. The correlation test between QUS measurements [TAI, TSI, EzHRI (Hepato-Renal Index with Automated regions of interest Recommendation)] and MR-PDFF indicated a concordance in TAI and TSI values, but not with EzHR.

Conclusions: The TAI and TSI tools can accurately measure liver fat content and can be used reliably in children for the assessment and grading of hepatosteatosis.

Keywords: Pediatric hepatosteatosis, hepatic fat quantification, tissue attenuation imaging, tissue scatter distribution imaging, magnetic resonance imaging-proton density fat fraction

ÖZ

Amaç: Bu çalışmanın amacı, çocuklarda karaciğer yağ içeriğinin manyetik rezonans görüntüleme proton yoğunluğu yağ fraksiyonu (MRI-PDFF) değerlerini referans alarak kantitatif ultrason (QUS) güvenilirliğini göstermek ve hepatosteatoz derecelendirilmesinde kantitatif US eşik değerlerini belirlemektir.

Yöntemler: Çalışma grubunu bilinen karaciğer hastalığı olmayan, 18 yaş altı çocuk hastalardan çalışmaya katılmaya gönüllü olanlar oluşturdu. Tüm hastalara MRI-PDFF taraması yapıldı ve doku zayıflama görüntüleme (TAI) ve doku saçılım dağılım görüntüleme (TSI) araçları kullanarak QUS görüntüleme yapıldı. MRI-PDFF'de ≥%5, ≥%16,3 ve ≥%21,7 kesme değerleri şu şekildedir: sırasıyla hafif, orta ve şiddetli steatoz için kullanıldı. Alıcı çalışma karakteristiği (AUROC) eğrilerinin altındaki alan farklı derecelerde hepatik steatozun saptanmasında TAI ve TSI'nın tanısal performansını değerlendirmek için kullanıldı.

Bulgular: Hepatosteatozun derecelendirilmesinde görülme sıklıkları S1;19 (%37), S2;5 (%10), S3;22 (%43). QUS ölçümleri tespitinde TAI ve TSI araçlarının AUROC'ları (MRI PDFF ≥%5), 0,95 idi [%95 güven aralığı (GA): 0,91-0,99] (p<0,001) ve 0,96 (%95 GA: 0,93-0,99) (p<0,001). Steatozun farklı dereceleri arasında ayrım yaparken, TAI aracı için 0,75, 0,86 ve 0,96 dB/cm/MHz değerleri sırasıyla %88, %88 ve %100 duyarlılığa sahiptir; ve değerleri 92,44, 96,64 ve 99,45, TSI aracı için sırasıyla %90, %92 ve %91,7 duyarlılığa sahiptir. QUS ölçümleri (TAI, TSI, EzHRI: otomatik ROI önerisi ile hepato-renal index) ve MR-PDFF değerleri arasındaki korelasyon testinde TAI ve TSI değerlerinde uyum olduğu ancak EzHRI ile uyumun olmadığı görüldü.

Sonuçlar: TAI ve TSI araçları karaciğer yağ içeriğini doğru bir şekilde ölçebilir ve hepatosteatozun değerlendirilmesi ve derecelendirilmesi için çocuklarda güvenilir bir şekilde kullanılabilir.

Anahtar kelimeler: Çocuk hepatosteatoz, quantitatif karaciğer yağ ölçümü, doku zayıflama görüntüleme, doku saçılım dağılım görüntüleme, manyetik rezonans görüntüleme-proton yoğunluğunun yağ fraksiyonu

Address for Correspondence: S. G. Bozbeyoglu, Goztepe Prof. Dr. Suleyman Yalcin City Hospital, Clinic of Radiology, Istanbul, Türkiye
E-mail: gulcinbozbeyoglu@hotmail.com **ORCID ID:** orcid.org/0000-0003-1593-4351

Cite as: Bozbeyoglu G, Asik M. Comparison of ultrasound-based techniques and magnetic resonance imaging proton density fat fraction in measuring the amount of hepatic fat in children with hepatosteatosis. Medeni Med J. 2025;40:46-52

Received: 12 December 2024
Accepted: 18 April 2025
Epub: 22 May 2025
Published: 26 June 2025

INTRODUCTION

Fatty liver is defined as the presence of intracellular fat content of 5% or more in hepatocytes[1]. Fatty liver has become the most common chronic liver disease worldwide, with publications reporting an incidence of up to 30% in the general population[2]. Early diagnosis is crucial, as the advanced stages of fatty liver can lead to serious complications such as steatohepatitis, portal hypertension, cirrhosis, and hepatocellular carcinoma.

Currently, the gold standard for the definitive diagnosis of liver fat quantification is liver biopsy. However, in cases of heterogeneous fat distribution in the liver, biopsy results may vary depending on the sampled location. Furthermore, because biopsies are an invasive procedure, it is challenging to repeat them for long-term monitoring of steatosis[3].

Magnetic resonance imaging-proton density fat fraction (MRI-PDFF) is a non-invasive technique that offers accurate quantification of liver fat as an alternative to biopsy[4,5]. It also has advantages, such as being operator-independent and unaffected by body mass index (BMI). On the other hand, ultrasound (US) is a non-invasive, easily accessible, repeatable, and cost-effective method. With the addition of recent quantitative methods, US holds significant potential for diagnosis and monitoring in pediatric patients, particularly in the coming years.

In grayscale US examinations, fatty liver is subjectively classified and graded (grade 0-3). Conventional US has over 90% sensitivity in detecting hepatic steatosis (HS) when at least 20% of hepatocytes are affected. However, it has been reported to be less sensitive to detect lower degrees of steatosis. It is also known to be operator-dependent and subject to inter-operator variability[6].

For these reasons, a non-invasive, easy-to-apply, and quantitative US (QUS) method, similar to grayscale US, has been developed, particularly for use in pediatric patients. In the QUS device we use (Samsung Medison Co Ltd), tissue attenuation imaging (TAI) and tissue scatter distribution imaging (TSI), are utilized to measure hepatic fat content. This method provides users with numerical data on the degree of liver fat and allows for comparative analysis in follow-ups.

However, according to manufacturers, the cut-off values for steatosis grading differ between devices. Currently, there are insufficient studies to validate the accuracy of QUS and to establish standardized cut-off values, particularly in pediatric patients.

The aim of this study is to demonstrate the reliability of QUS in pediatric patients by referencing MRI-PDFF values and to determine the QUS cut-off values for the diagnosis of HS in children.

MATERIALS and METHODS

Approval of our single-center prospective study was obtained from the University of Health Sciences Istanbul Medeniyet University Goztepe Training and Research Hospital Clinical Research Ethics Board in accordance with the provisions of the Declaration of Helsinki (decision no: 2023/0889, date: 13.12.2023). Informed consent forms were obtained from the parents of all participating patients.

Patients who presented with a diagnosis or suspicion of HS and were referred for abdominal US examination between January and June 2024 were included in the study. Patients with homogeneous hepatosteatosis liver parenchyma were included in the study, and cases with heterogeneous and geographic-pattern hepatosteatosis were excluded. Demographic characteristics of the patients were recorded, and their BMI and body surface area (BSA) were calculated. Laboratory data (ALT, AST, GGT, albumin, total bilirubin, triglycerides, total cholesterol, LDL cholesterol) were retrieved from the hospital information system for pediatric patients under 18 years of age without known liver disease (Table 1).

Patients with primary or metastatic liver disease, a history of liver surgery, liver trauma, or hepatobiliary infectious-inflammatory diseases were excluded from the study.

Quantitative US Imaging

QUS imaging was performed on all patients after a minimum of 6 hours of fasting. Abdominal US examinations were conducted by a pediatric radiologist with over 15 years of experience (G.B) and a radiologist with 12 years of experience (M.A). The US device used was a Samsung RS Prestige 85 with a 1-7 MHz convex curved-array probe.

Patients were evaluated in the supine position. The cranio-caudal long axis of the liver was measured through the midclavicular line for each patient. Subsequently, QUS imaging was obtained through the right intercostal space by having patients place their right hand beneath their head.

Initially, a numerical EzHRI value was obtained by comparing the renal, and liver parenchyma. Next, TAI and TSI measurements were performed sequentially, ensuring measurements were taken from the same location. TAI and TSI values were measured from at least three different locations in the right liver lobe.

Table 1. Demographic characteristics of the patients, laboratory and physical examination findings.	
Variance	**n (%), mean ± SD**
Sex	
M	37(72.5)
F	14 (27.5)
Age	13.04±3.30
Liver KK lengh	147.45±21.71
ALT	43.27±36.08
AST	31.05±22.17
GGT	28.58±20.71
Albumin	47.64±4.56
Total bilirubin	0.47±0.32
LDL	89.11±21.33
TGS	118.41±62.93
HDL	44.45±10.38
Total cholesterol	151.41±28.60
BMI	29.56±7.81
BSA	1.78±0.39

CC: Cranio-caudal, ALT: Alanine aminotransferase, AST: Aspartat aminotransferaz GGT: Gamma-glutamyl transpeptidaz, LDL: Low-density lipoprotein, TGS: Trigliserid, HDL: High-density lipoprotein, BMI: Body mass index, BSA: Body surface area, SD: Standard deviation

Care was taken to exclude vascular structures from the measurements and to obtain measurements at least 3 cm deep from the liver capsule. Examinations were performed while the patients held their breath. Both QUS techniques were successfully and easily applied.

As shown in Figure 1, TAI is a tool that measures energy loss due to the attenuation of US signals from the liver, depending on liver fat concentration[7,8]. For accurate measurements, the ROI should be kept away from major vascular structures and artefactual areas, with measurements taken at least 3 cm below the liver capsule.

Measurement reliability was ensured by selecting optimal areas with an R^2 value of 0.6 or higher, as determined by the manufacturer. In areas with an R^2 value below 0.6, the device issued a warning, and measurements could not be taken. This feature facilitates standardization among operators.

TSI, on the other hand, is a tool that measures signal distribution based on backscattered signals, as shown in Figure 2. The distribution of scattering signals changes depending on hepatic fat content[9,10].

For both TAI and TSI, at least three measurements were obtained in a single breath-hold. The mean, median, and interquartile range (IQR) values of the measurements were recorded (Figure 3).

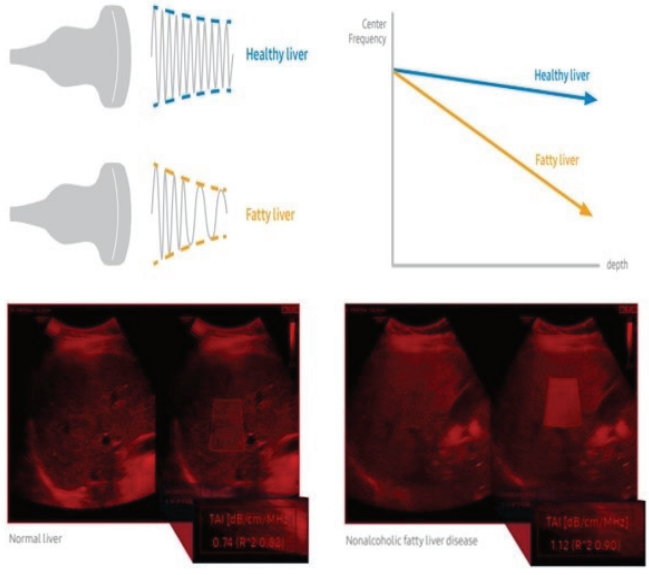

Figure 1. TAI, the quantitative tool that measures the attenuation of signals from the liver, shows that attenuation, as shown in Figure 1 above, causes a change in center frequency at greater depth, while a more severe fatty liver is associated with greater attenuation.

TAI: Tissue attenuation imaging

Magnetic Resonance Imaging-Proton Density Fat Fraction Method

After US imaging, all patients underwent MRI-PDFF scans on the same day using a 1.5 Tesla MRI scanner (GE, 360 Explorer) equipped with a body coil. A single breath-hold 3D volumetric imaging sequence, MRI-PDFF (IDEAL IQ), was performed with the following scanning parameters: TR 17.1 ms, TE 3.8 ms, imaging matrix 224x192, slice thickness 10 mm, field of view 40 cm, and bandwidth 100 kHz in the axial plane. A low flip angle of 8 degrees was set.

Elliptical regions of interest (ROIs) of 3 cm² were used for MRI-PDFF measurements. At least three ROI values were taken from the right liver lobe (segments 5, 6, 7, and 8), and their averages were recorded. The images were independently reviewed by two radiologists blinded to the US findings, and the average of their measured values was calculated.

Based on previously published studies, the accepted MRI-PDFF cut-off values for HS were as follows: mild (S1) ≤5%, moderate (S2) 16.3%, and severe (S3) 21.7% steatosis[11].

Statistical Analysis

The Kolmogorov-Smirnov test was used to show the normal distribution of the data. Frequency and percentage were used for categorical data, and mean standard deviation and maximum and minimum values were used for continuous data. Spearman correlation analysis was used to evaluate the correlation between QUS values such as TSI, TAI, EzHRI, and MRI-PDFF values. ROC curve analysis was performed to determine the diagnostic performance of QUS data in detecting hepatosteatosis grades from S0 to S3, corresponding to grades S0, S1, and S2 of ≥5%, ≥16.3% and ≥21.7%, respectively. The p-value less than 0.05 was considered statistically significant. The SPSS 24.0 software (IBM Corp, Armonk, NY) was used to perform statistical analyses.

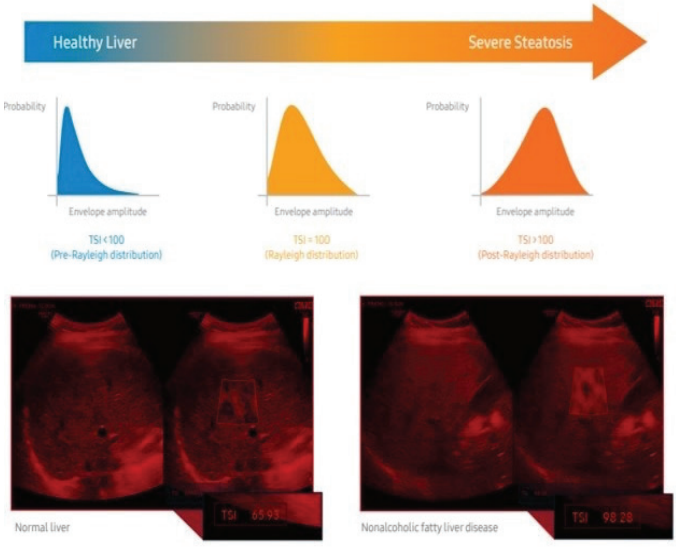

Figure 2. Figure 2 below shows TSI, which measures the correlation between the backscattered signals and the Rayleigh distribution to assess the scattered signal distribution.

TAI: Tissue attenuation imaging

RESULTS

The study included 51 patients [37 male (72.5%)]. The mean age of the patients was 13.04±3.30 (range: 5-17 years). Demographic values, laboratory findings showing liver function tests, and physical examination findings (such as BMI, BSA) of the patients are shown in Table 1.

According to MRI-PDFF values, steatosis was not detected in 8 patients [S0: 5 (10%)]. Steatosis grading was done from S1 to S3, and the values of this grading were ≥5%, ≥16.3%, and ≥21.7%, respectively. Their frequency was found as follows in our patient group: S1: 19 (37%), S2: 5 (10%), S3: 22 (43%). In the correlation test between QUS measurements (TAI, TSI, EzHRI) and MRI-PDFF values, it was seen that there was agreement in TAI and TSI values, but no agreement with EzHRI (Table 2).

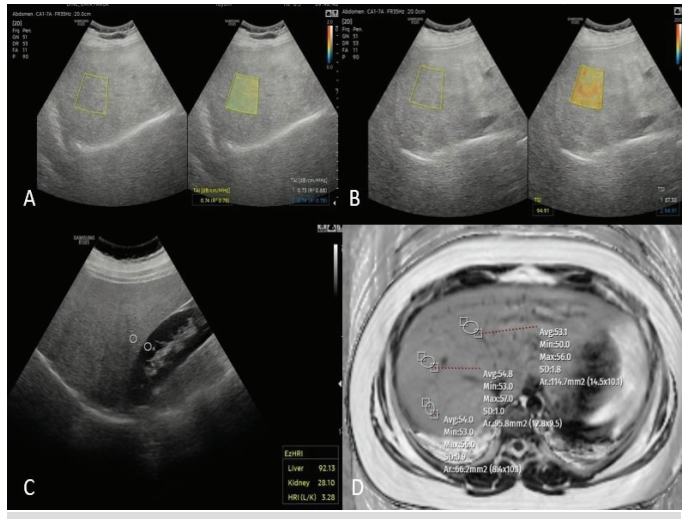

Figure 3. The median values of measurements were 0.74 dB/cm/ MHz and 94.91 for TAI (Figure 3A) and TSI (Figure 3B) techniques in a 10-year-old male patient with grade 1 hepatosteatosis. EzHRI value (Figure 3C) is 3.28. MRI-PDFF value is 9.38 % (Figure 3D).

TAI: Tissue attenuation imaging, TSI: Tissue scatter distribution imaging, MRI: Magnetic resonance imaging, PDFF: Proton density fat fraction

Table 2. QUS measurements with MRI PDFF.				
MRI-PDFF hepatosteatosis grade	**TAI (dB/cm/MHz) Median (IQR)**	**TSI median (IQR)**	**EzHRI median (IQR)**	**n (%)**
S0 (<%5)	0.64 (0.61-0.66)	83.87 (71.14-87.44)	2.29 (1.85-2.55)	5 (10)
S1 (≥5%-<16.3%)	0.70 (0.67-0.77)	89.24 (88.41-96.00)	2.63 (2.64-3.03)	19 (37)
S2 (≥16.3%-<21.7)	0.82	98.97 (97.02-100.01)	3.47 (3.34-3.55)	5 (10)
S3 (≥21.7%)	0.84	101.94 (100.85-102.65)	3.68 (3.57-3.85)	22 (43)

TAI: Tissue attenuation imaging, QUS: Quantitative Ultrasound, MRI: Magnetic resonance imaging, PDFF: Proton density fat fraction, IQR: Interquartile range, TSI: Tissue scatter distribution imaging

In the correlation analysis, it was seen that there was a correlation between TAI (r=0.790, p<0.001) and TSI (r=0.591, p<0.001) measurements and MRI-PDFF values, while there was no correlation between EzHRI (r=0.294, p=0.36) value and MRI-PDFF.

According to the evaluation made with ROC curve analysis, the results of TAI and TSI in diagnosing hepatosteatosis (accepted MRI-PDFF ≥5%) were as follows: AUROC: 0.817, 95% CI: (0.73-0.93) (p=0.005) and AUROC: 0.628, 95% CI: (0.70-0.88) (p=0.047).

The sensitivity and specificity of the TAI value of 0.67 dB/cm/MHz in diagnosing hepatosteatosis (MRI-PDFF ≥5%) were found to be 77% and 75%, respectively. In the TSI measurement, the sensitivity at the value of 88.03 was 70% and the specificity was 73%.

DISCUSSION

In recent years, the terminology of HS has evolved, and it is now internationally recognized as fatty liver disease associated with metabolic syndrome, which includes dyslipidemia, obesity, and insulin resistance. This metabolic syndrome is well-known to be linked to cardiovascular risk[12,13]. Therefore, early diagnosis is crucial, and one of the primary non-invasive methods gaining prominence, especially in children, is QUS. In our study, the effectiveness of QUS in diagnosing HS in pediatric patients was demonstrated; showing strong correlation with MRI.

In our study, we demonstrated that QUS is an effective non-invasive method for diagnosing HS in pediatric patients, showing a strong correlation with MRI-PDFF. The Samsung Prestige RS85 device used in our study employed TAI and TSI parameters to calculate HS percentage, with cut-off values of 0.67 and 88.03, respectively. TAI demonstrated an AUROC value of 0.817, indicating good diagnostic performance with 77% sensitivity and 75% specificity. In contrast, TSI exhibited a lower AUROC value, highlighting differences in diagnostic performance. Additionally, the EzHRI parameter did not show a statistically significant results or a correlation with MRI-PDFF.

Interestingly, previous studies conducted in adult populations reported a strong diagnostic performance for EzHRI, identifying a cut-off value of 1.2 as optimal for detecting steatosis with 100% sensitivity[14]. Additionally, a recent pediatric study found a similar optimal cutoff value (AUROC 0.98, specificity 92.9), indicating good diagnostic performance[15]. The discrepancy between our findings and these previous studies might be attributed to differences in sample size, population characteristics, or study design.

The incidence of HS in children is increasing, largely due to sedentary lifestyles, fast-food consumption, and screen dependency. HS poses severe risks, including parenchymal inflammation and fibrosis (in about 20-25% of cases), carcinoma, and mortality. Therefore, accurate, non-invasive, and easily applicable diagnostic techniques are essential. Our findings suggest that QUS, particularly using TAI, is a reliable and practical tool for diagnosing HS in children, especially in settings where MRI is unavailable.

When comparing our findings with the literature, it is evident that studies have reported the growing role of QUS in liver fat quantification. The American Institute of US in Medicine and RSNA Quantitative Imaging Biomarkers Alliance have standardized US protocols for fat quantification. In 2022, Ferraioli et al.[16] reported attenuation-based QUS techniques with MRI-PDFF as the reference standard. In recent studies, the receiver operating characteristic (ROC) curves for QUS showed an area under the curve (AUC) of 0.84-0.93 for steatosis grade 1, 0.86-0.93 for grade 2, and 0.79-0.93 for grade 3 (17,18). Similarly, Labyed and Milkowski[19] reported a high correlation (r=0.87) between US-derived fat fraction and MRI-PDFF. Our results are consistent with these findings, emphasizing the robustness of QUS for pediatric HS diagnosis.

Guidelines published by the Expert Committee on HS and the North American Society for Pediatric Gastroenterology, Hepatology, and Nutrition recommend alanine aminotransferase (ALT) as the best screening test for detecting steatosis in children; however, B-mode US is not recommended due to insufficient sensitivity and specificity. In our study, elevated ALT levels were observed. However, serum markers such as aminotransferases are relatively insensitive and not specific for detecting HS. Liver enzyme tests systematically underestimate the true extent of disease and have low prognostic value for the development of non-alcoholic steatohepatitis[20].

Transient elastography via FibroScan, while effective, shows variability in threshold values and higher measurement failure rates in patients with high BMI. In contrast, QUS offers better accessibility and cost-efficiency without sacrificing diagnostic accuracy. Moreover, recent advancements in US-based technologies (such as ATI and TAI) are promising but vary in diagnostic performance, as shown by Zhu et al.[21] in a study comparing TAI, ATI, and controlled attenuation parameter (CAP). When compared with 1 proton MR spectroscopy (1H-MRS), TAI also demonstrated the highest correlation (the study). Their study showed moderate-to-good AUCs for detecting HS. However, in cases of severe HS, the significantly attenuated signals limit the system's ability to evaluate steatosis effectively.

On the contrary, in a steatosis study conducted on 305 children, the CAP demonstrated higher sensitivity (72%), compared to B-mode US (42%)[22]. Moreover, liver stiffness values in children with HS were significantly higher (approximately 0.5 kPa) than those without steatosis. While this increase may not be clinically significant, it underscores that steatosis is not always a benign condition due to the potential risk of steatohepatitis. Indeed, advanced fibrosis was present at diagnosis in 15% of children, suggesting that the disease may be more severe in children than in adults[23]. Therefore, early diagnosis is of great importance in the management of children.

In 2021, Bende et al.[24] conducted studies on US-guided attenuation parameter measurements, which showed a strong correlation with CAP, with a correlation coefficient of 0.73. The AUROC values for predicting S1, S2, and S3 steatosis were above 0.83 and up to 0.90, indicating high accuracy.

Similarly, a study by Tada et al.[25] involving 126 participants used MRI-PDFF to assess chronic liver disease, reporting AUROC values of 0.92, 0.87, and 0.92 for predicting S1, S2, and S3 steatosis, respectively. Several studies have also validated MRI-PDFF or H-MRS as reference standards in numerous clinical trials[26].

Despite their high sensitivity, these techniques are expensive and not routinely utilized for HS quantification[27]. Consequently, US remains the most preferred method for clinical screening and follow-up due to its accessibility and affordability.

In a recent study, TAI demonstrated high diagnostic performance and a strong correlation in differentiating degrees of HS, whereas TSI did not show a linear dependence on the severity of steatosis[28]. According to the literature and the aforementioned studies that used MRI-PDFF as a reference, it is evident that when MRI is unavailable, there is a need for less expensive and non-invasive imaging techniques, such as US, which is more practical and easier to perform in children.

The limitations of our study include its single-center nature and the small sample size of patients. Another limitation is that potential confounding factors such as inflammation or fibrosis cannot be completely eliminated.

CONCLUSION

In conclusion, as the prevalence of fatty liver disease continues to rise and associated complications become more apparent, the need for reliable non-invasive diagnostic methods has grown. Our study demonstrated that QUS, particularly using TAI and TSI parameters, provides a practical and accessible alternative to MRI-PDFF in diagnosing HS in children. The strong agreement between TAI and TSI values and MRI enhances the reliability of QUS. In contrast to previous studies showing good diagnostic performance, the inconsistency of EzHRI suggests that further large-scale research is necessary to evaluate the consistency and applicability of this parameter across different populations.

Ethics

Ethics Committee Approval: Approval for this study was obtained from the Clinical Research Ethics Committee of the Istanbul Medeniyet University Göztepe Training and Research Hospital of the Health Sciences University (decision no: 2023/0889, date: 13.12.2023).

Informed Consent: Informed consent forms were obtained from the parents of all participating patients.

Footnotes

Author Contributions

Concept: S.G.B., M.A., Design: S.G.B., M.A., Data Collection and/or Processing: S.G.B., M.A., Analysis and/or Interpretation: S.G.B., M.A., Literature Search: S.G.B., M.A., Writing: S.G.B., M.A.

Conflict of Interest: The authors have no conflict of interest to declare.

Financial Disclosure: The authors declared that this study has received no financial support.

REFERENCES

1. Kleiner DE, Brunt EM, Van Natta M, et al. Design and validation of a histological scoring system for nonalcoholic fatty liver disease. Hepatology. 2005;41:1313-21.
2. Younossi ZM. Non-alcoholic fatty liver disease - a global public health perspective. J Hepatol. 2019;70:531-44.
3. Vuppalanchi R, Unalp A, Van Natta ML, et al. Effects of liver biopsy sample length and number of readings on sampling variability in nonalcoholic Fatty liver disease. Clin Gastroenterol Hepatol. 2009;7:481-6.
4. Raptis DA, Fischer MA, Graf R, et al. MRI: the new reference standard in quantifying hepatic steatosis? Gut. 2012;61:117-27.
5. Idilman IS, Keskin O, Elhan AH, Idilman R, Karcaaltincaba M. Impact of sequential proton density fat fraction for quantification of hepatic steatosis in nonalcoholic fatty liver disease. Scand J Gastroenterol. 2014;49:617-24.
6. Dasarathy S, Dasarathy J, Khiyami A, Joseph R, Lopez R, McCullough AJ. Validity of real time ultrasound in the diagnosis of hepatic steatosis: a prospective study. J Hepatol. 2009;51:1061-7.
7. Kim H, Varghese T. Attenuation estimation using spectral cross-correlation. IEEE Transactions on Ultrasonics, Ferroelectrics, and Frequency Control. 2007;54:510-19.
8. Liao YY, Yang KC, Lee MJ, Huang KC, Chen JD, Yeh CK. Multifeature analysis of an ultrasound quantitative diagnostic index for classifying nonalcoholic fatty liver disease. Sci Rep. 2016;6:35083.
9. Mohana Shankar P. A general statistical model for ultrasonic backscattering from tissues. IEEE Trans Ultrason Ferroelectr Freq Control. 2000;47:727-36.
10. Po-Hsiang T, Yung-Liang W. Application of ultrasound nakagami imaging for the dagnosis of fatty liver. J Med Ultrasound. 2006;24:47-9.
11. Middleton MS, Heba ER, Hooker CA, et al. Agreement between magnetic resonance imaging proton density fat fraction measurements and pathologist-assigned steatosis grades of liver biopsies from adults with nonalcoholic steatohepatitis. Gastroenterology. 2017;153:753-61.
12. Eslam M, Sanyal AJ, George J. Toward more accurate nomenclature for fatty liver diseases. Gastroenterology. 2019;157:590-53.
13. Arulanandan A, Ang B, Bettencourt R, et al. Association between quantity of liver fat and cardiovascular risk in patients with nonalcoholic fatty liver disease independent of nonalcoholic steatohepatitis. Clin Gastroenterol Hepatol. 2015;13:1513-20.e1.
14. Borges VF, Diniz AL, Cotrim HP, Rocha HL, Andrade NB. Sonographic hepatorenal ratio: a noninvasive method to diagnose nonalcoholic steatosis. J Clin Ultrasound. 2013;41:18-25.
15. Polti G, Frigerio F, Del Gaudio G, et al. Quantitative ultrasound fatty liver evaluation in a pediatric population: comparison with magnetic resonance imaging of liver proton density fat fraction. Pediatr Radiol. 2023;53:2458-65.
16. Ferraioli G, Kumar V, Ozturk A, Nam K, de Korte CL, Barr RG. US Attenuation for liver fat quantification: an AIUM-RSNA QIBA pulse-echo quantitative ultrasound initiative. Radiology. 2022;302:495-506.
17. Bae JS, Lee DH, Lee JY, et al. Assessment of hepatic steatosis by using attenuation imaging: a quantitative, easy-to-perform ultrasound technique. Eur Radiol. 2019;29:6499-6507.
18. Dioguardi Burgio M, Ronot M, Reizine E, et al. Quantification of hepatic steatosis with ultrasound: promising role of attenuation imaging coefficient in a biopsy-proven cohort. Eur Radiol. 2020;30:2293-301.
19. Labyed Y, Milkowski A. Novel method for ultrasound-derived fat fraction using an integrated phantom. J Ultrasound Med. 2020;39:2427-38.
20. Eslam M, Sanyal AJ, George J, International Consensus Panel. MAFLD: a consensus-driven proposed nomenclature for metabolic associated fatty liver disease. Gastroenterology. 2020;158:1999-2014.e1.
21. Zhu Y, Yin H, Zhou D, et al. A prospective comparison of three ultrasound-based techniques in quantitative diagnosis of hepatic steatosis in NAFLD. Abdom Radiol (NY). 2024;49:81-92.
22. Ferraioli G, Calcaterra V, Lissandrin R, et al. Noninvasive assessment of liver steatosis in children: the clinical value of controlled attenuation parameter. BMC Gastroenterol. 2017;17:61.
23. Vos MB, Abrams SH, Barlow SE, et al. NASPGHAN clinical practice guideline for the diagnosis and treatment of nonalcoholic fatty liver disease in children: recommendations from the expert committee on NAFLD (ECON) and the North American Society of Pediatric Gastroenterology, hepatology and nutrition (NASPGHAN). J Pediatr Gastroenterol Nutr. 2017;64:319-34.
24. Bende F, Sporea I, Şirli R, et al. Ultrasound-guided attenuation parameter (UGAP) for the quantification of liver steatosis using the controlled attenuation parameter (CAP) as the reference method. Med Ultrason. 2021;23:7-14.
25. Tada T, Kumada T, Toyoda H, et al. Utility of attenuation coefficient measurement using an ultrasound-guided attenuation parameter for evaluation of hepatic steatosis: comparison with MRI-determined proton density fat fraction. AJR Am J Roentgenol. 2019;212:332-41.
26. Tamaki N, Ajmera V, Loomba R. Non-invasive methods for imaging hepatic steatosis and their clinical importance in NAFLD. Nat Rev Endocrinol. 2022;18:55-66.
27. Jeon SK, Lee JM, Joo I, Yoon JH, Lee G. Two-dimensional convolutional neural network using quantitative US for noninvasive assessment of hepatic steatosis in NAFLD. Radiology. 2023;307:e221510.
28. Zhu Y, Yin H, Zhou D, et al. A prospective comparison of three ultrasound-based techniques in quantitative diagnosis of hepatic steatosis in NAFLD. Abdom Radiol (NY). 2024;49:81-92.

DOI: 10.4274/MMJ.galenos.2025.24804
Medeni Med J 2025;40:53-60

Original Article

Loneliness in Retirement

Emeklilikte Yalnızlık

Alen GREŠ[1], Nika SPASIĆ[2], Dijana STAVER[3]

[1]University Hospital Center Zagreb, Department of Psychiatry and Psychological Medicine, Zagreb, Croatia
[2]General Hospital Pula, Clinic of Psychiatry, Zagreb, Croatia
[3]University Psychiatric Hospital Vrapče, Zagreb, Croatia

ABSTRACT

Objective: Loneliness has been identified as a subjective unpleasant feeling of emptiness and distress, affecting diverse age groups, particularly retirees. Retirement is a major life event characterized by the cessation of professional activities and the loss of regular income. These phenomena are often combined and their relationship can be complex.

Methods: The research encompassed 75 randomly selected outpatients at the University Hospital Center Zagreb, Department for Psychiatry and Psychological Medicine in Zagreb Croatia with an anxiety disorder who were in remission and met the inclusion criteria. The participants were divided into three groups of 25 respondents: five years before retirement, one year before retirement, and one year after retirement. The participants were tested once using psychological tests: The University of California, Los Angeles (UCLA); and the Mini International Neuropsychiatric Interview.

Results: This study examined loneliness among 75 participants across retirement phases. UCLA Loneliness Scale scores increased significantly from pre to post-retirement ($p<0.001$), peaking one year after retirement. Emotional loneliness, particularly feelings of isolation, rose sharply, while social loneliness increased gradually. A One-Way Analysis of Variance confirmed a significant effect of retirement on loneliness, $F(2.72)=24,561$, $p<0.001$, with an impact level of $\eta^2=0.405$. A substantial impact is observed on emotional and social well-being.

Conclusions: Study results indicate a significant increase in loneliness among retired individuals. Transition to retirement can have an impact on individuals' emotions and social interactions. There is a need to support retirees in establishing new daily routines.

Keywords: Loneliness, retirement, anxiety disorder, social interactions, support

ÖZ

Amaç: Yalnızlık, başta emekliler olmak üzere çeşitli yaş gruplarını etkileyen, öznel ve hoş olmayan bir boşluk ve sıkıntı hissi olarak tanımlanmıştır. Emeklilik, mesleki faaliyetlerin sona ermesi ve düzenli gelirin kaybı ile karakterize edilen önemli bir yaşamsal olaydır. Bu olgular genellikle bir arada görülür ve aralarındaki ilişki karmaşık olabilir.

Yöntemler: Araştırma, Hırvatistan'ın Zagreb kentindeki Zagreb Üniversite Hastanesi Psikiyatri ve Psikolojik Tıp Bölümü'nde anksiyete bozukluğu için ayakta tedavi gören ve remisyonda olan ve dahil edilme kriterlerini karşılayan rastgele seçilmiş 75 hastayı kapsamaktadır. Katılımcılar emeklilikten beş yıl önce, emeklilikten bir yıl önce ve emeklilikten bir yıl sonraki gruplar olarak 25'er kişilik üç gruba ayrılmışlardır. Katılımcılar psikolojik testler [California Üniversitesi, Los Angeles (UCLA) yalnızlık ölçeği ve Mini Uluslararası Nöropsikiyatrik Görüşme] kullanılarak bir kez test edilmişlerdir.

Bulgular: Bu çalışmada, 75 katılımcı arasında emekliliğin aşamalarındaki yalnızlık incelenmiştir. UCLA Yalnızlık Ölçeği puanları emeklilik öncesinden emeklilik sonrasına önemli ölçüde artmış ($p<0,001$) ve emeklilikten bir yıl sonra zirveye ulaşmıştır. Duygusal yalnızlık, özellikle de izolasyon hissi keskin bir şekilde yükselirken, sosyal yalnızlık kademeli olarak artmıştır. Tek yönlü varyans analizi, emekliliğin yalnızlık üzerinde anlamlı bir etkisi olduğunu doğrulamıştır [$F(2,72)= 24.561$, $p<0,001$, etki düzeyi $\eta^2=0,405$]. Duygusal ve sosyal refah üzerinde de önemli bir etki gözlenmiştir.

Sonuçlar: Çalışma sonuçları, emekli bireyler arasında yalnızlıkta önemli bir artış olduğunu göstermektedir. Emekliliğe geçiş, bireylerin duyguları ve sosyal etkileşimleri üzerinde etkili olabilir. Emeklilerin yeni günlük rutinler oluşturmalarında desteklenmeleri gerekmektedir.

Anahtar kelimeler: Yalnızlık, emeklilik, aksiyete bozukluğu, sosyal etkileşimler, destek

INTRODUCTION

"... how hard it is to be weak. How hard it is to be alone and to be old, yet so young!"

Tin Ujević

Loneliness can be defined as a subjective experience of social isolation based on frustrated needs for belonging and a sense of dissonance between the expected and the actually existing quality of social relationships[1]. It is a truly universal experience, which means that every person will encounter loneliness at some point in their

Address for Correspondence: A. Greš, MD, University Hospital Center Zagreb, Department of Psychiatry and Psychological Medicine, Zagreb, Croatia
E-mail: alengres@gmail.com **ORCID ID:** orcid.org/0009-0003-7189-9340

Cite as: Greš A, Spasić N, Staver D. Loneliness in retirement. Medeni Med J. 2025;40:53-60

Received: 11 March 2025
Accepted: 03 May 2025
Published: 26 June 2025

life[2]. The concept of loneliness has been discussed since Ancient Greece. Aristotle himself emphasized that a person who is not social cannot be anything other than a beast or a god; *i.e.*, he cannot be a fully human being. There are many classifications of loneliness, but the most renowned one is the Weiss typology of loneliness, which distinguishes between emotional and social loneliness[3,4]. Recent reasearchs claims that loneliness can manifest itself through a number of different dimensions of human existence. On a biological level, loneliness can be characterized as internal stress. On the psychological level, it creates a subjective feeling of rejection and pain. On a deeper spiritual level, it affects questions of meaning[5].

Loneliness has become an epidemic problem in contemporary society, which we cannot ignore, because it has produced serious psychological and health consequences[6]. In the European context, loneliness disproportionately affects the elderly. The significance of this issue is accentuated by Europe's large and growing elderly population. The increase in life expectancy has contributed to later retirements. The phenomenon of individuals working full-time or part-time in retirement has become increasingly prevalent in the 21st century[7,8].

Loneliness is not the same as solitude. Solitude is an objective indicator that a person does not have other people around him or her, while loneliness is a subjective experience of insufficient or deficient relationships with other people[9]. The positive aspect of loneliness can be beneficial. Furthermore, it encourages a person to seek and establish relationships. Importantly, the study discovers and eliminates its psychological causes[10].

In contrast, severe or prolonged episodes of loneliness can act as chronic stressors that damage well-being and health. Addressing this issue requires a substantial investment in social relationships[11]. As individuals age, there is an increasing probability of encountering health limitations and illnesses that may impede their capacity for social engagement[12].

Retirement represents the culmination of a phase in the life of every individual who no longer has professional activities, loses regular salary for the work performed, and brings the working life to a definitive conclusion. According to many experts, retirement is characterized by elevated stress levels and the dissolution of previously held roles and responsibilities[13]. Before the advent of globalization, modern technology, and an organized pension system, people worked as long as their health allowed them. There was no limit that marked when a person was ready for retirement[14].

There are two categories of retirement: voluntary and involuntary. Voluntary retirement refers to an employee's decision to leave their position prior to reaching the statutory retirement age. Involuntary retirement is caused by external factors, not by personal choice. It has been shown to negatively affect depression, life satisfaction, and stress levels[15]. In the retirement phase, an individual ceases to be an active member of the working world. This period of life is often accompanied by a sense of mortality and a fear of death[16]. It is not possible to assert that the process is the same for everyone because we do not all age in the same way, influenced by a combination of psychological, biological, and social factors. The spirit and nature of each individual is the foundation of their unique identity[17].

Despite numerous medical discoveries and achievements of the modern era, death still eludes human control. The terms "illness" and "death" are commonly associated with old age and retirement[18,19]. As indicated by the biological aspect of aging, individuals experience a decline in physical strength and an increase in physical dependence on others. The social institution creates structures to govern the dependence of people considered helpless[20]. The notion of retirement can evoke a concept that sounds scary and intimidating to any of us. A significant proportion of retirees have adult children who themselves have their own families, which is a common occurrence concomitant with retirement[21].

Assuming that an individual is in good health when entering the third age upon retiring, they will have a significant amount of free time at their disposal. After many years of work, these situations can have a negative effect on the transition to retirement[22]. Prejudices are frequently correlated with advanced age: a tendency to get sick, being unproductive, impaired cognitive function, depression, and express dissatisfaction[23]. In addition to the fears that accompany the transition to retirement, older adults must confront prejudicial attitudes that are prevalent in society[24].

The study hypothesizes that loneliness increases significantly during the transition to retirement, with the highest levels observed post-retirement. The objective of this study was to examine the effects of retirement on the degree of loneliness experienced by individuals with anxiety disorders.

MATERIALS and METHODS

Study Design

A 12-week December 5th, 2024-March 4th, 2025 randomized controlled trial was carried out at the University Hospital Center Zagreb, Department for Psychiatry and Psychological Medicine in Zagreb, Croatia. A total of 75 outpatient participants who met the inclusion criteria were randomly assigned to three age groups, with 25 participants per group. Five years before, one year before, and one year after involuntary retirement.

Inclusion criteria required the following: Participants to have a diagnosed anxiety disorder, be aged 55-66 years, and have stable remission maintained for ≥6 months. Exclusion criteria comprised: Psychotic decompensation, antipsychotics, current depression, antidepressants, suicide attempts, or substance/alcohol use within the preceding 6 months.

All participants underwent psychiatric examination, including general questionnaires and psychological testing including the University of California, Los Angeles (UCLA) test to measure loneliness levels and the Mini International Neuropsychiatric Interview (MINI) to exclude depression and psychosis.

Measuring Instruments

1. General questionnaire (sociodemographic and medical data).

Gender: m/f, level of education (elementary, high school, university), marital status-married, widowed, divorced, single, offspring yes/no, if yes, how many children, employment status: employed or unemployed. Family history, suicide attempt, diagnosis.

2. The short form of the UCLA Scale was used to measure loneliness[25]. This scale quantifies loneliness as a unidimensional construct. It has seven items with five points. Participants were instructed to indicate on a five-point rating scale how much each statement applied to them, ranging from 1 (does not apply to me at all) to 5 (completely applies to me). The total score is derived as a linear combination of the scores from all seven items, with higher scores indicating greater levels of loneliness. The UCLA scale was utilized in a Croatian sample comprising different age groups. The scale has been found to possess satisfactory discriminant validity[26].

3. MINI was utilized to rule out the presence of depressiveness and psychoticism, as it is a structured interview according to the criteria from the Diagnostic and Statistical Manual of Mental Disorders. The psychiatric interview is consistent with a biopsychosocial approach to mental disorders, and it is crucial to grant the patient the opportunity to articulate in his own words his experiences and concerns. The formulation of a diagnosis and the acquisition of additional pertinent data are facilitated by specific questions. This comprehensive approach enables a thorough evaluation of the patient's condition and the development of a tailored treatment plan. The patient must be informed of the rationale behind the psychiatric interview, such as diagnosis, research, treatment determination, or the assessment of capacity to work or disability, along with any other pertinent rights[27].

Statistical Analysis

The statistical methods used for data analysis of this study were descriptive statistics: numbers, percentages, means, and means and standard deviations (SDs). Statistical analyses were conducted using IBM SPSS version 19.0. tables and figures were created in MS Excel.

Ethical Approval

This study was approved by the Ethical Committee of the University Hospital Center Zagreb, Croatia, class: 8.1-24/266-2, number: 02/013 AG, dated December 4th, 2024, before recruitment of the first participant. Participants were provided with a detailed explanation of the study protocol, and written informed consent was obtained from each individual. All procedures were carried out in accordance with the ethical principles outlined in the Declaration of Helsinki.

RESULTS

Demographic Characteristics

The final sample included 75 participants. Women comprised the majority at 54.7%, while men accounted for 45.3%. The majority of participants (68%) were younger than 65 years, while 32% were 65 years or older. As anticipated, the analysis revealed a statistically significant difference in the distribution of age groups. The result was significant ($p<0.001$) because all retired participants belonged to the older age group.

Over half of the participants were married (56%), while 32% were divorced, 9.3%, were single, and a minority (2.7%) were widowed. Importantly, marital status was evenly distributed across all age groups ($p=0.49$). Education level was also well distributed across groups ($p=0.40$), with the majority (50.7%) having completed high school, 32% holding a university degree, and 17.3% having finished elementary school.

As shown in Table 1, 60% of participants were employed, while 33.3% were retired and 6.7% were unemployed. Given the structure of the sample, it was expected that the employment distribution would not be equal (p<0.001). The majority of participants (89.3%) had children, while 10.7% were childless. However, no statistically significant difference was observed between the groups in this regard (p=0.37).

Psychiatric diagnoses were evenly distributed among the three groups (p=0.80), with 50.7% diagnosed with F41 disorders and 49.3% diagnosed with F43.2 disorders. Regarding the hereditary aspect of psychiatric illness, 24% of participants reported having a family member with a mental illness, with the difference between groups is approaching statistical significance (p=0.07). Only one person had a history of a suicide attempt.

Table 1. Demographic characteristics.

Category	Subcategory	p-value
Sex	Female: 54.7%	0.42
	Male: 45.3%	
Age	<65: 68%	<0.001*
	≥65: 32%	
Marital status	Single: 9.3%	0.49
	Married: 56%	
	Divorced: 32%	
	Widowed: 2.7%	
Education	Elementary: 17.3%	0.40
	High school: 50.7%	
	University: 32%	
Employment	Unemployed: 6.7%	<0.001*
	Employed: 60%	
	Retired: 33.3%	
Children	Yes: 89.3%	0.37
	No: 10.7%	
Diagnosis	F41: 50.7%	0.80
	F43.2: 49.3%	
Family history	Yes: 24%	0.07*
	No: 76%	
Suicide attempt	Yes: 1.3%	0.36
	No: 98.7%	

*As indicated by the symbol

This indicates a statistically significant difference or association when compared between the studied categories and other categories. The p-value for that specific category is statistically significant, typically at a threshold of p<0.05.

University of California, Los Angeles Loneliness Scale Analysis

As seen in the descriptive statistics for the UCLA total score in Table 2, the mean UCLA loneliness score increased across the three groups. The lowest mean score was observed five years before retirement (M=13.32, SD=3.26), followed by one year before retirement (M=15.20, SD=2.55), with the highest mean score found one year post-retirement (M=18.96, SD=2.83).

A One-Way Analysis of Variance (ANOVA) revealed a significant effect of retirement on loneliness levels, F (2, 72) = 24.561, p<0.001, with a large effect size η^2=0.405, indicating that approximately 40.5% of the variance in loneliness scores can be explained by retirement status. This strong effect size suggests a substantial increase in feelings of loneliness after retirement.

Post-hoc Tukey honestly significant difference (HSD) analysis indicated that loneliness scores one year after retirement were significantly higher than both one year prior (p<0.001) and five years prior to retirement (p<0.001). Notably, the difference between five and one year prior to retirement was not statistically significant (p=0.07).

Further analysis of item-level UCLA loneliness responses revealed differences across time points. UCLA item 3, "I feel isolated from others," showed the largest increase, with mean scores rising from M=2.3 (five years before) to M=2.5 (one year before) and peaking at M=2.8 (one year after retirement). Similarly, UCLA item 4, "I feel alone," increased from M=2.2 to M=2.4 before reaching M=2.7 after retirement. These results suggest that emotional loneliness, characterized mainly by feelings of isolation, post-retirement, is the most affected aspect of loneliness.

Social loneliness also increased but more gradually. UCLA item 1, measuring lack of companionship, rose from M=1.9 (five years before) to M=2.1 (one year before) and M=2.4 (one year after). A similar trend was observed

Table 2. UCLA total score descriptive statistics.

Group	N	Mean	SD	Minimum	Maximum
5 years before	25	13.32	3.262	9	23
1 year before	25	15.2	2.55	8	20
1 year after	25	18.96	2.835	11	22

SD: Standard deviation, UCLA: University of California, Los Angeles

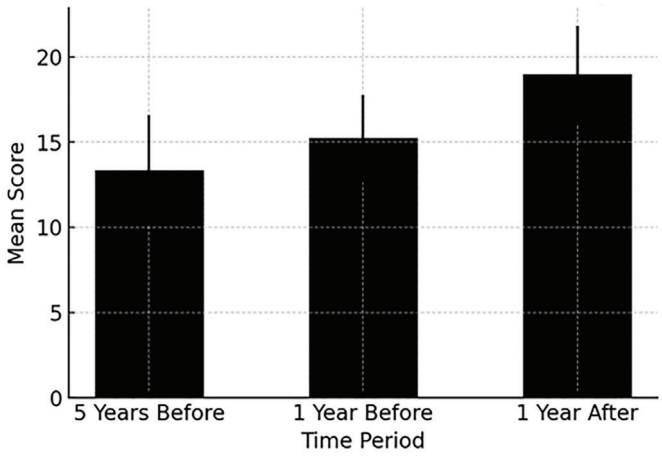

Figure 1. Mean UCLA total score across groups.
UCLA: University of California, Los Angeles

in UCLA item 2, assessing feelings of being left out (M=2.0→M=2.2→M=2.5). These findings suggest retirees maintain social interactions, but experience a gradual decline in social belonging.

Lastly, perceived social support slightly declined. Items four, five, and six increased by 0.2 points from five years before to one year after retirement. Notably, UCLA item 7, "There are people who really understand me," saw a larger rise (M=2.2→M=2.5), indicating a rising sense of emotional detachment.

DISCUSSION

The objective of the present study was to assess the likelihood of increased loneliness in patients prior to and following retirement. Our results suggest that emotional loneliness characterized by feelings of isolation, loneliness, or misunderstanding increases more sharply after retirement than social loneliness, which is defined as a lack of companionship and feelings of being left out.

Sociodemographic Data

The final sample included 75 participants. Women comprised the majority (54.7%), while 45.3% were men. The majority of participants (68%) were younger than 65 years, while 32% were 65 years or older. Over half of the participants were married (56%), while 32% were divorced, 9.3% were single, and a minority (2.7%) were widowed. Importantly, marital status was evenly distributed across all age groups (p=0.49). Education level was also evenly distributed across groups (p=0.40), with the majority (50.7%) having completed high school, 32% holding a university degree, and 17.3% having finished elementary school.

Psychiatric diagnoses were evenly distributed among the three groups (p=0.80), with 50.7% diagnosed with F41 and 49.3% diagnosed with F43.2. Regarding the hereditary aspect of psychiatric illness, 24% of participants reported having a family member with a mental illness, with the difference between groups approaching statistical significance (p=0.07). Only one person had a history of suicide attempt.

Analysis of the University of California, Los Angeles Loneliness Scale

The mean UCLA loneliness score increased gradually from five years prior to retirement to one year prior to retirement, peaking one year after retirement, according to the UCLA total score shown in Table 2. Findings indicate a notable increase in emotional loneliness post-retirement. Retirement has a statistically significant impact on loneliness levels [F (2.72)= 24,561, p<0.001], according to the results of the one-way ANOVA, with a substantial effect size (η^2=0.405). According to the research, loneliness was significantly higher after retirement, underscoring the necessity of focused interventions like social support networks.

The results showed significantly higher scores one year after retirement compared to pre-retirement levels (p<0.001). Post-hoc Tukey HSD tests confirmed that loneliness levels were significantly higher after retirement. However, the difference between five and one year before retirement was not statistically significant (p=0.07), indicating that loneliness is a result of the transition itself. These results emphasize the necessity of focused assistance in early retirement to lessen emotional and social difficulties.

In a study by Hawkley et al.[28], researchers examined data from two surveys involving adults older than 50 years in the ultrasonography. The researchers' findings indicated that after the age of 50, which was the earliest age of participants in their study, loneliness tended to decrease until about age 75, after which it began to increase again[28]. In our study, we had a sample ranging in age from 55 to 66 years. The present study focused on the phenomenon of loneliness, highlighting the impact of major life transitions and identifying fluctuations in loneliness.

Interestingly, the same part of the brain (the anterior insula) is activated during experiences of pain and loneliness, which points to a similar emotional quality in both experiences[29].

Carr and Fang [30] conducted a study exploring the qualitative experiences of existential loneliness among

80 older adults residing in retirement communities in the United Kingdom and Australia. The study provided substantial insight into the inner lives of older people. The study identified several core themes, including the loss of close relationships, absence of physical touch and intimacy, declining physical health, and the lack of an emotional vocabulary to articulate experiences of existential loneliness. The study concluded that transition to retirement living is linked to the experience of existential loneliness[30].

Our study further examined loneliness in the context of retirement. We identified emotional loneliness (*e.g.*, feelings of isolation) as a key component, contributing to a deeper understanding of loneliness in eldery population and retirees.

Research by Shin et al.[31] found that involuntary retirement is linked to higher levels of loneliness. However, the study also indicated that involuntarily retired individuals with strong positive social support had relatively lower levels of loneliness. The findings suggested that social support may alleviate the negative impacts of involuntary retirement. No one can be forever young or healthy, and just as caring for children is considered a family obligation, so is caring for the elderly and infirm[31].

Guthmuller et al.[32] study indicates that individuals can adapt to retirement by increasing their activity levels. This leads to a reduction in feelings of loneliness and social isolation. The heterogeneity analysis indicates that this phenomenon is particularly evident among the more highly educated[32].

The results in our study also indicate that more highly educated individuals were less lonely prior to retirement. As individuals grow older, very often, their social circle tends to contract. Friends and family live far away. This can create some difficulties in maintaining social connections and establishing new relationships, particularly if health issues restrict their ability to stay active and mobile.

Sharma and Prince[33] research, had a sample of 600 retired people. The results indicated that loneliness has a negative and significant impact on the health of retired individuals. While self-esteem and physical activity have a positive and significant impact on their health, further studies are needed to understand the mechanisms involved. The study demonstrated a negative association between health and loneliness, indicating that increased loneliness contributes to a decline in both quality of life and overall health among adults[33].

Both studies emphasize that retirement is a critical period where the loss of structured social interactions and emotional support can lead to increased loneliness. They also emphasize the need for interventions to address these challenges. These findings are comparable to ours.

Findings from the study by Chen and Feeley[34] indicated that emotional support from a spouse or partner, as well as from friends, played a significant role in alleviating feelings of loneliness. In a survey conducted by Hajek et al.[35], regression analyses revealed that loneliness increased with advancing age; transitions from being married and cohabiting with a spouse or registered partner to other marital statuses; reductions in log income; declines in self-rated health and functional ability; increases in depressive symptoms; and decreases in cognitive functioning. Notably, loneliness was not associated with changes in the presence of chronic diseases. The data were drawn from Waves 5 to 7 of the Survey of Health, Ageing and Retirement in Europe, comprising an analytical sample of 101.909 observations[35].

Loneliness in retirement can have significant effects on both mental and physical health. Current research is mainly focused on the connection of loneliness with mortality, mental, and cardiovascular health. It is more likely that lonely people will resort more often to unhealthy behaviors like alcohol consumption, smoking, substance abuse, or excessive food intake and use them as psychological relief mechanisms[36,37].

The study by Jutengren and Ståhl[38] included a sample of 601 job-retired, community-dwelling older adults (386 females and 215 males) aged between 65 and 97 years. The results indicated that the mediation model provided a substantially better fit to the data compared to the main effects regression model. These findings suggest that emotional expressivity plays a mediating role in the relationship between social loneliness and its previously identified predictors[38].

The present study shares certain parallels with other research in the field. Loneliness was observed among retired individuals, and furthermore, the impact of retirement on social connectedness was highlighted. It is imperative to acknowledge the emotional and social dimensions of loneliness. Additionally, there is a need for interventions to address loneliness in retired individuals.

Contribution

The primary contribution of our research is its strong statistical significance. Furthermore, the present study provides valuable insights that enable a deeper

exploration of loneliness. It highlights retirement-specific loneliness dynamics, differentiation of loneliness types (emotional and social loneliness), and providing practical implications. Given the inherently subjective nature of loneliness, future studies could benefit from incorporating qualitative methods such as open-ended questions or in-depth interviews to provide richer insights.

Study Limitations

The present study was subject to several limitations. Firstly, the relatively modest sample size may have reduced the study's power. Secondly, the study did not incorporate additional laboratory tests. The absence of a control group and cross-sectional design are important limitations of the study. Consequently, future research should prioritize expanding the sample size in order to achieve better statistical power.

CONCLUSION

The transition to retirement represents a critical life event, as it often initiates significant changes across multiple domains of an individual's life. Newly retired individuals frequently report heightened feelings of loneliness during this period. Loneliness, particularly emotional loneliness, spikes after retirement, while social loneliness increases more gradually. They may feel as though they don't have any social roles and may have less contact with other people. This is a serious health problem. Further research is needed to enhance retirees' quality of life.

Ethics

Ethics Committee Approval: This study was approved by the Clinical Hospital Center Zagreb Ethics Committee (approval no: 02/013 AG, date: 04.12.2024).

Informed Consent: Participants were provided with a detailed explanation of the study protocol, and written informed consent was obtained from each individual.

Foonotes

Authorship Contributions

Concept: A.G., N.S., D.S., Design: A.G., N.S., D.S., Data Collection or Processing: A.G., N.S., D.S., Analysis or Interpretation: A.G., N.S., Literature Search: A.G., N.S., D.S., Writing: A.G., N.S., D.S.

Conflict of Interest: No conflict of interest was declared by the authors.

Financial Disclosure: The authors declare that this study received no financial support

REFERENCES

1. Cacioppo JT, Cacioppo S. Loneliness in the modern age: An evolutionary theory of loneliness. Exp Soc Psychol. 2018;58:127-97.
2. Kaplan D, Berkman B. The Oxford handbook of social work in health and aging. 2nd ed. New York: Oxford University Press; 2016.
3. Lacković-Grgin K. Usamljenost: fenomenologija, teorije i istraživanja. 1st ed. Jastrebarsko: Naklada Slap; 2008.
4. Šolak R, Dragičević J. Efekti percipirane socijalne podrške na usamljenost. CIVITAS. 2021;11:46-61.
5. Spitzer M. Usamljenost: Neprepoznata bolest. Zagreb: Naklada Ljevak; 2019.
6. Nuyen J, Tuithof M, de Graaf R, et al. The bidirectional relationship between loneliness and common mental disorders in adults: Findings from a longitudinal population-based cohort study. Soc Psychiatry Psychiatr Epidemiol. 2020;55:1297-310.
7. Das A. Is loneliness adaptive? A dynamic panel model study of older U.S. adults. J Gerontol B Psychol Sci Soc Sci. 2021;76:1430-40.
8. World Health Organization. Social isolation and loneliness among older people: Advocacy brief [Internet]. 2021. Available from: https://www.who.int/publications/i/item/9789240030749
9. Cohen-Mansfield J, Hazan H, Lerman Y, Shalom V. Correlates and predictors of loneliness in older-adults: a review of quantitative results informed by qualitative insights. Int Psychogeriatr. 2016;28:557-76.
10. Marčinko D, et al. Usamljenost i depresija. 1st ed. Zagreb: Medicinska naklada; 2024.
11. Huxhold O, Fiori KL, Windsor T. Rethinking social relationships in adulthood: the differential Investment of Resources Model. Pers Soc Psychol Rev. 2022;26:57-82.
12. Huxhold O, Fiori KL, Windsor TD. The dynamic interplay of social network characteristics, subjective well-being, and health: The costs and benefits of socio-emotional selectivity. Psychol Aging. 2013;28:3-16.
13. Giné-Garriga M, Jerez-Roig J, Coll-Planas L, et al. Is loneliness a predictor of the modern geriatric giants? Analysis from the survey of health, ageing, and retirement in Europe. Maturitas. 2021;144:93-101.
14. Repetti M. Retirement. In: Handbook on migration and ageing. 1st ed. Cheltenham: Edward Elgar Publishing; 2023. p.35-44.
15. van der Heide I, van Rijn RM, Robroek SJ, Burdorf A, Proper KI. Is retirement good for your health? A systematic review of longitudinal studies. BMC Public Health. 2013;13:1180.
16. Ong AD, Uchino BN, Wethington E. Loneliness and health in older adults: A mini-review and synthesis. Gerontology. 2016;62:443-9.
17. Hawkley LC, Browne MW, Cacioppo JT. How can I connect with thee? Let me count the ways. Psychol Sci. 2005;16:798-804.
18. Greš A, Staver D, Šakić B, Radovančević LJ. Thanatological perspectives in geriatrics and gerontopsychiatry. Scr Med. 2023;54:297-9.
19. Greš A, Staver D, Radovančević L. Dysthanasia. Scr Med. 2025;56:201-4.
20. Bara M, Podgorelec S. Društvene teorije umirovljenja i produktivnog starenja. Etnološka tribina. 2015;45:58-71.

21. Štifanić M. Društveni aspekti starenja i obolijevanja. Diacovensia. 2018;26:505-27.

22. Sharma P, Asthana H, Gambhir IS, Ranjan JK. Death anxiety among elderly people: Role of gender, spirituality and mental health. Indian J Gerontol. 2019;33:240-54.

23. Erber J. Aging and Older Adulthood. 3rd Chichester: Wiley-Blackwell; 2013.

24. Mali J. Ana Štambuk: Stavovi starijih osoba prema smrti i umiranju. Rev Za Soc Polit. 2019;26:267-9.

25. Allen RL, Oshagan H. The UCLA loneliness scale: Invariance of social structural characteristics. Pers Individ Differ. 1995;19:185-95.

26. Lacković-Grgin K, Nekić M, Penezić Z. Usamljenost žena odrasle dobi: Uloga percipirane kvalitete bračnog odnosa i samostišavanja. Suvremena Psihologija. 2009;12:7-22.

27. American Psychiatric Association. DSM-5: Dijagnostički i statistički priručnik za duševne poremećaje. 5th ed. Jukić V, Arbanas G, translators. Zagreb: Naklada Slap; 2013.

28. Hawkley LC, Wroblewski K, Kaiser T, Luhmann M, Schumm LP. Are U.S. older adults getting lonelier? Age, period, and cohort differences. Psychol Aging. 2019;34:1144-57.

29. Lam JA, Murray ER, Yu KE, et al. Neurobiology of loneliness: A systematic review. Neuropsychopharmacology. 2021;46:1873-87.

30. Carr S, Fang C. A gradual separation from the world: A qualitative exploration of existential loneliness in old age. Ageing Soc. 2023;43:1436-56.

31. Shin O, Park S, Amano T, Kwon E, Kim B. Nature of retirement and loneliness: The moderating roles of social support. J Appl Gerontol. 2020;39:1292-302.

32. Guthmuller S, Heger D, Hollenbach J. Werbeck A. The impact of retirement on loneliness in Europe. Sci Rep. 2024;14:26971.

33. Sharma E, Prince JB. Measuring the impact of loneliness, physical activity, and self esteem on the health of the retired people. Ment Health Soc Incl. 2024;28:893-909.

34. Chen Y, Feeley TH. Social support, social strain, loneliness, and well-being among older adults: An analysis of the health and retirement study. J Soc Pers Relat. 2014;31:141-61.

35. Hajek A, Gyasi RM, König HH. Factors associated with loneliness among individuals aged 80 years and over: Findings derived from the nationally representative "Old Age in Germany (D80+)" study. Arch Gerontol Geriatr. 2024;123:105443.

36. Mesar M, Domitrović A. Usamljenost starijih osoba na potresom pogođenom području Sisačko-moslavačke županije. Epoha zdravlja. 2023;16:27-8.

37. Murray J, Craigs CL, Hill KM, Honey S, House A. A systematic review of patient reported factors associated with uptake and completion of cardiovascular lifestyle behaviour change. BMC Cardiovasc Disord. 2012;12:120.

38. Jutengren G, Ståhl F. Determinants of social loneliness among older adults in job retirement and the role of emotional expressivity. Aging Ment Health. 2024;28:1153-61.

DOI: 10.4274/MMJ.galenos.2025.86729
Medeni Med J 2025;40:61-71

Original Article

Comprehensive Classification of Variations of the Anterior Part of the Circle of Willis in Fresh Cadavers Anterior Communicating Artery

Taze Kadavralarda Willis Halkasının Ön Bölümündeki Varyasyonların Kapsamlı Sınıflandırılması

Gkionoul NTELI CHATZIOGLOU[1], Emine NAS[2,3], Aysin KALE[2], Kardelen AKTAS[2], Osman COSKUN[2], Özcan GAYRETLI[2]

[1]Istanbul Health and Technology University Faculty of Medicine, Department of Anatomy, Istanbul, Türkiye
[2]Istanbul University Faculty of Medicine, Department of Anatomy, Istanbul, Türkiye
[3]Istanbul University Institute of Health Sciences Department of Anatomy, Istanbul, Türkiye

ABSTRACT

Objective: The goal of our study is to evaluate and classify the variations of the anterior communicating artery (AComA) on fresh cadavers from the Türkiye population.

Methods: In this study, 182 fresh cadavers were analysed and classified according to the number, shape and course of the AcomA.

Results: In our study, typical AcomA was the most common with a rate of 86 (47.25%), while variations of the AcomA were found in the remaining 96 (52.75%) cases. Among these variations, in 11.46% (11/96) of cases, AcomA variations were identified as distal and proximal duplications according to the number of branches they represented; 68.75% (66/96) of cases were identified by their shape (X-shaped, single/double fenestration, hypoplasia, or aplasia); and, in 19 cases, it was characterized by course (median artery or oblique course). The rate of variations was 65% (26/40) in females and 49.29% (70/142) in males. In our study, the X-shaped and single fenestration variations were recorded as the most common.

Conclusions: The results of the study are important for cerebrovascular surgery and radiological interventions. It emphasises the importance of recognising and considering variations. The study will contribute to the understanding of cerebrovascular diseases and the development of treatment strategies.

Keywords: Anterior communicating artery, variation, circle of Willis, fresh cadaver

ÖZ

Amaç: Bu çalışmanın amacı, Türk popülasyonuna ait taze kadavralar üzerinde arteria communicans anterior'un (AcomA) varyasyonlarını tanımlamak ve sınıflandırmaktır.

Yöntemler: Bu çalışmada toplamda 182 taze kadavra incelendi ve AcomA'nın sayısı, şekli ve seyrine göre sınıflandırılması gerçekleştirildi.

Bulgular: Çalışmamızda, tipik AcomA %47,25 oranıyla en sık görülürken, geri kalan 96 olguda AcomA'un varyasyonlarına rastlandı. Bu varyasyonlar arasında 11/96 olguda distal ve proksimal duplikasyon, 66/96 olguda şekline göre (X-şekilli, fenestrasyona sahip, hipoplazik veya aplazik) ve 19 olguda seyrine göre (median arter veya oblik seyir) AcomA varyasyonları tespit edildi. Varyasyon oranı kadınlarda 26/40 ve erkeklerde 70/142 idi. Çalışmamızda, X şekilli ve tek fenestrasyon gösteren varyasyonları en sık görülen varyasyonlar olarak kaydedildi.

Sonuçlar: Çalışmanın sonuçları serebrovasküler cerrahi ve radyolojik girişimler için önemlidir. Varyasyonları tanımanın ve dikkate almanın önemini vurgulamaktadır. Çalışma, serebrovasküler hastalıkların anlaşılmasına ve tedavi stratejilerinin geliştirilmesine katkıda bulunacaktır.

Anahtar kelimeler: Arteria communicans anterior, varyasyon, Willis halkası, taze kadavra

Address for Correspondence: G. Nteli Chatzioglou, Istanbul Health and Technology University Faculty of Medicine, Department of Anatomy, Istanbul, Türkiye
E-mail: gkionoul.chatzioglou@istun.edu.tr **ORCID ID:** orcid.org/0000-0003-3728-6930

Cite as: Nteli Chatzioglou G, Nas E, Kale A, Aktaş K, Coşkun O, Gayretli Ö. Comprehensive classification of variations of the anterior part of the circle of willis in fresh cadavers anterior communicating artery. Medeni Med J. 2025;40:61-71

Received: 19.11.2024
Accepted: 06.05.2025
Published: 26 June 2025

INTRODUCTION

The cerebral arteries forming the Circle of Willis are very important in terms of collateral circulation of the brain. There are a number of vital anastomoses between the arteries forming the polygon[1]. In case of stenosis or occlusion of any of the arteries, these anastomotic connections ensure the continuity of collateral circulation. Variations such as aplasia and hypoplasia are risk factors for cerebrovascular events. Knowledge of both the normal anatomy of the arteries forming the cerebral arterial circle and the existing variations are extremely important for the radiologic and surgical interventions planned for this region[2-4].

The anterior communicating artery (AcomA), which connects the anterior cerebral arteries (ACAs) on both sides, is sometimes absent or may be double. From this artery, branches named anteromedial central arteries of varying numbers branch off and supply the optic chiasm, hypothalamus, cingulate gyrus, lamina terminalis, and preolfactory area[1,5,6].

This study was conducted to find variations in the AcomA, which stabilises cerebral blood flow when the main channels fail or are insufficient for different reasons. The AcomA shows many morphological variations. The adequacy or lack of recovery after vascular occlusion depends partly on the anatomical condition of the component vessel of the Circle of Willis[1,7-10]. Therefore, knowledge of such variations is of clinical importance.

MATERIALS and METHODS

Approval from the ethics committee of our study was completed in two stages. In the first stage, after obtaining permission from the scientific committee of the Forensic Medicine Institute (Istanbul, Türkiye), an ethics committee application was made; approval was obtained from Istanbul Medical Faculty Clinical Research Ethics Committee (date: 04/10/2024, decision no: 19).

Since our study was performed on autopsied cadavers, "informed consent" was not obtained. All procedures were carried out in accordance with the ethical rules and the principles of the Declaration of Helsinki. The study was conducted on the fresh cadavers received by Department of Morgue Specialization of the Forensic Medicine Institute, Ministry of Justice (Istanbul, Türkiye) for autopsy from 2022 to 2024.

Autopsy Procedure and Brain Examination

During the autopsy, the scalp was incised coronally using a scalpel and carefully pulled back. The temporalis muscle and its fascia were dissected, and any remaining fascial tissue on the bone was meticulously scraped away. The calvaria was then removed using a bone saw, followed by the careful removal of the dura mater to expose the underlying brain tissue.

The brain was gently retracted posteriorly from the frontal lobes, and the cranial nerves were severed at their osseous entry points to isolate the brainstem. A transverse incision was made at the brainstem near the level of the foramen magnum, allowing the complete extraction of the brain.

Subsequently, the arachnoid mater covering the cerebral arteries was dissected to fully expose the vessels of the cerebral arterial circle (Circle of Willis). The ACAs and AcomAs were examined *in situ* to preserve their natural anatomical relationships and photographed for documentation. High-resolution images were captured using a 20-megapixel Sony RX100 VII camera.

Exclusion criteria were determined as follows: before the autopsy procedure, during the autopsy, and after the brain tissue was removed.

Dissection Technique

In the first stage of dissection, the scalp was removed. The fascia covering the temporalis muscle and the muscle itself was peeled off. The calvaria was then incised with a saw according to autopsy procedures. After the dura mater was dissected, the brain tissue was exposed. The brain was deviated posteriorly from the frontal lobe, and the visible cranial nerves were cut at their entry points to the cranium. Finally, the brain stem was dissected transversely, and the brain tissue was removed from the cranium. The adherent layer of arachnoidea mater under the dura mater and just above the brain tissue was removed, and the cerebral arteries were exposed. The ACA and AcomA cerebral arteries were photographed inferiorly, without altering the normal anatomical position[11]. Photographs were taken with a Sony RX100 VII model (20 megapixel) camera.

Morphometric Evaluation of Anterior Communicating Artery

The outer diameter of the AcomA was measured from its midpoint. The measurement was performed perpendicular to the course of the AcomA using the "straight line" measurement tool in the Image J program. Arteries with a diameter of less than 1 mm were called hypoplastic in accordance with the literature[4], and included in our classification.

Morphological Evaluation of Anterior Communicating Artery

The AcomA was classified into 3 groups according to the number of branches, shape, and course. The AcomA cases that did not fit this classification were considered to be typical AcomA or Type 1 (Figure 1) and unilateral ACA A1 hypoplasia or Type 9.

Variations of Anterior Communicating Artery According to the Number of Branches (Figure 2)

1. Proximal duplication of AcomA or Type 8 (Figure 2A and Figure 2B): The variation is defined as a combination of an additional AcomA, with a contralateral A1 or A2 segment of the anterior cerebral artery. Proximal duplication of AcomA was defined as having the first artery measured at a distance of 1-2.5 mm away from the second artery.

2. Distal duplication of AcomA or Type 6 (Figure 2C and Figure 2D): The variation is a combination of an additional AcomA and a contralateral A1 or A2 segment of the anterior cerebral artery. Distal duplication of AcomA is considered if the first artery is >2.5 mm away from the second artery.

Variations of Anterior Communicating Artery According to the Shape (Figure 3)

3. The X-shaped or Type 2 (Figure 3A and Figure 3B): In this variation, the transverse AcomA, which joins the anterior cerebral arteries of both sides, is either absent or is so short that it forms an X-shape.

4. Double fenestration of AcomA or Type 11 (Figure 3C and Figure 3D): Double fenestration occurs when the lumen splits into two and merges after a certain distance.

5. Single fenestration of AcomA or Type 3 (Figure 3E and Figure 3F): A single fenestration is present when a lumen forms on AcomA.

6. Aplasia of AcomA or Type 7 (Figure 3G and Figure 3H): It is defined as the absence of the anterior communicating artery.

7. Hypoplasia of AcomA or Type 5 (Figure 3J and Figure 3K): The variation occurs when the diameter is less than 1 mm.

Variations of Anterior Communicating Artery According to the Course (Figure 4)

8. Median artery or Type 4 (Figure 4A and 4B): This variation describes a branch arising from the median line of the AcomA and extending between the hemispheres.

9. Oblique course of AcomA or Type 10 (Figure 4C and Figure 4D): This variation defines a branch that runs obliquely to connect the contralateral anterior cerebral arteries of both sides.

Statistical Analysis

Descriptive statistics were used to determine the general distribution of the morphometric measurements obtained in the study. The average, standard deviation, minimum, and maximum values were observed.

An analysis of variance (ANOVA) test was used to determine whether there was a significant difference between AcomA types. Kruskal-Wallis H-test was applied when the data did not conform to normal distribution and the assumption of homogeneity of variance was not met. In cases where a significant difference was found as a result of ANOVA or the Kruskal-Wallis test, post-hoc

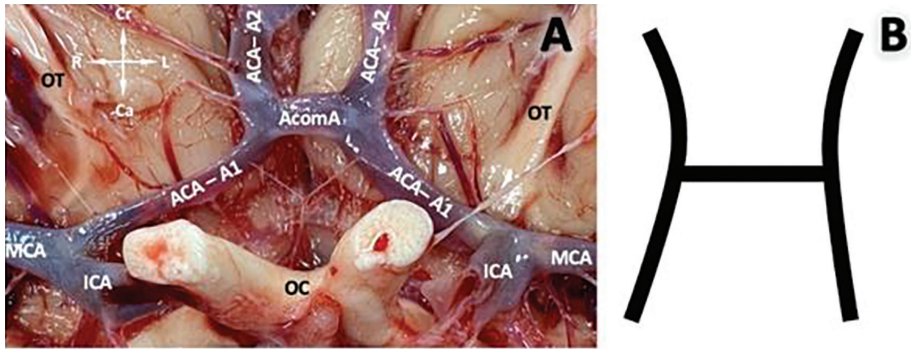

Figure 1. Demonstration of typical anterior communicating artery (AcomA). Typical AcomA of cadaver (A) and illustration (B) anterior cerebral artery (ACA)-A2: A2 segment of ACA, ACA-A1, A1 segment of ACA.

AcomA: Anterior communicating artery, ICA: Internal carotid artery, OT: Olfactory tract, OC: Optic chiasm, MCA: Middle cerebral artery, Cr: Cranial, Ca: Caudal; R: Right L: Left

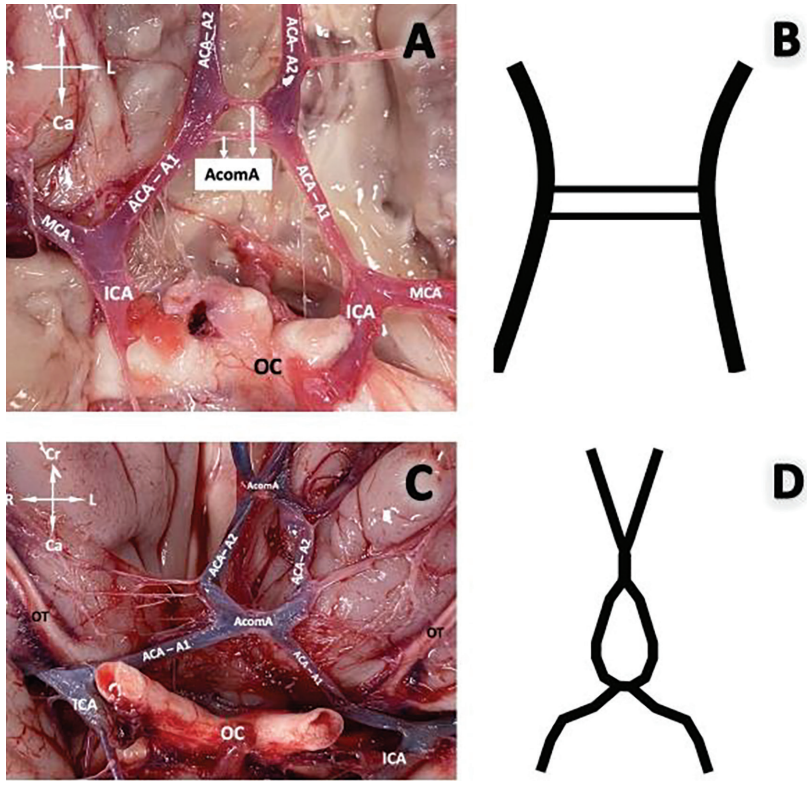

Figure 2. Various variations of the AcomA according to the number of branches. Proximal duplication of AcomA of cadaver (A), and illustration (B). Distal duplication of AcomA of cadaver (C) and illustration (D). Anterior cerebral artery (ACA)-A2, A2 segment of ACA; ACA-A1, A1 segment of ACA.

AcomA: Anterior communicating artery, ICA: Internal carotid artery, OT: Olfactory tract, OC: Optic chiasm, MCA: Middle cerebral artery, Cr: Cranial, Ca: Caudal, R: Right, L: Left

analyses were performed to determine which groups were different. The Bonferroni correction method was used in these analyses.

The Chi-square test was employed to determine whether there was a statistically significant difference between gender (female and male) and AcomA types. Fisher's exact test was applied when the expected frequency was not greater than 5 or the expected frequency was less than 1. Finally, ANOVA was used to examine whether there was a statistical difference among body mass index (BMI) and various AcomA types. The Kruskal-Wallis H-test was applied when the data were not normally distributed, and the variances of the groups were not homogeneous (checked by Levene's test). When a significant difference was found from ANOVA or the Kruskal-Wallis test post-hoc analyses (Bonferroni correction) were used to determine which groups were different. All statistical analyses were performed with Jamovi (Version 2.6), computer software (https://www.jamovi.org)[12].

RESULTS

Participant Demographics

The study included 182 cadavers, comprising 40 females (21.98%) and 142 males (78.02%).

Age: The mean age was 52.7±19.9 years for females and 48.5±17.5 years for males (Table 1).

Anthropometric Data:

Mean height: 170.19±9.59 cm

Mean weight: 77.37±19.18 kg

BMI Distribution:

Normal BMI: Mot prevalent (44.5%)

Low BMI: Least represented (4.39%)

The Classification of Acom A and the Correlations Between Gender and Body Mass Index

In 96 of 182 cadavers, 9 different variations according to the distribution of AcomA were observed. In total, 11,

Table 1. Summary of gender, age, height, weight and BMI data of the case								
					BMI			
	n	Age (mean±SD)	Height (cm) (mean±SD)	Weight (kg) (mean±SD)	Low (<18.5) n (%)	Normal (18.5-24.9) n (%)	Overweight (25-29.9) n (%)	Obese (≥30) n (%)
Male	142	48.48±17.48	173.64±5.69	78.07±17.58	7 (4.93)	66 (46.48)	39 (27.47)	30 (21.12)
Female	40	52.70±19.87	157.95±10.59	74.87±24.12	1 (2.5)	15 (37.5)	5 (12.5)	19 (47.5)
Total	182	49.40±18.05	170.19±9.59	77.37±19.18	8 (4.39)	81 (44.5)	44 (24.18)	49 (26.93)
BMI: Body mass index, SD: Standard deviation								

66 and 19 variations were described according to the number of branches, the shape and the course of AcomA, respectively. The most common variations were X-shaped, 36.36% (24/66), and single fenestration, 34.85% (23/66), variations in the group classified according to shape, among which 66 cases were identified. Hypoplastic AcomA, aplastic AcomA, and double fenestration AcomA were found in 13, 4, and 2 cases, respectively. In the classification according to the course of AcomA in 19 cases, AcomA including median artery was seen in 16/19 cases, and oblique course of AcomA was seen in only 3/19 cases. Finally, the AcomA classified according to the number of branches was detected in a total of 11 brains. Among these, distal duplication of distal AcomA was the most common with 7/11 cases, where the first AcomA was 9.78±3.59 mm (minimum: 5.48, maximum: 16.03) away from the second branch of AcomA, while proximal duplication was detected in 4/11 cases, where the first AcomA was 2.00±0.38 mm (1.43-2.24) away from the second branch of AcomA. When these variations were analyzed according to gender, X-shaped AcomAs were the most common variations in 17 of 142 male cases, and 7 of 40 female cases. The least common variation was double fenestration of the AcomA in both sexes (Table 2).

Morphological variations of the AComA were investigated, and these variations were classified according to the course of the AComA. In addition, these morphological variations were typed from Type 1 to Type 11. ANOVA and Kruskal-Wallis H-tests were performed to test whether there was a statistically significant difference among 11 types of AcomA. The p-values of ANOVA (p=0.018) and Kruskal-Wallis H (p=0.022) results indicated significant differences between the types. Therefore,

Table 2. Distribution of the courses of anterior communicating arteries according to genders.				
AcomA	**Male n (%)**	**Female n (%)**	**Total n (%)**	**P-values (ANOVA p=0.018, Kruskal-Wallis tests p=0.022)**
				Post-hoc analysis
Typical AcomA (Type 1)	**67/142 (47.18)**	**12/40 (30)**	**79/182 (43.40)**	Type 1 vs. Type 2: **p=0.045**
Unilateral ACA A1 hipoplasia **(Type 9)**	6/142 (4.22)	1/40 (2.5)	7/182 (3.84**)**	Type 1 vs. Type 3: **p=0.012**
Variations of anterior communicating artery according to the number of branches				
Distal duplication of AcomA **(Type 6)**	6/142 (4.22)	1/40 (2.5)	7/182 (3.86)	Type 1 vs. Type 4: **p=0.001**
Proximal duplication of AcomA **(Type 8)**	3/142 (2.12)	1/40 (2.5)	4/182 (2.2)	Type 2 vs. Type 3: p=0.067
Variations of anterior communicating artery according to the shape				
The X-shaped **(Type 2)**	17/142 (11.97)	7/40 (17.5)	24/182 (13.18)	Type 3 vs. Type 4: **p=0.034**
Single fenestration of AcomA **(Type 3)**	17/142 (11.97)	6/40 (15)	23/182 (12.63)	Type 5 vs. Type 6: p=0.089
Hypoplasia of AcomA **(Type 5)**	9/142 (6.33)	4/40 (10)	13/182 (7.14)	Type 6 vs. Type 7: **p=0.021**
Aplasia of AcomA **(Type 7)**	2/142 (1.42)	2/40 (5)	4/182 (2.2)	Type 7 vs. Type 8: **p=0.045**
Double fenestration of AcomA **(Type 11)**	1/142 (0.7)	1/40 (2.5)	2/182 (1.2)	Type 8 vs. Type 9: **p=0.012**
Variations of anterior communicating artery according to the course				
Median artery **(Type 4)**	13/142 (9.15)	3/40 (7.5)	16/182 (8.79)	Type 9 vs. Type 10: **p=0.034**
Oblique course of AcomA (Type 10)	2/142 (1.42)	1/40 (2.5)	3/182 (1.64)	Type 10 vs. Type 11: p=0.067
ANOVA: Analysis of variance, AcomA: Anterior communicating artery, ACA: Anterior cerebral artery				

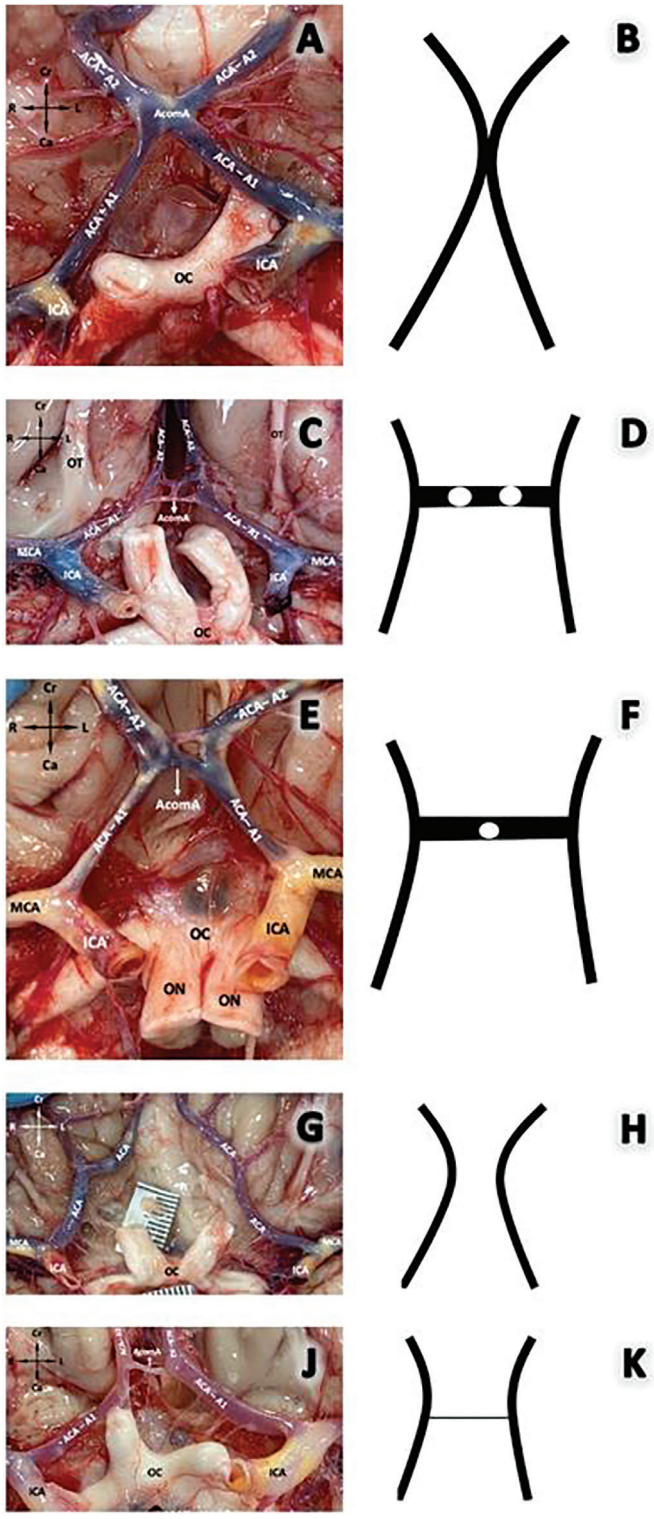

Figure 3. Various variations of the AcomA according to its shape. The X-shaped of cadaver (A) and illustration (B), Double fenestration of AcomA of cadaver (C), and illustration (D), Single fenestration of AcomA of cadaver (E) and illustration (F), Aplasia of AcomA of cadaver (G), and illustration (H), Hypoplasia of AcomA of cadaver (J), and illustration (K). ACA-A2, A2 segment of anterior cerebral artery. ACA-A1, A1 segment of anterior cerebral artery.

AcomA: Anterior communicating artery, ICA: Internal carotid artery, OT: Olfactory tract, OC: Optic chiasm, MCA: Middle cerebral artery, Cr: Cranial, Ca: Caudal, R: Right, L: Left

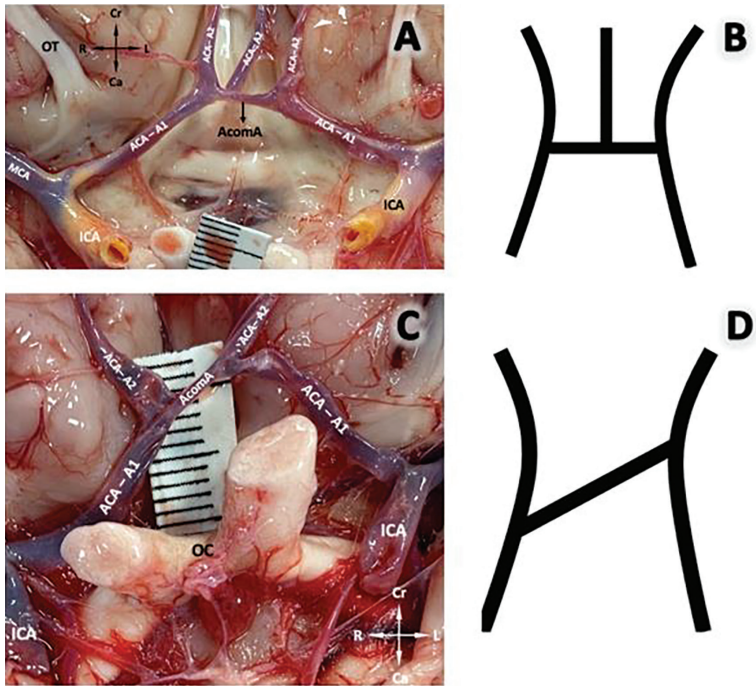

Figure 4. Various variations of the AcomA according to its course. Median artery of cadaver (A), and illustration (B), Oblique course of AcomA of cadaver (C) and illustration (D). ACA-A2, A2 segment of ACA, ACA-A1, A1 segment of ACA.

AcomA: Anterior communicating artery, ICA: Internal carotid artery, OT: Olfactory tract, OC: Optic chiasm, MCA: Middle cerebral artery, Cr: Cranial, Ca: Caudal, R: Right, L: Left

post-hoc analyses were performed to determine between which groups the significant difference occurred. The Bonferroni correction method was used in these analyses. Accordingly, significant differences were found between Types 1, 2, 3, 4, 6, 7, 8, 9, and 10 AcomA types. However, no significant difference was found in Type 2 vs. Type 3, Type 5 vs. Type 6, and Type 10 vs. Type 11 comparisons. (Table 2). After the evaluation of AcomA types between the sides, the distribution of AcomA types according to gender was also analysed. Accordingly, it was analysed whether there was a statistically significant difference between the different types of AcomA between genders. For this purpose, the χ^2 test was used (p=0.045). When the assumptions of the Chi-square test were not fulfilled, Fisher's exact test was applied (p=0.038). Although the results of both tests were similar, there was a statistically significant correlation between sex and AcomA types. It was determined that AcomA types such as Type 1, Type 3, and Type 4 were observed at different frequencies between males and females (Table 3). For example, Type 1 was the most common type of AcomA in both males and females. However, it was more common in males. Rarer AcomA types, such as Type 10 and Type 9, were found to have similar frequencies in both genders (Table 3).

In our study, most of the sample consisted of cadavers with normal BMI (81/182), (Table 4). Of the sample group, 49 were obese, 44 were overweight, and 8 had a low BMI. In the normal BMI group, Type 1 was observed in 54.32% of cases (44 out of 81). There were 8 cases of both Type 2 and Type 4 AcomA variations among cadavers with normal BMI, constituting 9.88% (8/81) in each group, respectively. However, the variations with Type 8 and Type 9 were the least common, 1.23% (1/81). In the obese BMI group, Type 1 was observed in 32.65% of (16-49) cases. Similarly, the most common variations were Type 2 14.28% (7/49) and Type 3 14.28% (7/49), while the least common were Type 6 2.04% (1/49) and Type 10 2.04% (1/49). No cadavers with Type II (0/49) were found. In cases of overweight BMI, Type 1 was determined in 43.18% (19/44) cadavers. Additionally, Type 3 was the most commonly seen, 6.82% (3/44), AcomA variation in this group, and Type 8, 2.27% (1/44), and Type 10, 2.27% (1/44), were the least common types seen. Type 7 (0/44), Type 9 (0/44), and Type 11 (0/44) were not encountered in this category of BMI. Finally, the cases with low BMI were analyzed according to the various types of AcomA. In four of eight cadavers, the AcomA was observed as Type 2. Also, Type 5 (2/8) and

Table 3. Distribution of the types of anterior communicating arteries according to subtypes of BMI.					
Types of AcomA	**BMI**				**Total**
	Low (<18.5)	**Normal (18.5-24.9)**	**Overweight (25-29.9)**	**Obese (>30)**	
Type 1	0	44	19	16	**79**
Type 2	4	8	5	7	**24**
Type 3	0	6	10	7	**23**
Type 4	0	8	3	5	**16**
Type 5	2	3	2	6	**13**
Type 6	0	3	3	1	**7**
Type 7	2	3	0	2	**7**
Type 8	0	1	1	2	**4**
Type 9	0	2	0	2	**4**
Type 10	0	1	1	1	**3**
Type 11	0	2	0	0	**2**
Total	**8**	**81**	**44**	**49**	**182**

BMI: Body mass index

Table 4. Statistical analysis between gender and AcomA type.				
Gender	**Type**	**Age (mean+SD)**	**BMI (mean+SD)**	**p-values (Chi-squared test/ Fisher's exact test)**
Female	Type 1 (n=12)	45.3+12.5	23.8+2.9	Chi-squared test: p=0.045* Fisher's exact test: p=0.038**
	Type 2 (n=8)	50.1+15.2	24.5+3.1	
	Type 3 (n=6)	48.7+14.8	25.2+3.4	
	Type 4 (n=5)	52.3+16.1	26.1+3.8	
	Type 5 (n=4)	47.5+13.9	22.9+2.7	
	Type 6 (n=3)	49.0+14.5	21.6+2.8	
	Type 7 (n=2)	55.0+17.3	27.5+4.1	
	Type 8 (n=1)	58.0	26.8	
	Type 9 (n=2)	60.5+18.2	28.1+4.3	
	Type 10 (n=1)	62.0	29.0	
	Type 11 (n=1)	50.0	24.5	
Male	Type 1 (n=33)	44.2+11.8	24.8+3.0	
	Type 2 (n=12)	46.5+13.4	23.7+2.8	
	Type 3 (n=12)	47.8+14.1	25.0+3.3	
	Type 4 (n=10)	49.5+15.0	26.5+3.9	
	Type5 (n=6)	45.0+12.7	22.7+2.6	
	Type 6 (n=5)	47.0+13.8	21.3+2.7	
	Type 7 (n=5)	53.0+16.5	26.9+3.7	
	Type 8 (n=4)	56.0+17.0	27.0+3.8	
	Type 9 (n=4)	58.0+18.0	28.5+4.2	
	Type 10 (n=3)	60.0+18.5	29.2+4.0	
	Type 11 (n=2)	48.0+12.0	24.6+2.9	

*Chi-square test: A statistically significant difference was found between genders and artery types (p<0.05). **Fisher's exact test: This test was used because the assumptions of the chi-square test were not met. The results are similar.

BMI: Body mass index, SD: Standard deviation

Table 5. Statistical analysis between BMI findings and AcomA types.			
Type	**BMI (mean+SD)**	**P-value (ANOVA/Kruskal-Wallis)**	**Post-hoc analysis**
Type 6	21.45+2.89	0.023	Type 1 vs. Type 2: **p=0.045**
Type 5	22.78+2.56		Type 1 vs. Type 3: **p=0.012**
Type 2	23.89+2.98		Type 2 vs. Type 3: p=0.067
Type 11	24.56+2.78		Type 1 vs. Type 4: **p=0.001**
Type 1	24.56+3.12		Type 3 vs. Type 4: **p=0.034**
Type 3	25.12+3.45		Type 5 vs. Type 6: p=0.089
Type 4	26.34+4.01		Type 6 vs. Type 7: **p=0.021**
Type 8	26.89+3.45		Type 7 vs. Type 8: **p=0.045**
Type 7	27.12+3.78		Type 8 vs. Type 9: **p=0.012**
Type 9	28.34+4.12		Type 9 vs. Type 10: **p=0.034**
Type 10	29.12+3.89		Type 10 vs. Type 11: p=0.067
BMI: Body mass index, SD: Standard deviation, ANOVA: Analysis of variance			

Type 7 (2/8), cases were associated with low BMI. Cases of other AcomA types were not observed (Table 4).

BMI values of cadavers with various AcomA types (Type 1, Type 2, Type 3, ..., Type 11) were compared using ANOVA and Kruskal-Wallis tests. The p-value (0.023) obtained as a result of ANOVA/Kruskal-Wallis tests showed that there was a statistically significant difference among AcomA types corresponding to different BMI categories ($p<0.05$). This mean that cadavers with different AcomA types might have different BMI values. Post-hoc analyses were used to determine which group was significantly different, and it was found that there were significant differences among Type 1 and Type 2, Type 3 vs. Type 4, Type 3 and Type 4, Type 7 and Type 6, Type 7 and Type 8, Type 9 and Type 8, Type 9 and Type 10 AcomA types in terms of BMI values. BMI averages of cadavers with Type 9 and Type 10 AcomA types were higher than those of the other groups. BMI averages of cadavers with Type 5 and Type 6, AcomA types were found to be lower than the other groups (Table 5).

DISCUSSION

In our study, the variations of AcomA were observed in 96/182 fresh cadavers. The remaining 86 cases were included in the category of typical AcomA. these variations (96/182) have been classified in various ways, including the number, course, or shape of AcomA[7]. Each of these had a subtype, and the most common AcomA variation among all the main classifications were those classified according to shape. In the literature, AcomA has been reported to vary between 6.27% and 59.38%[13,14]. This rate was found to be 52.75% in our study on fresh cadavers. To date, studies related to the variations of AcomA have been performed on fresh cadavers, fixed cadavers, magnetic resonance imaging angiography and computed tomography angiography (CTA)[14-18].

In the 182 recently deceased cadavers analyzed in the study, 96 variations related to the AcomA were detected. The most common variation was the X-shaped AcomA (24/96), and the AcomA with single fenestration (23/96), while the rarest variation was AcomA with double fenestration (2/96). The prevalence of fenestration variations reported in the literature is between 0.9% and 2%[2,7,19]. Fenestration-related variations, which were relatively high in our study, play an essential role in aneurysms. The fact this ratio was higher in our study than in the literature may be due to the characteristics of sample used in the study or the effects of post-mortem processes that may cause fenestration structures to become more prominent. In general, fenestrations in arteries are associated with a significant increase in the risk of rupture. They are also linked to aneurysm formation due to developmental problems such as weakness in the tunica layers of the arterial wall[20,21]. When the demographic data of the cadaver samples were analysed, the effect of factors such as gender on the variation types was observed. Kardile et al.[7] reported that AcomA showed variation in 18/48 (37.5%) females and 20/52 (38.46%) males. In our study, variations of AcomA were found in 26/40 females and 70/142 males. This high rate in female cases is thought to be due to factors such as lower reporting or diagnosis rates compared to male cases[7].

The anterior cerebral arteries and the anterior communicating artery are critical components of the Willis polygon and play an important role in maintaining the continuity of cerebral blood circulation. Morphological variations of AcomA may be especially effective in the pathophysiology of cerebrovascular diseases. In our study, structural variations such as hypoplasia, aplasia, and fenestration

were determined. It has been reported in the literature that such variations may affect the incidence of cerebrovascular events and may cause technical difficulties in surgical interventions[1,5,22]. Particularly hypoplastic and aplastic variations may increase the risk of complications during surgical interventions by decreasing the adequacy of collateral circulation[23]. Therefore, detection of these variations in preoperative angiographic evaluations is of great importance for the success of surgical planning.

Advanced imaging modalities, such as 3D reconstruction or maximum intensity projection images, may be useful for the identification of AcomA. Among the possible variants of AcomA, absence, double, fenestrated, and triple AcomA have been reported in the literature. Other rare cases include AcomA X, Y, V, H, or N[19]. There is some controversy in the literature about the frequency of anatomical variants of AcomA. Some authors describe the absence of the AcomA as the most common atypical vascular variant with a prevalence of approximately 14%[24] and 19%[15], while other authors claim that definite absence of the anterior communicating artery is found in 5% of surgical dissections[21]. This disagreement may arise from the fact that among the limitations of some studies was the inability of CTA source images to visualize very small arteries, possibly leading to the misdiagnosis of some hypoplastic arteries as aplastic arteries[15]. For this reason, the findings of studies that are illustrated by the use of dissection become more important.

Study Limitations

Limitations of this study include that the sample group was taken from only from one region and that only fresh cadavers were examined. In future research, similar studies on larger and more diverse populations will increase the generalisability of the findings. Furthermore, increasing the sample size would enable a more robust and statistically significant evaluation of correlation results stratified by BMI or sex. Given the considerable variability in AcomA types and despite the relatively large sample size used in this study, the interpretation of correlation findings between these types remains limited. Distribution of results by subtypes may not yield ethically applicable and generalizable results due to the inherent heterogeneity observed.In addition, prospective studies evaluating the clinical outcomes of these variations will provide more data for surgical and radiological applications.

CONCLUSION

This study has examined and classified the morphological variations of the AcomA on fresh cadavers in a sample from Türkiye. The findings provide important clinical information, especially for cerebrovascular surgery and radiological interventions. Variations such as hypoplasia, aplasia and fenestration identified in the study may affect the haemodynamics of cerebral vessels, alter the adequacy of collateral circulation and predispose to aneurysm formation. Therefore, the detection of these variations in preoperative imaging processes may help to plan surgical and endovascular interventions more safely and effectively. It should be kept in mind that hypoplastic and aplastic variations, especially, may lead to adverse complications due to insufficient blood flow during surgery.

This study contributes to the literature by being performed on fresh cadavers. The data obtained by dissection reveal the anatomical details of the vascular structures more accurately compared to previous studies performed with imaging methods. Moreover, the higher rate of fenestration-related variations in this study compared to the rates reported in the literature, suggests that more research should be conducted on the clinical effects of these variations. These anatomical differences should be taken into consideration in the diagnosis and treatment of cerebrovascular diseases.

Ethics

Ethics Committee Approval: Approval was obtained for this study from the Istanbul Medical Faculty Clinical Research Ethics Committee (date: 04/10/2024, decision no: 19).

Informed Consent: Since our study was performed on autopsied cadavers, "informed consent" was not obtained.

Footnotes

Author Contributions

Surgical and Medical Practices: G.N.C., E.N., Concept: G.N.C., Design: G.N.C., E.N., Data Collection or Processing: G.N.C., K.A., Analysis or Interpretation: G.N.C., E.N., Literature Search: G.N.C., O.C., Writing: G.N.C., A.K., Ö.G.

Conflict of Interest: No conflict of interest was declared by the authors.

Financial Disclosure: The authors declare that this study received no financial support.

REFERENCES

1. Standring S. Gray's Anatomy: The anatomical basis of clinical practice. Standring S. editor. 41st ed. Amsterdam: Elsevier; 2016.
2. Osborn AG. Diagnostic cerebral angiography. 2nd ed. Philadelphia: Lippincott Williams Wilkins; 1999.
3. Nas E, Chatzioglou GN, Şahan O, et al. Anatomical features of posterior cerebral arteries and basilar artery in 170 Anatolian fresh cadavers: İmplications for surgical planning and intervention. World Neurosurg. 2024;184:255-65.
4. Nas E, Nteli Chatzioglou G, Gayretli Ö. Anatomical evaluation of P1 segment of posterior cerebral artery and posterior communicanting artery in 340 human hemispheres: A proposal for morphological classification. Surg Radiol Anat. 2024;46:685-95.
5. Arıncı K, Elhan A. Anatomi. 2nd ed. Ankara: Güneş Tıp Kitabevleri; 2020.
6. Moore KL, Dalley AF. Agur AMR. Clinically oriented anatomy. 8th ed New Delhi: Wolters Kluwer; 2018.
7. Kardile PB, Ughade JM, Pandit SV, et al. Anatomical variations of anterior communicating artery. Anatomical variations of anterior communicating artery. J Clin Diagn Res. 2013;7:2661-4.
8. Chamanhali AA, Rajanna S, Kadaba JS. Comparative anatomy of the circle of Willis in man, cow, sheep, goat and pig. Neuroanatomy. 2008;7:54-65.
9. Yaşargil MG. Microneurosurgery, Volume I: Microsurgical anatomy of the basal cisterns and vessels of the brain, diagnostic studies, general operative techniques and pathological considerations of the intracranial aneurysms. 1st ed. Stuttgart-New York: Thieme Stratton Inc; 1984.
10. Rhoton AL Jr. Rhoton's Cranial Anatomy and Surgical Approaches. 1st ed. New York: LSC Communications, Oxford University Press; 2019.
11. Barut C, Ertilav H. Guidelines for standard photography in gross and clinical anatomy. Anat Sci Educ. 2011;4:348-56.
12. The jamovi Project. jamovi (Version 2.6) [Computer software]. 2024. Available from: https://www.jamovi.org
13. Vare AM, Bansal PC. Arterial pattern at the base of the human brain. J Anat Soc India. 1970;19:71-9.
14. Yokuş A, Toprak N, Gündüz AM, et al. Anterior cerebral artery and anterior communicating artery variations: Assessment with magnetic resonance angiography. World Neurosurg. 2021;155:203-9.
15. Krzyżewski RM, Tomaszewski KA, Kochana M, et al. Anatomical variations of the anterior communicating artery complex: Gender relationship. Surg Radiol Anat. 2015;37:81-6.
16. Gunnal SA, Wabale RN, Farooqui MS. Variations of anterior cerebral artery in human cadavers. Neurol Asia. 2013;18:249-59.
17. Kannabathula AB, Rai G, Sunam H. Anatomical variations of anterior cerebral artery and anterior communicating artery: a cadaveric study. Int J Anat Res. 2017;5:3882-90.
18. Fredon F, Baudouin M, Hardy J, et al. An MRI study of typical anatomical variants of the anterior communicating artery complex. Surg Radiol Anat. 2021;43:1983-8.
19. López-Sala P, Alberdi N, Mendigaña M, Bacaicoa MC, Cabada T. Anatomical variants of anterior communicating artery complex: A study by computerized tomographic angiography. J Clin Neurosci. 2020;80:182-7.
20. Orakdogen M, Emon ST, Somay H, Engin T, Is M, Hakan T. Vascular variations associated with intracranial aneurysms. Turk Neurosurg. 2017;27:853-62.
21. Dimmick SJ, Faulder KC. Normal variants of the cerebral circulation at multidetector CT angiography. Radiographics. 2009;29:1027-43.
22. Krasny A, Nensa F, Saldalcioglu IE, et al. Association of aneurysms and variation of the A1 segment. J Neurointerv Surg. 2014;6:178-83.
23. Abla AA, Wilson DA, Williamson RW, et al. The relationship between ruptured aneurysm location, subarachnoid hemorrhage clot thickness, and incidence of radiographic or symptomatic vasospasm in patients enrolled in a prospective randomized controlled trial. J Neurosurg. 2014;120:391-7.
24. Jiménez Sosa MS, Cantú González JR, Morales Avalos R, et al. Anatomical variants of anterior cerebral arterial circle: A study by multidetector computerized 3D tomographic angiography. Int J Morphol. 2017;35:1121-8.

DOI: 10.4274/MMJ.galenos.2025.73848
Medeni Med J 2025;40:72-79

Original Article

The Role of Combined C-reactive Protein and Albumin Indices in Predicting Prolonged Hospital Stay in Acute Pancreatitis: A Prospective Observational Study

Akut Pankreatitte Uzamış Hastane Yatışını Öngörmede Kombine C-reaktif Protein ve Albümin İndekslerinin Rolü: Prospektif Gözlemsel Bir Çalışma

Abdullah ALGIN[1], Serdar OZDEMIR[1], Mustafa Ahmet AFACAN[2], Kaan YUSUFOGLU[2], Abuzer OZKAN[3]

[1]University of Health Sciences Türkiye, Umraniye Training and Research Hospital, Clinic of Emergency Medicine, Istanbul, Türkiye
[2]University of Health Sciences Türkiye, Haydarpasa Numune Training and Research Hospital, Clinic of Emergency Medicine, Istanbul, Türkiye
[3]University of Health Sciences Türkiye, Taksim Training and Research Hospital, Clinic of Emergency Medicine, Istanbul, Türkiye

ABSTRACT

Objective: To evaluate the predictive ability of indices based on the combination of C-reactive protein (CRP) and albumin, namely the CRP/albumin ratio (CAR), Glasgow prognostic score (GPS), and modified GPS (mGPS), for prolonged hospital stay in patients with acute pancreatitis.

Methods: This prospective observational study was conducted on patients monitored in the emergency department of a tertiary university hospital. The patients' demographic data, vital signs, laboratory parameters, comorbidities, and length of hospital stay were prospectively recorded. Based on their length of hospital stay, the patients were divided into two groups: prolonged stay (>7 days) and non-prolonged stay. The indices were compared between these groups.

Results: There were statistically significant differences in CAR, GPS, and mGPS between the prolonged and non-prolonged hospital stay groups ($p<0.001$ for all; chi-square test). The area under the curve values of CAR, GPS, and mGPS were calculated as 0.677 [95% confidence interval (CI): 0.601-0.753, $p<0.001$], 0.637 (95% CI: 0.570-0.704, $p<0.001$), and 0.671 (95% CI: 0.602-0.740, $p<0.001$), respectively. According to multivariate analysis, CAR [odds ratio (OR)=1.017, 95% CI (1.003-1.03), p=0.015], GPS [OR=2.894, 95% CI (1.632-5.13), $p<0.001$], and mGPS [OR=3.757, 95% CI (2.108-6.70), $p<0.001$] were found to be independent predictors of prolonged hospital stay.

Conclusions: CAR, GPS, and mGPS are independent predictors of prolonged hospital stay in patients with acute pancreatitis. The findings also suggest that incorporating CRP levels into prognostic calculations may yield more accurate results compared to scores based solely on albumin levels.

Keywords: Emergency departments, acute pancreatitis, C-reactive protein, albumin, hospital stay

ÖZ

Amaç: Bu çalışmanın amacı, C-reaktif protein (CRP) ve albüminin kombinasyonuna dayalı indekslerin-CRP/albümin oranı (CAR), Glasgow prognostik skoru (GPS) ve modifiye GPS (mGPS)-akut pankreatitli hastalarda uzamış hastane yatış süresini öngörmedeki etkinliğini değerlendirmektir.

Yöntemler: Bu prospektif gözlemsel çalışma, üçüncü basamak bir üniversite hastanesinin acil servisinde takip edilen hastalar üzerinde gerçekleştirildi. Hastaların demografik verileri, vital bulguları, laboratuvar parametreleri, eşlik eden hastalıkları ve hastanede kalış süreleri prospektif olarak kaydedildi. Yatış sürelerine göre hastalar iki gruba ayrıldı: uzamış yatış (>7 gün) ve kısa yatış. Belirtilen indeksler bu gruplar arasında karşılaştırıldı.

Bulgular: CAR, GPS ve mGPS değerleri, uzamış ve kısa yatış grupları arasında istatistiksel olarak anlamlı farklılık gösterdi (tüm testler için $p<0,001$; ki-kare testi). CAR, GPS ve mGPS için eğri altındaki alan (AUC) sırasıyla 0,677 [%95 güven aralığı (GA): 0,601-0,753], 0,637 (%95 GA: 0,570-0,704) ve 0,671 (%95 GA: 0,602-0,740) olarak bulundu. Çok değişkenli analizde CAR [olasılık oranı (OA)=1.017, %95 GA: 1.003-1,03, p=0,015), GPS (OA=2,894, %95 GA: 1,632-5,13, $p<0,001$) ve mGPS (OA=3,757, %95 GA: 2,108-6,70, $p<0,001$) bağımsız öngörücüler olarak saptandı.

Sonuçlar: CAR, GPS ve mGPS, akut pankreatitli hastalarda uzamış hastane yatışını öngören bağımsız belirteçlerdir. Bulgular ayrıca, yalnızca albümin düzeylerine dayalı skorlara kıyasla CRP düzeylerinin dahil edilmesinin prognostik doğruluğu artırabileceğini göstermektedir.

Anahtar kelimeler: Acil servis, akut pankreatit, C-reaktif protein, albümin, hastane kalış

Address for Correspondence: Algın A, University of Health Sciences Türkiye, Umraniye Training and Research Hospital, Clinic of Emergency Medicine, Istanbul, Türkiye
E-mail: dralgin@hotmail.com **ORCID ID:** orcid.org/0000-0002-9016-9701

Cite as: Algin A, Ozdemir S, Afacan MA, Yusufoglu K, Ozkan A. The role of combined C-reactive protein and albumin indices in predicting prolonged hospital stay in acute pancreatitis: a prospective observational study. Medeni Med J. 2025;40:72-79

Received: 25 April 2025
Accepted: 05 June 2025
Published: 26 June 2025

INTRODUCTION

Acute pancreatitis (AP) is among the most common gastrointestinal emergencies requiring hospitalization worldwide and represents a significant public health concern due to its high morbidity and mortality rates. While mild forms often resolve spontaneously, severe cases can lead to serious complications such as multiple organ failure and necrotizing pancreatitis, necessitating intensive care[1,2]. The severity of AP can prolong hospital stays, increase treatment costs, and cause productivity loss, particularly among individuals of working age. These outcomes have serious implications not only for individual health but also for healthcare systems and economic burden[3-5].

One of the main challenges in managing AP is predicting which patients will develop severe disease during its early stages. Mortality rates can reach up to 20% in severe AP cases and may exceed 50% in those with sepsis and multiple organ failure[2,4,6,7]. Therefore, early identification of high-risk patients through reliable prognostic biomarkers is of critical importance for establishing appropriate treatment strategies and optimizing patient management[8,9]. Various biomarkers have been investigated to predict the course and prognosis of the disease, with the most frequently studied parameters being C-reactive protein (CRP) and albumin[10,11].

CRP is an acute-phase reactant synthesized by hepatocytes that plays a crucial role in systemic inflammatory responses[12-16]. In patients with AP, CRP levels have been shown to correlate with disease severity, and elevated CRP levels have been particularly associated with complications such as necrotizing pancreatitis, infection, and organ failure. CRP is considered a reliable biomarker for assessing disease severity, especially after the first 48 hours. However, it has also been demonstrated that CRP levels alone may have limited prognostic power and may not be sufficient for precise early-stage prediction[17]. Albumin, on the other hand, is a plasma protein reflecting inflammation and nutritional status, and its reduced levels have been associated with poor prognosis in critical illnesses and inflammatory states[18-21]. In patients with AP, hypoalbuminemia has been linked to enhanced inflammatory response, fluid imbalance, and poor clinical outcomes. Low albumin levels have been shown to increase the risk of mortality and complications, particularly in severe AP cases[20,21].

In recent years, growing attention has been given to the prognostic value of combining different biomarkers, leading to the development of new indices by evaluating CRP and albumin together[11,19]. The CRP/albumin ratio (CAR), Glasgow prognostic score (GPS), and modified GPS (mGPS) have been reported as important prognostic indicators in various inflammatory and critical illnesses[22-24]. However, there is still a lack of literature regarding the clinical relevance of these indices in AP.

This study aimed to evaluate the predictive ability of indices based on the combination of CRP and albumin, namely CAR, GPS, and mGPS, for prolonged hospital stay in patients with AP.

MATERIALS and METHODS

Study Population

This prospective observational study was conducted between February 1, 2023, and July 1, 2023, on patients monitored in the Emergency Department of Health Sciences University Türkiye Umraniye Training and Research Hospital Scientific Research Ethics Committee (approval number: B.10.1.TKH.4.34.H.GP.0.01/135, date: 10.04.2025). Patients diagnosed with AP who were hospitalized and aged over 18 years were included in the study. The diagnosis of AP was based on at least two of the following three criteria: (1) characteristic abdominal pain; (2) serum amylase and/or lipase level greater than three times the upper limit of normal; and (3) imaging findings consistent with AP on ultrasound or contrast-enhanced computed tomography. Patients with missing data (albumin or CRP) were excluded. Patients with chronic pancreatitis, active malignancy, or concomitant severe sepsis were also excluded.

The patients' demographic data (age and sex), vital signs (systolic and diastolic blood pressure, heart rate, and oxygen saturation), laboratory parameters (complete blood count, CRP, albumin, liver and renal function tests, electrolyte levels, and blood gas values), comorbidities, intensive care requirements, and length of hospital stay were prospectively recorded. To assess the inflammatory response, CAR, GPS, and mGPS were calculated (Table 1). The patients were divided into two groups based on length of hospital stay: prolonged stay (>7 days) and non-prolonged stay (≤7 days).

In line with previous literature indicating this threshold as clinically meaningful in predicting complication risk and healthcare utilization in AP, ≥7 days was defined as prolonged[5,8]

Statistical Analysis

Statistical analyses were performed using Jamovi software (v. 2.3.21). The normality of distribution for continuous variables was evaluated using the Shapiro-Wilk test. Non-normally distributed data were presented as median and interquartile range (IQR), and comparisons between groups were made using the Mann-Whitney U test. Categorical variables were expressed as frequencies and percentages, and the chi-square test was used for comparisons. To determine the predictive ability of prognostic scores for prolonged hospital stay, receiver operating characteristic analyses were conducted, and the area under the curve (AUC) values were calculated. Differences between AUC values were evaluated using the DeLong test. Logistic regression analysis was performed to identify independent predictors of prolonged hospital stay. Separate models were created for CAR, GPS, mGPS, and CRP to avoid the effect of collinearity. Model fit measures, including deviance, Akaike Information Criterion, and Nagelkerke's R^2, were also reported. A p-value of <0.05 was considered statistically significant.

RESULTS

A total of 152 patients were included in the study. The median age was 58 years, with an IQR of 39 to 74 years. In terms of sex distribution, 61 patients (40%) were female, and 91 patients (60%) were male.

Descriptive data pertaining to the study are presented in Table 2. Based on the duration of hospitalization, the patients were divided into two groups. Of the total 152 patients included in the study, 111 (73%) were classified under the prolonged hospital stay group, while 41 (27%) were categorized under the non-prolonged hospital stay group. The overall median length of hospital stay was 14 days (IQR: 7-23 days) in the whole sample, 19 days (IQR: 13-25 days) in the prolonged stay group, and 4 days (IQR: 3-7 days) in the non-prolonged stay group.

The median diastolic blood pressure was 82 mmHg (IQR: 66-93 mmHg) for all patients in the sample, 78 mmHg (IQR: 64-89 mmHg) in the prolonged stay group, and 85 mmHg (IQR: 74-95 mmHg) in the non-prolonged stay group. This difference between the two groups was statistically significant (p=0.029). The median CRP level was identified as 42 mg/L (IQR: 13-124 mg/L) for all patients. The median CRP level was 61 mg/L (IQR: 22-134 mg/L) in the prolonged stay group and 17 mg/L (IQR: 5-48 mg/L) in the non-prolonged stay group, also indicating a statistically significant difference (p<0.001). CAR, GPS, and mGPS demonstrated statistically significant differences between the two groups (p<0.001 for all; chi-square test). This table presents the comparisons of other parameters between the groups.

The AUC of mGPS in terms of discriminatory performance was measured as 0.671 (95% CI: 0.602-0.740, p<0.001). GPS demonstrated an AUC value of 0.637 (95% CI: 0.570-0.704, p<0.001). CAR exhibited the highest performance among the tested models, with an AUC of 0.677 (95% CI: 0.601-0.753, p<0.001) (Figure 1). Other diagnostic accuracy metrics are shown in Table 3, with the significance of the differences between AUC values given in Table 4.

The multivariate analysis, evaluating whether each parameter, is an independent predictor for prolonged hospital stay, is presented in Table 5.

DISCUSSION

In this prospective study, we evaluated the prognostic value of inflammation-based biomarkers-specifically the CAR, GPS, and mGPS-in predicting prolonged hospital stay among patients diagnosed with AP. Our findings demonstrated that all three parameters were significantly associated with extended hospitalization, with CAR emerging as the most diagnostically accurate tool.

Table 1. Calculation methods for the scoring systems used in the study.

Score	Calculation method	
CRP/albumin ratio	Calculated by dividing the C-reactive protein (mg/L) value by the albumin (g/dL) value.	
Glasgow prognostic score	Calculated based on CRP and albumin levels.	**CRP ≤ 10 mg/L and albumin ≥ 3.5 g/dL → 0 points**
		CRP > 10 mg/L or albumin < 3.5 g/dL → 1 points
		CRP > 10 mg/L and albumin < 3.5 g/dL → 2 points
Modified Glasgow prognostic score	In the mGPS system, a CRP level >10 mg/L receives 1 point even when serum albumin is ≥3.5 g/dL. This reflects the prognostic value of systemic inflammation, independent of the patient's nutritional status.	**CRP ≤ 10 mg/L → 0 points**
		CRP > 10 mg/L and albumin ≥ 3.5 g/dL → 1 points
		CRP > 10 mg/L and albumin < 3.5 g/dL → 2 points

Table 2. Baseline demographic, clinical, laboratory, and prognostic score characteristics of the study groups.				
Characteristic	**Total sample n = 152**	**Non-prolonged hospital stay group n = 41 (27%)**	**Prolonged hospital stay group n = 111 (73%)**	**p-value**
Demographic characteristics				
Age	58 (39-74)	62 (44-74)	58 (36-74)	0.52
Sex				0.36
Female	61 (40%)	14 (34%)	47 (42%)	
Male	91 (60%)	27 (66%)	64 (58%)	
Comorbidities				
Diabetes mellitus	22 (14%)	4 (9.8%)	18 (16%)	0.32
Hypertension	64 (42%)	20 (49%)	44 (40%)	0.31
Coronary artery disease				0.18
Congestive heart failure	5 (3.3%)	3 (7.3%)	2 (1.8%)	0.12
Chronic kidney disease	5 (3.3%)	0 (0%)	5 (4.5%)	0.32
Initial vital parameters				
Systolic blood pressure (mmHg)	131 (122-149)	132 (125-159)	131 (121-147)	0.13
Diastolic blood pressure (mmHg)	**82 (66-93)**	**85 (74-95)**	**78 (64-89)**	**0.029**
Heart rate (beats per minute)	84 (74-96)	87 (78-96)	82 (74-92)	0.26
Oxygen saturation (%)	97 (95-98)	97 (96-99)	97 (94-98)	0.57
Laboratory parameters				
White blood cell count (cells/μL)	13.7 (9.0-15.8)	11.4 (9.0-16.5)	13.7 (9.0-15.8)	0.88
Neutrophil count (cells/μL)	11.2 (6.4-13.8)	9.0 (6.3-14.1)	11.2 (6.4-12.8)	0.89
Lymphocyte count (cells/μL)	1.52 (1.15-2.04)	1.39 (1.09-1.57)	1.53 (1.15-2.14)	0.14
Platelet count (cells/μL)	270 (222-350)	257 (239-350)	270 (221-350)	0.83
Eosinophil count (cells/μL)	0.10 (0.03-0.17)	0.10 (0.01-0.24)	0.10 (0.04-0.17)	0.95
Monocyte count (cells/μL)	0.68 (0.48-0.86)	0.67 (0.49-0.87)	0.68 (0.48-0.86)	0.89
Hemoglobin (g/dL)	14.00 (11.90-15.20)	13.20 (11.90-15.20)	14.10 (11.90-15.20)	0.62
Red cell distribution width (%)	13.85 (12.90-14.90)	13.90 (13.50-14.50)	13.80 (12.90-14.95)	0.48
Aspartate aminotransferase (U/L)	93 (29-156)	72 (26-116)	106 (29-192)	0.16
Alanine aminotransferase (U/L)	71 (32-184)	48 (32-139)	74 (32-196)	0.17
Albumin (g/dL)	4.05 (3.74-4.41)	4.00 (3.90-4.39)	4.05 (3.64-4.41)	0.59
Total bilirubin (mg/dL)	1.22 (0.54-2.01)	1.27 (0.54-2.10)	1.20 (0.54-1.90)	0.99
Direct bilirubin (mg/dL)	0.44 (0.20-1.00)	0.56 (0.30-1.00)	0.43 (0.20-1.00)	0.24
Amylase (U/L)	408 (222-1,054)	338 (212-610)	451 (244-1,111)	0.20
Lipase (U/L)	1,138 (518-1,811)	1,057 (406-1,265)	1,219 (750-2,074)	0.051
Lactate dehydrogenase (U/L)	306 (228-376)	284 (228-315)	313 (240-379)	0.11
Blood urea nitrogen (mg/dL)	32 (26-40)	32 (29-38)	32 (25-41)	0.91
Creatinine (mg/dL)	0.90 (0.76-1.10)	0.89 (0.79-1.02)	0.90 (0.75-1.10)	0.89
Sodium (mEq/L)	135.6 (133.1-139.0)	135.3 (133.0-139.2)	136.0 (133.3-139.0)	0.82
Potassium (mEq/L)	4.21 (4.01-4.60)	4.15 (3.92-4.45)	4.27 (4.03-4.62)	0.065
Calcium (mg/dL)	8.75 (8.50-9.14)	8.70 (8.50-9.10)	8.80 (8.50-9.14)	0.67
Glucose (mg/dL)	118 (95-157)	119 (95-173)	115 (99-150)	0.89
C-reactive protein (mg/L)	**42 (13-124)**	**17 (5-48)**	**61 (22-134)**	**<0.001**
pH	7.40 (7.36-7.43)	7.41 (7.39-7.43)	7.39 (7.34-7.42)	0.14

Table 2. Continued				
Characteristic	**Total sample n = 152**	**Non-prolonged hospital stay group n = 41 (27%)**	**Prolonged hospital stay group n = 111 (73%)**	**p-value**
Partial pressure of carbon dioxide (mmHg)	40 (36-44)	40 (36-44)	40 (37-44)	0.33
Bicarbonate (mEq/L)	23.05 (21.80-25.30)	23.50 (22.10-24.50)	22.80 (21.60-25.40)	0.54
Base excess (mEq/L)	-0.3 (-3.0-1.1)	-0.2 (-1.7-1.1)	-1.2 (-3.0-1.1)	0.42
Lactate (mmol/L)	1.69 (1.35-2.35)	1.84 (1.38-2.39)	1.68 (1.31-2.33)	0.61
C-reactive protein/albumin ratio	**11 (3-29)**	**4 (1-11)**	**13 (5-33)**	**<0.001**
Modified Glasgow prognostic score				**<0.001**
0	32 (21%)	20 (49%)	12 (11%)	
1	91 (60%)	17 (41%)	74 (67%)	
2	29 (19%)	4 (9.8%)	25 (23%)	
Glasgow prognostic score				**<0.001**
0	28 (18%)	16 (39%)	12 (11%)	
1	95 (62%)	21 (51%)	74 (67%)	
2	29 (19%)	4 (9.8%)	25 (23%)	
Outcome measures				
Intensive care unit admission	17 (11%)	5 (12%)	12 (11%)	0.78
Length of hospital stay	**14 (7-23)**	**4 (3-7)**	**19 (13-25)**	**<0.001**

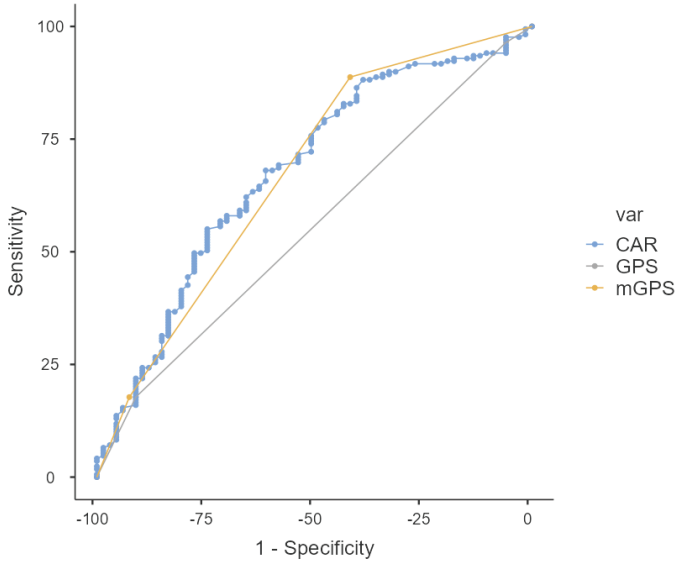

Figure 1. Receiver operating characteristic (ROC) curves of the C-reactive protein/albumin ratio, Glasgow Prognostic Score, and Glasgow prognostic score for predicting prolonged hospital stay.

ROC Curve: Combined

AP is a condition with a highly variable clinical trajectory. While most cases are self-limiting, a subset of patients progresses to severe disease requiring prolonged hospitalization and intensive support. Early risk stratification remains a cornerstone for guiding appropriate clinical management and resource allocation[1-5]. In this regard, systemic inflammation plays a pivotal role in disease progression and complications. Scoring systems such as GPS and mGPS, which integrate inflammatory markers, have previously been applied in oncology and infectious diseases[23-25]. Our results support their broader applicability in inflammatory diseases such as AP.

Among the evaluated scores, CAR demonstrated the strongest association with prolonged length of stay and remained an independent predictor in multivariate logistic regression analysis [odds ratio (OR): 1.017, p=0.015]. This underscores the additive prognostic value of combining CRP, a marker of acute phase response, with albumin, a marker of nutritional and inflammatory status[12,19]. Importantly, CAR offers a simple, cost-effective, and rapidly accessible tool for early risk evaluation, especially valuable features in settings with limited resources or delayed access to imaging.

When comparing GPS and mGPS, our study found that mGPS had significantly superior diagnostic performance, as supported by the DeLong test (p<0.001). This finding suggests that including CRP levels in risk stratification provides enhanced prognostic accuracy compared to albumin-only models. These observations are in line with prior research. For example, Wang et al.[26] demonstrated that GPS predicted 28-day mortality in severe AP patients, in the ICU, and Bardakçı et al.[27] reported that

Table 3. Diagnostic test performance of the parameters for prolonged hospital stay.				
	C-reactive protein/ albumin ratio	**C-reactive protein/ albumin ratio**	**Glasgow prognostic score**	**Modified Glasgow prognostic score**
Area under the curve	0.677	0.677	0.637	0.671
Cut-off	≥2.7	≥11.8*	≥1*	≥1*
Sensitivity	88.2%	55.0%	99.4%	88.8%
Specificity	37.3%	74.6%	1.5%	41.8%
Accuracy	73.7%	60.6%	71.6%	75.4%
Prevalence	71.6%	71.6%	71.6%	71.6%
Positive predictive value	78.0%	84.5%	71.8%	79.4%
Negative predictive value	55.6%	39.7%	50.0%	59.6%
Post-test disease probability	78.0%	84.5%	71.8%	79.4%
Post-test health probability	55.6%	39.7%	50.0%	59.6%
Positive likelihood ratio	1.41	2.17	1.01	1.52
Negative likelihood ratio	0.317	0.603	0.396	0.269
*Optimal cut-off value based on Youden's index				

Table 4. DeLong test for differences between the AUC values of the scoring systems.					
	AUC difference	**Confidence interval (lower)**	**Confidence interval (upper)**	**Correlation**	**p-value**
Modified Glasgow prognostic score vs. Glasgow prognostic score	0.127	0.070	0.185	0.561	**<0.001**
Modified Glasgow prognostic score vs. C-reactive protein to albumin ratio	-0.006	-0.062	0.051	0.707	0.843
Glasgow prognostic score vs. C-reactive protein/albumin ratio	-0.133	-0.205	-0.061	0.406	**<0.001**
AUC: Area under the curve					

mGPS outperformed traditional scores such as Ranson and APACHE II in identifying severe cases[25]. Our study extends these findings by focusing on length of hospital stay as a functional outcome, which is closely tied to disease severity and resource burden.

CAR has also been studied in AP mortality prediction. Kaplan et al.[28] found that CAR values >16.28 were associated with a 19-fold increase in mortality risk, while Zhao et al.[29] reported its association with organ failure and necrosis. In alignment with those studies, our results suggest that CAR is also a reliable predictor of disease severity as reflected by hospitalization length.

From a clinical perspective, inflammation-based biomarkers like CAR, GPS, and mGPS provide practical, low-cost alternatives to complex scoring systems such as APACHE II or Ranson. They allow early triage and may facilitate timely decision-making, especially in high-volume emergency departments or low-resource healthcare environments.

Study Limitations

This study has several limitations. First, it was conducted at a single center, which may restrict the generalizability of the findings. Second, long-term outcomes such as readmission, recurrence, or late complications were not assessed. Third, although laboratory markers were evaluated, integration with radiological and detailed clinical scoring systems (e.g., CTSI) was not performed. Future multicenter studies incorporating longitudinal outcomes and multimodal prognostic approaches are needed to validate and expand upon these results.

CONCLUSION

In conclusion, this study demonstrated that CAR, GPS, and mGPS are independent predictors of prolonged hospital stay in patients with AP. Among them, CAR showed the highest diagnostic performance. The inclusion of CRP in inflammation-based prognostic scores appears to enhance predictive accuracy, supporting the use of mGPS over GPS in this clinical context. Given

Table 5. Multivariate analysis evaluating whether each parameter is an independent predictor of prolonged hospital stay.

Model fit measures			Multivariate analysis							
			Predictor	**Estimate**	**SE**	**Z**	**p-value**	**Odds ratio**	**95% CI (lower)**	**95% CI (upper)**
Model 1	Deviance	264	Intercept	15.895	0.83272	1.91	0.056	4.901	0.958	25.07
	Akaike information criterion	270	Diastolic blood pressure (mmHg)	-0.0132	0.00973	-1.35	0.176	0.987	0.968	1.01
	Nagelkerke's R^2	0.0799	**C-reactive protein/ albumin ratio**	0.0171	0.00698	2.44	**0.015**	1.017	1.003	1.03
Model 2	Deviance	257	Intercept	12.037	0.86482	1.39	0.164	3.333	0.612	18.15
	Akaike information criterion	263	Diastolic blood pressure (mmHg)	-0.0162	0.00983	-1.64	0.100	0.984	0.965	1.00
	Nagelkerke's R^2	0.118	**Glasgow prognostic score**	10.627	0.29242	3.63	**<0.001**	2.894	1.632	5.13
Model 3	Deviance	249	Intercept	0.9906	0.8699	1.14	0.255	2.693	0.489	14.81
	Akaike information criterion	255	Diastolic blood pressure (mmHg)	-0.0157	0.0100	-1.56	0.118	0.984	0.965	1.00
	Nagelkerke's R^2	0.166	**Modified Glasgow prognostic score**	13.237	0.2948	4.49	**<0.001**	3.757	2.108	6.70
Model 4	Deviance	263	Intercept	156.449	0.82812	1.89	0.059	4.780	0.943	24.23
	Akaike information criterion	269	Diastolic blood pressure (mmHg)	-0.01335	0.00966	-1.38	0.167	0.987	0.968	1.01
	Nagelkerke's R^2	0.0849	**C-reactive protein**	0.00506	0.00195	2.59	**0.010**	1.005	1.001	1.01

SE: Standard error, CI: Confidence interval

their simplicity and accessibility, these biomarkers may aid in early risk stratification and decision-making. Nevertheless, further validation through multicenter, prospective studies is warranted before these scores can be routinely adopted into clinical algorithms.

Ethics

Ethics Committee Approval: Approval for this study was received from the Scientific Research Ethics Committee of the Health Sciences University Türkiye Ümraniye Training and Research Hospital (approval number: B.10.1.TKH.4.34.H.GP.0.01/135, date: 10.04.2025).

Informed Consent: Since this study is a prospective observational study, patient consent is not required.

Footnotes

Author Contributions

Concept: A.A., M.A.A., A.O., Design: A.A., M.A.A., A.O., Data Collection and/or Processing: A.A., S.O., Analysis and/or Interpretation: A.A., S.O., K.Y., A.O., Literature Search: A.A., K.Y., Writing: A.A., S.O.

Conflict of Interest: The authors have no conflict of interest to declare.

Financial Disclosure: The authors declared that this study has received no financial support.

REFERENCES

1. Zerem E, Kurtcehajic A, Kunosić S, Zerem Malkočević D, Zerem O. Current trends in acute pancreatitis: diagnostic and therapeutic challenges. World J Gastroenterol. 2023;29:2747-63.
2. Akoglu EU, Özdemir S, Ak R, Ozturk TC. The discriminative power of inflammatory markers in patients with mild-to-moderate acute pancreatitis: mean platelet volume, neutrophil-lymphocyte ratio, lymphocyte-monocyte ratio, and neutrophil-monocyte product. South Clin Ist Euras. 2021;322:159-64.
3. Li CL, Jiang M, Pan CQ, Li J, Xu LG. The global, regional, and national burden of acute pancreatitis in 204 countries and territories, 1990-2019. BMC Gastroenterol. 2021;21:332.
4. İslam MM, Osoydan Satıcı M, Ademoğlu E, et al. The role of delta neutrophil index in early identification of severe acute

pancreatitis in adult patients: a prospective diagnostic accuracy study. Med Sci Discov. 2023;10:487-94.

5. Özdemir S, Altunok İ, Algın A. Relationship of the systemic immuno-inflammation index and hematological inflammatory index with mortality and hospitalization in acute pancreatitis: a cross-sectional study. Frontiers in Emergency Medicine. 2023;7:e13.
6. Aggarwal A, Manrai M, Kochhar R. Fluid resuscitation in acute pancreatitis. World J Gastroenterol. 2014;20:18092-103.
7. Prajapati R, Manay P, Sugumar K, Rahandale V, Satoskar R. Acute pancreatitis: predictors of mortality, pancreatic necrosis and intervention. Turk J Surg. 2021;37:13-21.
8. Altunok İ, Özdemir S. Relationship between platelet indices and prolonged hospitalization in patients with acute pancreatitis: a retrospective observational study. J Contemp Med. 2022;12:743-8.
9. Özkan A, Duman C, Özdemir S. The role of hemoglobin, albumin, lymphocyte, platelet (HALP) score in acute pancreatitis - an analytical study. SABD. 2024;14:33-8.
10. Çalım A, Ersoy Ç. Can CRP/Albumin Ratio, A Non-invasive Test, Predict the Severity of Acute Pancreatitis?. Bagcilar Med Bull. 2025: doi:10.4274/BMB.galenos.2025.55265.
11. Karabuga B, Gemcioglu E, Konca Karabuga E, Baser S, Ersoy O. Comparison of the predictive values of CRP, CRP/albumin, RDW, neutrophil/lymphocyte, and platelet/lymphocyte levels in determining the severity of acute pancreatitis in patients with acute pancreatitis according to the BISAP score. Bratisl Lek Listy. 2022;123:129-35.
12. Özdemir S, Algin A. Evaluation of the ability of the C- reactive protein-to-albumin ratio to predict short-term mortality in patients with COVID-19. J Clin Med Kaz. 2021;18: 35-9.
13. Black S, Kushner I, Samols D. C-reactive Protein. J Biol Chem. 2004;279:48487-90.
14. Ozdemir S, Akca HŞ, Algin A, Eroğlu SE. Can C- reactive protein-to-albumin ratio be a predictor of short-term mortality in community-acquired pneumonia? Ann Clin Anal Med. 2021;12:1043-8.
15. Moutachakkir M, Lamrani Hanchi A, Baraou A, Boukhira A, Chellak S. Immunoanalytical characteristics of C-reactive protein and high sensitivity C-reactive protein. Ann Biol Clin (Paris). 2017;75:225-9.
16. Özdemir S. Inflammation: Complexity and significance of cellular and molecular responses. Journal of Acute Disease. 2024;13:3-7.
17. Ozdemir S. Emergency Department Applications of Inflammatory Markers: A Narrative Review. Ibnosina Journal of Medicine and Biomedical Sciences 2024;16:135-41.
18. Özkan A, Akça HŞ. The role of combined hematological inflammatory indices in predicting poor outcomes in patients with acute pancreatitis. J Contemp Med. 2022;12:832-8.
19. Li S, Zhang Y, Li M, Xie C, Wu H. Serum albumin, a good indicator of persistent organ failure in acute pancreatitis. BMC Gastroenterol. 2017;17:59. Erratum in: BMC Gastroenterol. 2017;17:86.
20. Özdemir S, Altunok İ. Comparison of the predictive ability of the blood urea nitrogen/albumin, C-reactive protein/albumin, and lactate/albumin ratios for short-term mortality in SARS-CoV-2-infected patients. Avicenna J Med. 2023;13:43-8. Erratum in: BMC Gastroenterol. 2017;17:86.
21. Amri F, Rahaoui M, Aissaoui H, et al. Is serum albumin a pivotal biomarker in anticipating acute pancreatitis outcomes? BMC Gastroenterol. 2024;24:234.
22. Ozkan A, Ozsivri K, Algin A, Ozdemir S. Can the blood urea nitrogen to serum albumin ratio predict a prolonged hospital stay in patients with acute cholecystitis? Ann Med Res. 2023;30:914-9.
23. Ozturk E, Elibol T, Kilicaslan E, Kabayuka B, Erdogan Ozunal I. Prognostic nutritional index predicts early mortality in diffuse large B-cell lymphoma. Medeni Med J. 2022;37:85-91.
24. Algin A, Ozkan A, Yusufoglu K, Ozdemir S, Afacan MA. The role of C-reactive protein and albumin combined ındexes in predicting the need for ıntubation in acute heart failure: A prospective observational study. North Clin Istanb. 2025: https://northclinist.com/jvi.aspx?un=NCI-76032&volume=#
25. Komolafe O, Pereira SP, Davidson BR, Gurusamy KS. Serum C-reactive protein, procalcitonin, and lactate dehydrogenase for the diagnosis of pancreatic necrosis. Cochrane Database Syst Rev. 2017;4:CD012645.
26. Wang R, Ji P, Zhang Z, He M. Predictive value of Glasgow prognostic score in patients with severe acute pancreatitis. Asian J Surg. 2021;44:1427-8.
27. Bardakçı O, Akdur G, Das M, Sıddıkoğlu D, Akdur O, Beyazit Y. Comparison of different risk stratification systems for prediction of acute pancreatitis severity in patients referred to the emergency department of a tertiary care hospital. Ulus Travma Acil Cerrahi Derg. 2022;28:967-73.
28. Kaplan M, Ates I, Akpinar MY, et al. Predictive value of C-reactive protein/albumin ratio in acute pancreatitis. Hepatobiliary Pancreat Dis Int. 2017;16:424-30.
29. Zhao Y, Xia W, Lu Y, Chen W, Zhao Y, Zhuang Y. Predictive value of the C-reactive protein/albumin ratio in severity and prognosis of acute pancreatitis. Front Surg. 2023;9:1026604.

DOI: 10.4274/MMJ.galenos.2025.72273
Medeni Med J 2025;40:80-92

Original Article

Large-Scale Meta-Analysis of TNF-α rs1800629 Polymorphism in Schizophrenia: Evidence from 7,624 Cases and 8,933 Controls

Şizofrenide TNF-α rs1800629 Polimorfizminin Geniş Ölçekli Meta-Analizi: 7.624 Olgu ve 8.933 Kontrolden Elde Edilen Kanıtlar

Ghasem DASTJERDI[1], Bita FALLAHPOUR[2], Seyed Alireza DASTGHEIB[3], Amirhossein SHAHBAZI[4], Ahmadreza Golshan TAFTI[5], Mohammad BAHRAMI[6], Ali MASOUDI[7], Amirmasoud SHIRI[6], Fatemeh NEMATZADEH[8], Hossein NEAMATZADEH[7]

[1]Shahid Sadoughi Hospital, Shahid Sadoughi University of Medical Sciences, Department of Psychiatry, Yazd, Iran
[2]Razi Hospital, University of Social Welfare and Rehabilitation Sciences, Department of Psychiatry, Tehran, Iran
[3]Shiraz University of Medical Sciences, Department of Medical Genetics, School of Medicine, Shiraz, Iran
[4]Ilam University of Medical Sciences, Student Research Committee, School of Medicine, Ilam, Iran
[5]Shahid Beheshti University of Medical Sciences, Student Research Committee, School of Medicine, Tehran, Iran
[6]Shiraz University of Medical Sciences, Student Research Committee, School of Medicine, Shiraz, Iran
[7]Shahid Sadoughi University of Medical Sciences, Mother and Newborn Health Research Center, Yazd, Iran
[8]Islamic Azad University, Shabestar Branch, Department of Education, Shabestar, Iran

ABSTRACT

Objective: Schizophrenia is a multifaceted psychiatric disorder that affects about 1% of the world's population and arises from a combination of genetic, environmental, and neurodevelopmental influences. Recent studies highlight the role of immune system disturbances and neuroinflammation in its development, with tumor necrosis factor-alpha (TNF-α) identified as a pivotal cytokine. This meta-analysis aims to clarify the relationship between the TNF-α rs1800629 genetic variant and the risk of schizophrenia by synthesizing data from published research.

Methods: Two independent reviewers systematically searched PubMed, Web of Science, Embase, Cochrane Library, and Chinese National Knowledge Infrastructure for studies published up to January 19, 2024. Odds ratios and 95% confidence intervals were computed using a fixed-effects model, taking into account the absence of significant heterogeneity.

Results: A total of 33 case-control studies were included, encompassing 7,624 individuals with schizophrenia and 8,933 healthy controls from diverse backgrounds (21 studies on Asian populations, 11 on Caucasian, and one on a mixed group) conducted between 2001 and 2020. The pooled analysis did not reveal a significant link between the TNF-α rs1800629 polymorphism and susceptibility to schizophrenia under any genetic model. Further subgroup analyses by ethnicity (Asian, Caucasian), country (China, Poland), genotyping technique, and publication year also yielded no notable associations.

Conclusions: This comprehensive meta-analysis offers strong evidence that the TNF-α rs1800629 variant is not significantly associated with

ÖZ

Amaç: Şizofreni, dünya nüfusunun yaklaşık %1'ini etkileyen ve genetik, çevresel ve nörogelişimsel etkilerin bir kombinasyonundan kaynaklanan çok yönlü bir psikiyatrik bozukluktur. Son çalışmalar, bağışıklık sistemi bozukluklarının ve nöroinflamasyonun gelişimindeki rolünü vurgulamakta ve tümör nekroz faktörü-alfa (TNF-α) önemli bir sitokin olarak tanımlanmaktadır. Bu meta-analiz, yayınlanmış araştırmalardan elde edilen verileri sentezleyerek TNF-α rs1800629 genetik varyantı ile şizofreni riski arasındaki ilişkiyi netleştirmeyi amaçlamaktadır.

Yöntemler: İki bağımsız hakem PubMed, Web of Science, Embase, Cochrane Library ve Çin Ulusal Bilgi Altyapısı'nda 19 Ocak 2024 tarihine kadar yayınlanmış çalışmaları sistematik olarak taramıştır. Odds oranları ve %95 güven aralıkları, anlamlı derecedeki heterojenlik eksikliği dikkate alınarak sabit etkiler modeli kullanılarak hesaplanmıştır.

Bulgular: 2001-2020 yılları arasında yürütülen ve farklı geçmişlere sahip 7.624 şizofreni hastasını ve 8.933 sağlıklı kontrolü (21'i Asyalı, 11'i Kafkasyalı ve biri karma bir grup ile) kapsayan toplam 33 olgu kontrol çalışması çalışmaya dahil edildi. Karma analiz, TNF-α rs1800629 polimorfizmi ile şizofreniye yatkınlık arasında herhangi bir genetik model altında anlamlı bir bağlantı ortaya koymadı. Etnik köken (Asyalı, Kafkasyalı), ülke (Çin, Polonya), genotipleme tekniği ve yayın yılına göre yapılan diğer alt grup analizleri de anlamlı bir ilişki göstermedi.

Sonuçlar: Bu kapsamlı meta-analiz, TNF-α rs1800629 varyantının ne küresel olarak ne de belirli etnik gruplar içinde şizofreni riski ile

Address for Correspondence: Fallahpour B, MD, Razi Hospital, University of Social Welfare and Rehabilitation Sciences, Department of Psychiatry, Tehran, Iran
E-mail: hn6485@gmail.com **ORCID ID:** orcid.org/0009-0001-7811-0256

Received: 03 May 2025
Accepted: 10 June 2025
Published: 26 June 2025

Cite as: Dastjerdi G, Fallahpour B, Dastgheib SA et al. Large-scale meta-analysis of TNF-α rs1800629 polymorphism in schizophrenia: evidence from 7,624 cases and 8,933 controls. Medeni Med J. 2025;40:80-92

schizophrenia risk, either globally or within specific ethnic groups. These findings indicate that this polymorphism likely does not play a major role in schizophrenia susceptibility, underscoring the importance of future investigations into other TNF-α variants, gene-gene interactions, or alternative inflammatory mechanisms.

Keywords: Schizophrenia, tumor necrosis factor-alpha, rs1800629, polymorphism, meta-analysis, genetics

anlamlı bir ilişkisi olduğuna dair güçlü kanıtlar sunmaktadır. Bu bulgular, bu polimorfizmin şizofreniye yatkınlıkta muhtemelen önemli bir rol oynamadığını göstermekte ve diğer TNF-α varyantları, gen-gen etkileşimleri veya alternatif enflamatuvar mekanizmalarla ilgili gelecekteki araştırmaların önemini vurgulamaktadır.

Anahtar kelimeler: Şizofreni, tümör nekroz faktörü-alfa, rs1800629, polimorfizm, meta-analiz, genetik

INTRODUCTION

Schizophrenia is a chronic and multifaceted psychiatric illness that affects about 1% of people worldwide. It is marked by a combination of positive symptoms (such as hallucinations and delusions), negative symptoms (including social withdrawal and anhedonia), and cognitive deficits, all of which substantially diminish patients' quality of life and daily functioning[1,2]. The underlying causes of schizophrenia are complex, involving genetic predispositions, environmental exposures, and neurodevelopmental disturbances. Recent research increasingly points to the role of immune system dysfunction and neuroinflammatory processes in the development and progression of the disorder[3,4]. Among the inflammatory molecules implicated in schizophrenia, tumor necrosis factor-alpha (TNF-α) stands out as a key cytokine. Elevated TNF-α levels have been repeatedly documented in individuals with chronic schizophrenia and have been linked to greater severity of negative symptoms[5,6].

TNF-α acts as a pro-inflammatory cytokine, playing a pivotal role in immune regulation and, more recently, has been recognized for its influence on brain development, synaptic remodeling, and neuron survival[7,8]. Evidence suggests that both TNF-α and interleukin-6 are closely associated with the deficit syndrome subtype of schizophrenia, which is characterized by persistent and primary negative symptoms. This observation supports the idea that deficit schizophrenia may involve distinct immune-related pathophysiology[9]. Moreover, higher TNF-α concentrations have been shown to predict the intensity of specific negative symptoms, such as blunted affect and alogia, as well as overall negative symptom scores, indicating a direct contribution of inflammatory processes to clinical manifestations[10,11]. The hypothesis that inflammation plays a central role in schizophrenia is further reinforced by findings that immune-targeted therapies could offer new avenues for treating negative symptoms in individuals with this condition[12].

The TNF-α gene, situated on chromosome 6p21.3, harbors several functional variants that modulate cytokine expression and immune response mechanisms[13,14]. One notable variant is the rs1800629 single nucleotide polymorphism (SNP), also known as -308G>A, located in the gene's promoter region. This SNP has been widely investigated across various inflammatory and autoimmune diseases due to its regulatory effect on TNF-α production. Specifically, the substitution of guanine (G) with adenine (A) at position -308 is associated with increased TNF-α expression in individuals carrying the A allele compared to those with the G allele[15]. Research indicates that carriers of the A allele exhibit significantly reduced fractional anisotropy in broad brain regions, alongside more pronounced deficits in both immediate and delayed verbal memory recall and recognition, relative to individuals with the GG genotype[16]. These observations imply that the A allele, which drives higher TNF-α levels, may be linked to diminished fronto-temporal white matter connectivity and subsequent memory impairments in patients with schizophrenia[16,17].

Previous case-control studies investigating the association between TNF-α rs1800629 polymorphism and schizophrenia susceptibility have yielded inconsistent and sometimes contradictory results, likely due to differences in study populations, sample sizes, ethnic backgrounds, and methodological approaches[6]. While some studies have reported significant associations between specific genotypes and schizophrenia risk, others have found no significant relationship between the polymorphism and disease susceptibility[18]. Additionally, research has indicated that this polymorphism may act as a modulator for disease onset age and cognitive function rather than directly influencing susceptibility, as demonstrated in studies examining the related rs1800629 polymorphism, which showed associations with earlier onset age and cognitive deficits but not with overall disease risk[19]. The heterogeneity in study findings underscores the need for a comprehensive meta-analytical approach to synthesize existing evidence and provide more definitive conclusions about the role of rs1800629 in schizophrenia susceptibility.

Understanding genetic variants in inflammatory pathways has significant clinical and therapeutic implications. Given the influence of TNF-α

polymorphisms on treatment responses in conditions like autoimmune disorders[20], determining if the rs1800629 polymorphism is associated with schizophrenia could inform personalized medicine, guide treatment selection, and aid in developing targeted immunomodulatory interventions. This meta-analysis systematically evaluates case-control studies to determine if the TNF-α rs1800629 polymorphism is associated with increased schizophrenia susceptibility. It also assesses the magnitude of associations across populations and study designs, identifies sources of heterogeneity explaining inconsistencies in prior research, and provides recommendations for future genetic association studies in schizophrenia research.

MATERIALS and METHODS

Search Strategy

Since this meta-analysis did not involve the use of personal data or the recruitment of participants, ethical approval was unnecessary, and patient consent was not applicable. We performed an extensive literature search across a variety of electronic databases to identify publications examining the association between the TNF-α rs1800629 polymorphism and schizophrenia risk, with studies limited to those considered up to January 19, 2024. The databases searched included PubMed, EMBASE, Web of Science, Elsevier, Google Scholar, ScienceDirect, SciELO, Europe PMC, ResearchGate, Circumpolar Health Bibliographic Database, Cochrane Library, Current Contents, Linguamatics, Eye Health Organizations Database, WanFang, China Science and Technology Journal Database, VIP, Chinese Biomedical Database, Chinese National Knowledge Infrastructure, Scientific Information Database, PsycINFO, and ClinicalTrials.gov. To refine our search, we used combinations of keywords such as "schizophrenia", "TNF-α", "rs1800629", "polymorphism", "genetic susceptibility" and "association study", as well as related terms including "gene", "polymorphism", "DNA sequence", "single-nucleotide polymorphism", "SNPs", "genotype", "frequency", "mutation", "mutant", "allele", "variation", "variant" and "genetic predisposition". Additionally, we manually reviewed the reference lists of all relevant articles to ensure no pertinent studies were missed. There was no limitation regarding language or publication year; non-English articles were translated when necessary. Our review prioritized human studies published in English or Chinese, and in cases where multiple articles covered the same subjects, the most recent or those with larger sample sizes were selected.

Inclusion and Exclusion Criteria

We established clear criteria for study selection. The inclusion criteria were: (1) Only case-control or cohort studies that investigated the relationship between the TNF-α rs1800629 polymorphism and schizophrenia risk; (2) schizophrenia diagnosis had to be based on recognized clinical standards; (3) studies needed to provide genotype frequencies for both cases and controls to enable calculation of odds ratios (ORs) and 95% confidence intervals (CIs); (4) studies had to provide sufficient demographic information about participants; and (5) only studies published up to January 2024 were considered for relevance. Exclusion criteria were as follows: (1) Reviews, meta-analyses, abstracts, conference proceedings, case reports, letters to the editor, comments, and duplicate publications; (2) studies without a control group or with inappropriate selection criteria; (3) articles with duplicated data from the same author; (4) studies lacking gene frequency data that could not be supplemented; and (5) animal or *in vitro* research. If multiple publications reported on the same dataset, the study with the largest sample size or the most recent publication was included in the analysis.

Data Extraction

Two independent reviewers assessed the titles, abstracts, and search terms of identified studies to determine eligibility based on the established criteria regarding the TNF-α rs1800629 polymorphism and schizophrenia risk. Any disagreements were resolved through discussion or by consulting a third reviewer, and if needed, the original study authors were contacted for clarification. The screening process began with the evaluation of titles and abstracts to exclude irrelevant studies, followed by a detailed full-text review for final selection. From each eligible study, we extracted the following data: First author's name, participant ethnicity (categorized as Asian, Caucasian, African, Hispanic, or Mixed), publication year, genotyping method, country of study, total number of schizophrenia cases and controls, genotype frequencies of the TNF-α rs1800629 polymorphism in both groups, Hardy-Weinberg equilibrium (HWE) results, and minor allele frequencies (MAFs) among controls. When research groups published multiple related studies, we included the most recent, or the one with the largest sample size.

Statistical Analysis

To evaluate the association between the TNF-α rs1800629 polymorphism and the risk of developing schizophrenia, ORs with corresponding 95% CIs were

calculated. The statistical significance of the overall effect size was determined using the Z-test, with a p-value below 0.05 considered significant. Five genetic models were analyzed: allele comparison (B vs. A), homozygote comparison (BB vs. AA), heterozygote comparison (BA vs. AA), dominant model (BB+BA vs. AA), and recessive model (BB vs. BA+AA). Here, "A" represented the major allele, while "B" denoted the minor allele. To assess heterogeneity among studies, the Cochran Q-test was applied, with a significance threshold set at p≤0.10. The I^2 statistic was also used to quantify heterogeneity, with values ranging from 0% (no heterogeneity) to 100% (extreme heterogeneity): 0-25% indicated none, 25-50%, moderate, 50-75%, high, and 75-100%, very high heterogeneity[22,23]. Depending on the degree of heterogeneity, either the DerSimonian and Laird random-effects model or the Mantel-Haenszel fixed-effects model was used for pooling effect sizes. HWE in the control groups was checked using the chi-square test, and a p-value less than 0.05 indicated a significant deviation from equilibrium[24,25]. Subgroup analyses were performed based on ethnicity and schizophrenia subtype to explore sources of heterogeneity. Sensitivity analyses were conducted by sequentially removing individual studies to test the robustness of the results[26,27]. Potential publication bias was assessed through Begg's and Egger's tests, along with visual inspection of funnel plots for asymmetry. If bias was detected, the Duval and Tweedie "trim-and-fill" method was employed to adjust the results. All statistical analyses were performed using Comprehensive Meta-Analysis (CMA) software version 2.0 (Biostat, USA). A two-sided p-value less than 0.05 was considered statistically significant.

RESULTS

Characteristics of Selected Studies

A summary of the literature review and study selection process is depicted in Figure 1. The initial search identified 741 articles. After screening titles and abstracts, 312 duplicates and 218 articles related to cell or animal studies, reviews, case reports, and other non-eligible formats were excluded. The full texts of the remaining 211 articles were reviewed in detail, leading to the exclusion of 178 studies based on the set inclusion and exclusion criteria. Ultimately, 33 studies comprising 7,624 schizophrenia cases and 8,933 controls were included in the meta-analysis. Of these, 21 studies focused on Asian populations, 11 on Caucasian populations, and one on a mixed ethnic group. The studies were published between 2001 and 2020 and represented research from various countries, including Italy, Germany, Korea, Singapore, China, Finland, the United States, Canada, Japan, Poland, Pakistan, Saudi Arabia, and Türkiye. With the exception of three studies, the genotype distributions in the control groups conformed to HWE, as outlined in the study protocols. Detailed genotypic frequency data for all included studies are provided in Table 1.

Quantitative Synthesis

Overall Analysis

In the present meta-analysis, no statistically significant relationship was found between the TNF-α rs1800629 polymorphism and the risk of schizophrenia. This conclusion is based on the quantitative synthesis summarized in Table 2 and depicted in the forest plot (Figure 2), which presents results across multiple genetic models (allelic, homozygous, heterozygous, dominant, and recessive). For example, the pooled OR for the allelic comparison (A vs. G) was 1,148 (95% CI: 0.947-1.391, p=0.161), indicating only a slight, nonsignificant increase in risk. Similarly, the homozygous (AA vs. GG: OR=1,332, 95% CI: 0.785-2,260, p=0.289) and heterozygous (AG vs. GG: OR=1,081, 95% CI: 0.905-1,291, p=0.390) comparisons did not reveal significant associations. This lack of significant association was consistent across subgroup analyses stratified by ethnicity (such as Asian, Caucasian, and East Asian populations), country (e.g., China, Poland), HWE status, genotyping technique [polymerase chain reaction - restriction fragment length polymorphism (PCR-RFLP), ankle-brachial index (ABI)], and publication period (before and after 2010). For instance, among Asian populations, the OR for A vs. G was 1,198 (95% CI: 0.892-1,595, p=0.235), and for Caucasian populations, it was 1,043 (95% CI: 0.853-1,275, p=0.689), neither reaching statistical significance. However, a notable exception emerged in the subgroup analysis of studies published after 2010, where the combined AA+AG versus GG genotype model showed a significant association with schizophrenia risk, (OR=1,700, 95% CI: 1,073–2.693, p=0.024). When considering both AA and AG genotypes together, more recent research found a statistically significant increase in schizophrenia risk linked to the TNF-α rs1800629 polymorphism.

Heterogeneity Testing and Sensitivity Analysis

The heterogeneity analysis, as indicated by I2 values, reveals substantial variability across the different subgroups and genetic models. Specifically, the overall analysis shows high heterogeneity (I2=74.19% to 86.33%, p≤0.001). Similar trends are observed within ethnicity-based subgroups, with Asians, (I2=89.69% to 80.50%, p≤0.001), Caucasians, (I2=65.40% to 48.83%), and East Asians (I2=89.48% to 81.84%, p≤0.001) all exhibiting considerable heterogeneity. Country-based analyses in

countries, such as China (I2=90.62% to 53.49%, p≤0.011) and Poland (I2=97.01% to 83.22%, p=0.001 to 0.009), also demonstrate significant heterogeneity. Subgroups based on HWE and genotyping methods (PCR-RFLP and ABI) also show high levels of heterogeneity. Finally, stratification by publication year (before and after 2010) reveals high heterogeneity in both periods, suggesting that the observed associations are influenced by various confounding factors. These findings suggest that the overall effect estimates should be interpreted with caution, as the true effect may vary across different populations and study designs.

Publication Bias

The evaluation of publication bias related to the TNF-α rs1800629 polymorphism and its association with schizophrenia involved analyzing various genetic models and subgroups using Begg's and Egger's tests. The results indicated differing levels of publication bias across models (Figure 3). Specifically, Figure 3 (Begg's funnel plot) visually represents the publication bias test for the correlation between TNF-α rs1800629 polymorphism and schizophrenia development. For the A vs. G allele comparison, Begg's test returned a p-value of 0.675, and Egger's test yielded 0.288, both suggesting no significant bias.

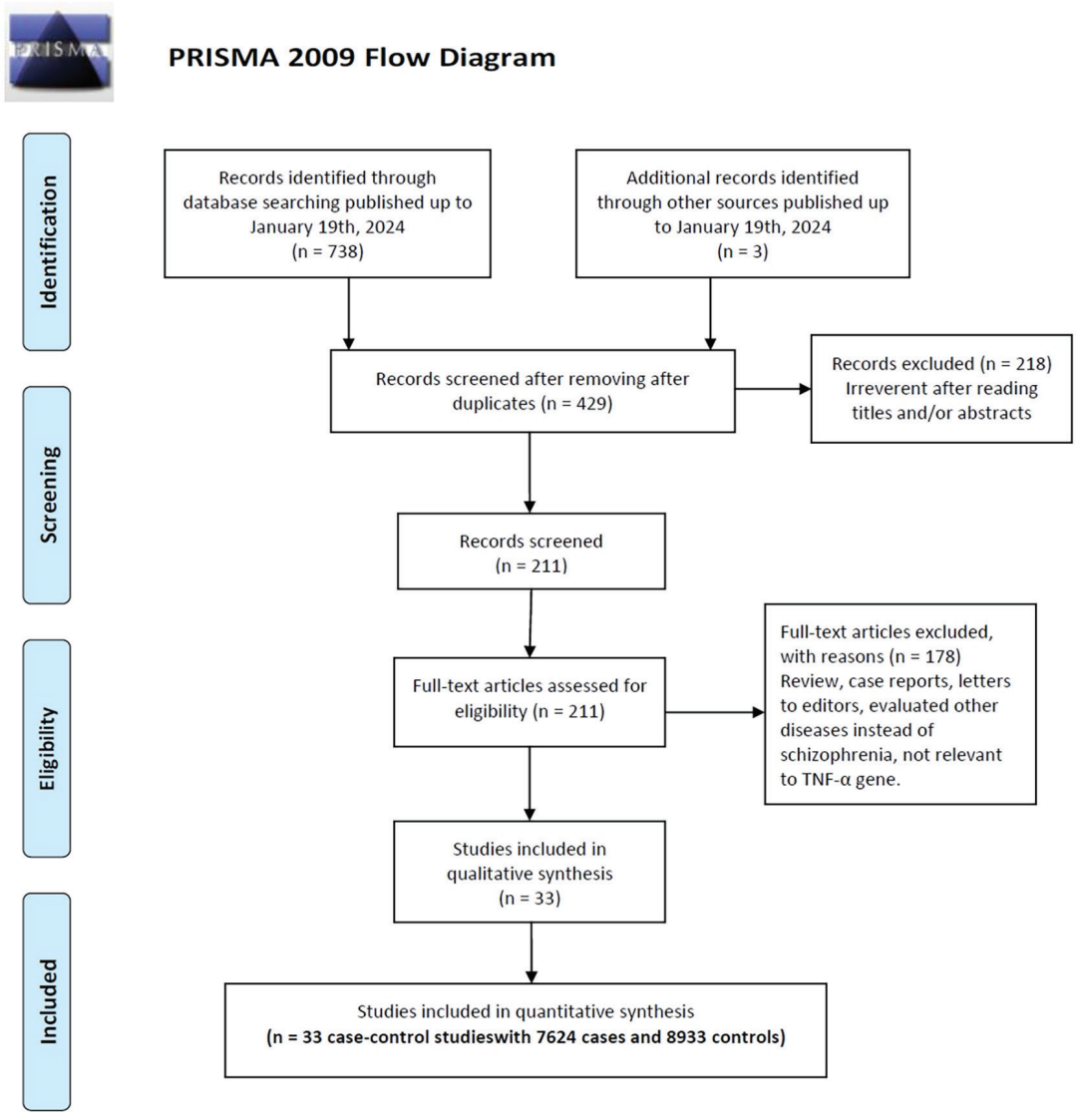

Figure 1. Diagram illustrating the process of study identification, screening, eligibility assessment, and final inclusion for this meta-analysis.

Table 1. Characteristics of studies included in this meta-analysis.

First author/year	Country (Ethnicity)	Genotyping method	SOC	Case/ control	Cases					Controls					MAFs	HWE
					Genotypes			Allele		Genotypes			Allele			
					GG	GA	AA	G	A	GG	GA	AA	G	A		
Boin 2001	Italy (Caucasian)	PCR-RFLP	HVS	84/138	55	23	6	133	35	109	29	0	247	29	0.105	0.167
Riedel 2002	Germany (Caucasian)	FRET	HVS	157/186	116	39	2	271	43	128	53	5	309	63	0.169	0.861
Meira-Lima 2003	Brazil (Mixed)	PCR-RFLP	HV	186/657	134	44	8	312	60	512	140	5	1164	150	0.114	0.169
Pae 2003	Korea (Asian)	PCR-RFLP	HVS	241/125	212	27	2	451	31	107	18	0	232	18	0.072	0.385
Tan 2003	Singapore (Asian)	PCR-RFLP	HVS	302/152	236	62	4	534	70	90	57	5	237	67	0.220	0.260
Tsai 2003	China (Asian)	PCR-RFLP	HVS	205/192	158	44	3	360	50	161	30	1	352	32	0.083	0.752
Yang 2003	China (Asian)	PCR-RFLP	HP	141/282	50	69	22	169	113	72	159	51	303	261	0.463	0.024
Duan 2004	China (Asian)	ABI 3100	HVS	314/340	269	44	1	582	46	295	42	3	632	48	0.071	0.280
Hashimoto 2004	Japan (Asian)	ABI 7000	HVS	297/458	288	9	0	585	9	451	7	0	909	7	0.008	0.869
Hanninen 2005	Finland (Caucasian)	ABI 7000	HBD	149/393	122	24	3	268	30	292	95	6	679	107	0.136	0.582
Kampman 2005	Finland (Caucasian)	ABI 7000	HBD	94/98	76	14	4	166	22	74	23	1	171	25	0.128	0.589
Duan 2006	China (Asian)	PCR-RFLP	HP	172/344	127	44	1	298	46	262	80	2	604	84	0.122	0.115
Pae 2006	Korea (Asian)	PCR-RFLP	HV	152/152	130	21	1	281	23	129	20	3	278	26	0.086	0.050
Shirts 2006	USA (Caucasian)	ABI 3700	NCB	244/276	173	64	7	410	78	195	73	8	463	89	0.161	0.713
Song 2006	China (Asian)	PCR-RFLP	HV	161/135	86	70	5	242	80	61	66	8	188	82	0.304	0.070
Zai 2006	Canada (Caucasian)	PCR-RFLP	HV	149/149	105	41	3	251	47	108	39	2	255	43	0.144	0.464
Sacchetti 2007	Italy (Caucasian)	PCR-RFLP	HVS	323/346	239	75	9	553	93	272	68	6	612	80	0.116	0.469
Watanabe 2007	Japan (Asian)	ABI 7900	HV	265/424	258	7	0	523	7	409	15	0	833	15	0.018	0.710
Czerski 2008	Poland (Caucasian)	PCR-RFLP	HV	348/351	267	78	3	612	84	242	98	11	582	120	0.171	0.779
Dai 2008	China (Asian)	PCR-RFLP	HP	155/310	113	42	0	268	42	262	48	0	572	48	0.077	0.139
Weidong 2008	China (Asian)	PCR-RFLP	HV	172/344	127	44	1	298	46	262	80	2	604	84	0.122	0.115
Hui 2010	China (Asian)	PCR-RFLP	HVS	253/319	221	32	0	474	32	279	40	0	598	40	0.063	0.232
Naz 2011	Pakistan (Asian)	PCR-RFLP	HVS	100/70	53	29	18	135	65	49	18	3	116	24	0.171	0.427
Jun 2011	China (Asian)	PCR-RFLP	HVS	57/30	38	17	2	93	21	25	4	1	54	6	0.100	0.155
Huijun 2011	China (Asian)	PCR-RFLP	HVS	346/323	315	31	0	661	31	283	40	0	606	40	0.062	0.235
Paul-Samojedny 2013	Poland (Caucasian)	PCR-RFLP	HBD	115/135	25	68	22	118	112	44	79	12	167	103	0.381	0.005
Wei 2013	China (Asian)	PCR-RFLP	HVS	161/135	86	70	5	242	80	61	66	8	188	82	0.304	0.070
Srinivas 2016	India (Asian)	KASPar Assay	NA	246/244	202	39	5	443	49	192	51	1	435	53	0.109	0.214
Kadasah 2017	KSA (Asian)	PCR	HV	180/200	4	176	0	184	176	110	76	14	296	104	0.260	0.859
Suchanek-Raif 2018	Poland (Caucasian)	PCR-ASA	HBD	401/606	273	123	5	669	133	445	144	17	1034	178	0.147	0.202
Feikang 2018	China (Asian)	PCR-RFLP	HVS	254/339	221	30	3	472	36	310	27	2	647	31	0.046	0.107
Lang 2019	China (Asian)	MALDI-TOF	HV	1087/576	762	105	220	1629	545	498	66	12	1062	90	0.078	0.001
Aytac 2020	Türkiye (Caucasian)	PCR-RFLP	HV	113/104	97	14	2	208	18	87	15	2	189	19	0.091	0.181

SOC: Source of controls; HV: Healthy volunteers; HVS: healthy volunteers screened fo rmental illnesses; HP: Health parents; HBD: Healthy blood donors; NCB: Neonatal cord blood; FRET: Fluorescence resonance energy transfer method; PCR: Polymerase chain reaction; RFLP: Restriction fragment length polymorphism; ABI: ABI Sequence Detection System, HWE: Hardy-Weinberg equilibrium; MAF: Minor allele frequency

Table 2. Summary risk estimates for association of TNF-α rs1800629 polymorphism with risk of schizophrenia.

Subgroup	Genetic model	Type of model	Heterogeneity		Odds ratio				Publication bias	
			I2 (%)	P_H	OR	95% CI	Z_{test}	P_{OR}	P_{Beggs}	P_{Eggers}
Overall	A vs. G	Random	86.33	≤0.001	1.148	0.947-1.391	1.403	0.161	0.675	0.288
	AA vs. GG	Random	74.77	≤0.001	1.332	0.785-2.260	1.061	0.289	0.417	0.333
	AG vs. GG	Random	75.70	≤0.001	1.081	0.905-1.291	0.860	0.390	0.232	0.148
	AA+AG vs. GG	Random	82.51	≤0.001	1.157	0.947-1.413	1.425	0.154	0.187	0.711
	AA vs. AG+GG	Random	74.19	≤0.001	1.261	0.757-2.101	0.890	0.374	0.678	0.223
Ethnicity										
Asians	A vs. G	Random	89.69	≤0.001	1.198	0.892-1.595	1.188	0.235	0.319	0.223
	AA vs. GG	Random	80.63	≤0.001	1.247	0.542-2.866	0.519	0.604	0.558	0.329
	AG vs. GG	Random	81.87	≤0.001	1.162	0.884-1.527	1.078	0.281	0.037	0.033
	AA+AG vs. GG	Random	87.06	≤0.001	1.253	0.919-1.707	1.428	0.153	0.123	0.721
	AA vs. AG+GG	Random	80.50	≤0.001	1.129	0.503-2.532	0.294	0.768	0.821	0.225
Caucasians	A vs. G	Random	65.40	0.001	1.043	0.853-1.275	0.407	0.689	1.000	0.898
	AA vs. GG	Random	51.79	0.023	0.997	0.812-1.223	0.032	0.974	0.533	0.764
	AG vs. GG	Random	52.39	0.021	1.025	0.844-1.246	0.253	0.801	0.876	0.477
	AA+AG vs. GG	Random	59.30	0.006	1.022	0.825-1.267	0.200	0.842	0.755	0.955
	AA vs. AG+GG	Random	48.83	0.034	1.131	0.639-2.003	0.424	0.672	0.436	0.772
East Asian	A vs. G	Random	89.48	≤0.001	1.110	0.809-1.523	0.646	0.518	0.363	0.289
	AA vs. GG	Random	83.55	≤0.001	1.011	0.389-2.630	0.023	0.981	0.160	0.275
	AG vs. GG	Random	62.30	≤0.001	0.997	0.817-1.218	-0.026	0.979	0.225	0.371
	AA+AG vs. GG	Random	82.22	≤0.001	1.071	0.811-1.416	0.484	0.628	0.448	0.307
	AA vs. AG+GG	Random	81.84	≤0.001	1.070	0.439-2.608	0.149	0.882	0.099	0.278
Country										
China	A vs. G	Random	90.62	≤0.001	1.220	0.851-1.748	1.083	0.279	0.200	0.246
	AA vs. GG	Random	86.06	≤0.001	1.196	0.399-3.585	0.319	0.749	0.371	0.398
	AG vs. GG	Random	53.49	0.011	1.069	0.879-1.299	1.299	0.668	0.299	0.317
	AA+AG vs. GG	Random	81.89	≤0.001	1.177	0.872-1.588	1.066	0.286	0.582	0.195
	AA vs. AG+GG	Random	84.74	≤0.001	1.245	0.447-3.463	0.419	0.675	0.283	0.414
Poland	A vs. G	Random	85.48	0.001	1.052	0.669-1.653	0.219	0.826	1.000	0.908
	AA vs. GG	Random	85.42	0.001	0.763	0.159-3.669	-0.338	0.735	0.296	0.283
	AG vs. GG	Random	97.01	0.009	1.126	0.693-1.830	0.480	0.631	1.000	0.957
	AA+AG vs. GG	Random	83.22	0.003	1.117	0.659-1.893	0.410	0.682	1.000	0.840
	AA vs. AG+GG	Random	83.22	0.003	0.702	0.172-2.865	-0.493	0.622	0.296	0.198
HWE	A vs. G	Random	75.69	≤0.001	1.094	0.932-1.284	1.095	0.274	0.784	0.983
	AA vs. GG	Random	74.57	≤0.001	1.347	0.739-2.453	973	0.331	0.381	0.450
	AG vs. GG	Random	76.83	≤0.001	1.100	0.911-1.327	988	0.323	0.535	0.236
	AA+AG vs. GG	Random	83.23	≤0.001	1.179	0.953-1.457	1.519	0.129	0.358	0.145
	AA vs. AG+GG	Random	47.62	0.005	1.066	0.678-1.675	0.276	0.782	0.673	0.774
Gentyping methods										
PCR-RFLP	A vs. G	Random	74.48	≤0.001	1.095	0.916-1.311	0.996	0.319	0.283	0.137
	AA vs. GG	Random	74.48	≤0.001	1.095	0.916-1.311	0.996	0.319	0.283	0.137
	AG vs. GG	Random	69.94	≤0.001	1.068	0.881-1.293	0.668	0.504	0.101	0.151
	AA+AG vs. GG	Random	69.94	≤0.001	1.068	0.881-1.293	0.668	0.504	0.101	0.151
	AA vs. AG+GG	Random	50.63	0.006	1.253	0.786-1.998	0.949	0.343	0.779	0.633

Table 2. Continued

Subgroup	Genetic model	Type of model	Heterogeneity		Odds ratio				Publication bias	
			I2 (%)	P_H	OR	95% CI	Z_{test}	P_{OR}	P_{Beggs}	P_{Eggers}
ABI	A vs. G	Random	65.23	0.015	0.952	0.750-1.205	-0.721	0.471	0.529	0.385
	AA vs. GG	Random	58.71	0.032	1.158	0.620-2.164	0.563	0.573	0.214	0.896
	AG vs. GG	Random	72.15	≤0.001	1.023	0.835-1.254	0.195	0.845	0.912	0.452
	AA+AG vs. GG	Random	61.98	0.008	0.987	0.799-1.220	-0.105	0.916	0.647	0.719
	AA vs. AG+GG	Random	49.36	0.045	1.311	0.701-2.451	0.992	0.321	0.488	0.555
Publication year										
Before 2010	A vs. G	Random	67.15	≤0.001	1.007	0.858-1.180	0.082	0.935	0.446	0.312
	AA vs. GG	Random	75.22	0.002	1.15	0.65 - 2.03	0.457	0.656	0.558	0.756
	AG vs. GG	Random	68.55	0.015	0.95	0.78 - 1.16	-0.828	0.413	0.924	0.235
	AA+AG vs. GG	Random	64.40	≤0.001	0.979	0.824-1.163	-0.240	0.810	0.843	0.611
	AA vs. AG+GG	Random	39.59	0.043	1.050	0.668-1.650	0.209	0.834	0.306	0.452
After 2010	A vs. G	Random	91.23	≤0.001	1.457	0.984-2.158	1.879	0.060	1.000	0.278
	AA vs. GG	Random	82.11	0.001	1.628	0.88 - 2.97	1.227	0.228	0.339	0.816
	AG vs. GG	Random	79.44	0.005	1.283	0.91 - 1.79	0.956	0.347	0.763	0.498
	AA+AG vs. GG	Random	89.68	≤0.001	1.700	1.073-2.693	2.262	0.024	0.275	0.693
	AA vs. AG+GG	Random	84.23	≤0.001	1.505	0.552-4.101	0.798	0.425	0.591	0.088

Similarly, the AA vs. GG model had p-values of 0.417 (Begg's) and 0.333 (Egger's), indicating an absence of substantial bias. The AG vs. GG comparison also showed no evidence of bias, with p-values of 0.232 and 0.148, respectively. However, subgroup analyses based on ethnicity revealed more complex results: in the Asian subgroup, the AG vs. GG model indicated significant publication bias with p-values of 0.037 (Begg's) and 0.033 (Egger's), suggesting a potential influence of publication bias for this genetic model within this specific ethnic group. Although no significant bias was found in other comparisons within this group, further investigation is required. For Caucasians and East Asians, results generally showed no significant publication bias, with p-values consistently above 0.05. When analyzing by country, Poland showed potential bias with A vs. G model p-values of 1.000 (Begg's) and 0.908 (Egger's), which may indicate a lack of studies showing a significant association in the Polish population for this specific allele comparison. In contrast, analyses for China revealed no publication bias in the assessed models. Examining the HWE subgroup, it was found that no significant publication bias was evident. Similarly, analyses based on genotyping methods (PCR-RFLP and ABI) and publication year (before and after 2010) generally indicated no substantial publication bias.

Minor Allele Frequencies

MAFs ranged from 0.008 to 0.463, demonstrating considerable geographical and ethnic variation. Asian populations exhibited lower MAFs in Japan (0.008) and China (0.071, 0.077) compared to Singapore (0.220) and healthy Chinese parents (0.463). Chinese studies showed diverse MAFs, some exceeding 0.300. Caucasian populations generally had higher MAFs, as seen in Germany (0.169) and Poland (0.171), while Finnish studies reported 0.136 and 0.128. These MAF differences are attributable to nationality, study design, and methodologies, underscoring the importance of population-specific genetic factors in genetic epidemiology. The results indicate a complex interaction of genetic and environmental influences on MAF distribution.

DISCUSSION

The association between the TNF-α rs1800629 polymorphism and schizophrenia susceptibility remains a complex and controversial topic, as evidenced by conflicting findings across various studies. While our CMA, encompassing 33 investigations with 7624 cases and 8933 controls, revealed no significant correlation between this polymorphism and schizophrenia risk across five

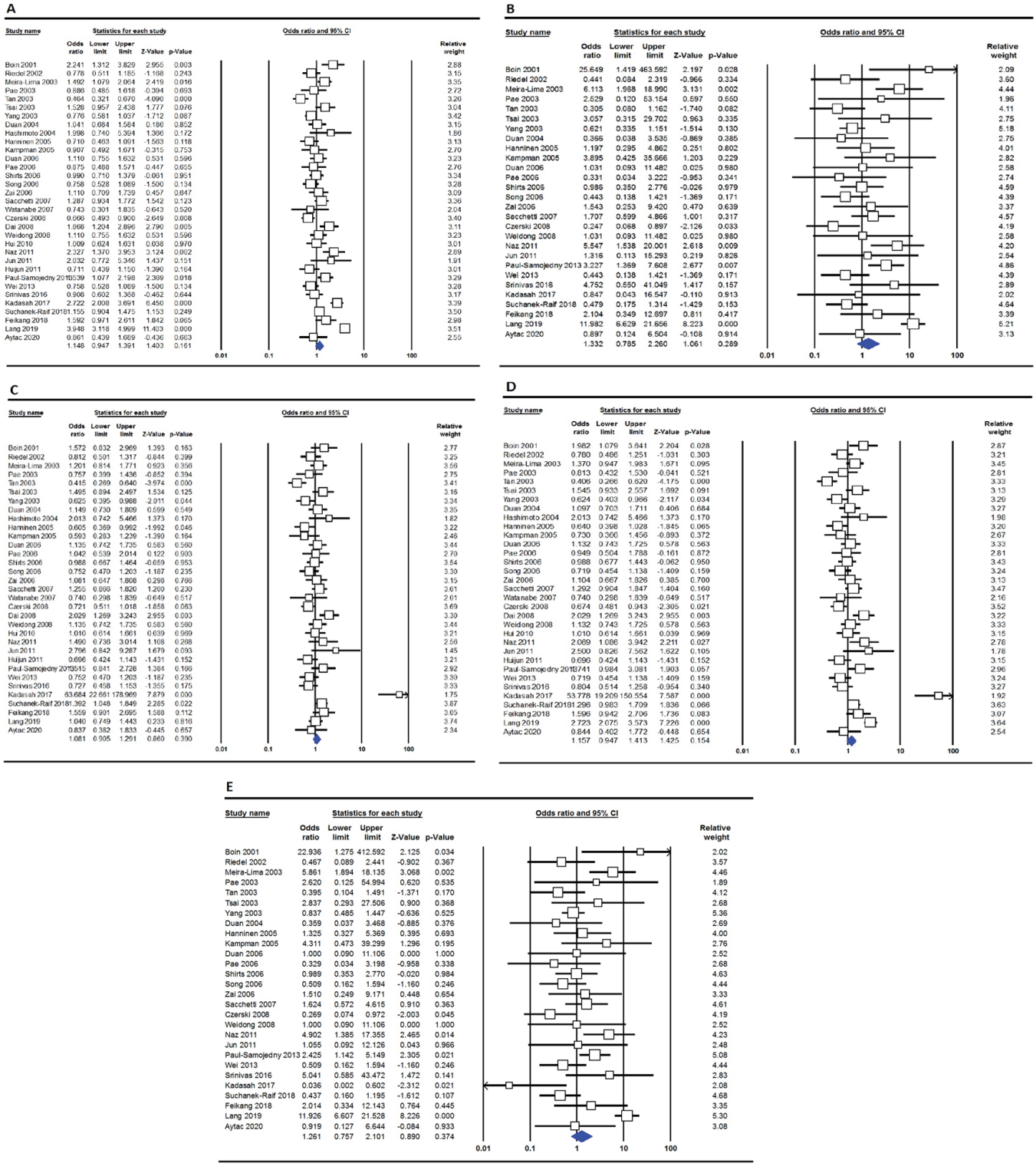

Figure 2. Forest plots depicting the association between the TNF-α rs1800629 genetic variant and schizophrenia risk across all included studies. Results are presented for five genetic models: A) Allelic comparison (A vs. G); B) Homozygote comparison (AA vs. GG); C) Heterozygote comparison (AG vs. GG); D) Dominant model (AA+AG vs. GG); and E) Recessive model (AA vs. AG+GG).

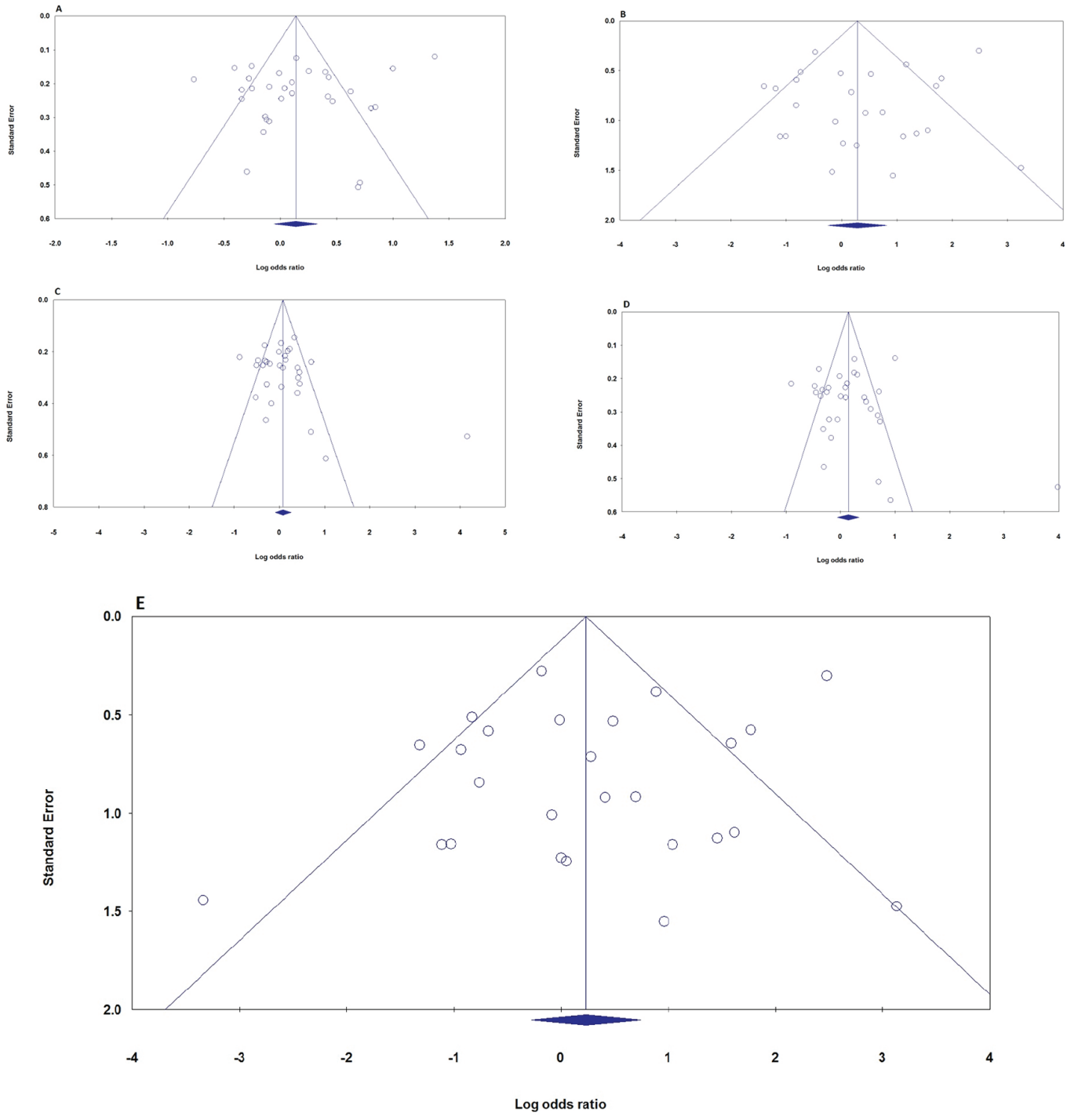

Figure 3. Begg's funnel plots evaluating potential publication bias in the analysis of the TNF-α rs1800629 polymorphism and schizophrenia risk. The plots correspond to: A) Allelic model (A vs. G); B) Homozygote model (AA vs. GG); C) Heterozygote model (AG vs. GG); D) Dominant model (AA+AG vs. GG); and E) Recessive model (AA vs. AG+GG).

genetic models, this contrasts with some prior research. For instance, Sacchetti et al.[28] (2007) reported a weak association between the AA genotype and schizophrenia susceptibility in Caucasoids, further supported by a replication case-control study indicating an association between the A allele and increased schizophrenia susceptibility, particularly in males, with correlations to a later schizophrenia onset at age. However, these initial observations have not been consistently replicated.

More recent meta-analyses, including those by Qin et al.[18] (2013) and He et al.[6] (2022), have found no substantial correlation between the TNF-α rs1800629 polymorphism and schizophrenia susceptibility. Qin et al.[16] analysis of 21 studies showed a lack of association among Caucasian and Asian subgroups, as well as between males and females. Similarly, He et al.[6] pooled analysis of 24 studies found no significant association. Further complicating the picture, studies have explored the influence of specific populations or other factors. Alfimova et al. found that childhood adversity influences the relationship between schizophrenia development and the TNF-α promoter polymorphism rs1800629, while Kang et al.[16] discovered that the A-allele at TNF-α rs1800629 is associated with reduced white matter connectivity in the fronto-temporal region in Korean patients; While Kang et al.[16] discovered that the A-allele at TNF-α rs1800629 is associated with reduced white matter connectivity in the fronto-temporal region in Korean patients[26]. Conversely, Aytec et al.[29] (2022) found no significant difference in the prevalence of TNF-α rs1800629 between Turkish individuals with schizophrenia and healthy controls, and Lang et al.[19] (2020) found no significant relationship between rs1800629 and schizophrenia or suicide. These discrepancies highlight the need for further research to clarify the role of this polymorphism in schizophrenia susceptibility, considering potential influences from ethnicity, environmental exposures, and interactions with other genes.

Clinical Implication

The meta-analysis suggests that the TNF-α rs1800629 polymorphism, on its own, is unlikely to be a strong predictor of schizophrenia risk across diverse populations. Clinically, this implies that routine screening for this specific polymorphism in individuals to assess their risk of developing schizophrenia is not currently warranted. However, clinicians should be aware of the potential for gene-environment interactions and the influence of ethnicity on genetic associations. Further research exploring these factors may refine risk prediction models in the future. It is important to consider other established risk factors and diagnostic criteria when assessing individuals for schizophrenia.

Study Limitations

The study entailed a thorough analysis of the network database. However, there are limitations to this meta-analysis. The primary constraint is that most studies focused on Asian and Caucasian populations, making it challenging to evaluate the impact of TNF-α rs1800629 polymorphism on other groups. This limitation could impact the true association between the polymorphism and schizophrenia. Due to limited data, the relationship between TNF-α rs1800629 polymorphism and the clinical features of schizophrenia could not be fully explored. The analysis was unadjusted; however, an analysis that considered factors like gender, family history of schizophrenia, pregnancy complications, and exposure to toxins or viruses could have been more beneficial. Genetic and environmental interactions were not examined due to insufficient original data. Therefore, further validation with a larger, diverse sample is necessary to confirm the study's findings. Future research should also account for the potential influence of other genetic polymorphisms and lifestyle factors on schizophrenia development. Additionally, exploring the role of epigenetic modifications in conjunction with TNF-α rs1800629 polymorphism could offer a more comprehensive understanding of the underlying mechanisms involved in schizophrenia susceptibility. Collaborative efforts among researchers from diverse ethnic backgrounds and regions could help overcome current limitations and provide a more nuanced perspective on the relationship between TNF-α rs1800629 polymorphism and schizophrenia. Ultimately, a multidisciplinary approach encompassing genetics, epigenetics, environmental factors, and clinical characteristics is crucial for advancing our understanding of the complex etiology of schizophrenia.

CONCLUSION

In summary, our comprehensive analysis does not support a consistent link between the TNF-α rs1800629 polymorphism and increased susceptibility to schizophrenia. However, these findings should be interpreted with caution due to considerable heterogeneity among studies and the limited representation of ethnic groups, as the current meta-analysis primarily included Asian and Caucasian populations. To better understand the potential involvement of TNF-α rs1800629 in schizophrenia, future research should incorporate larger and more ethnically diverse cohorts. Additionally, exploring gene-gene and gene-environment interactions

will be essential for a more complete understanding of the genetic and environmental factors that contribute to schizophrenia risk.

Ethics

Ethics Committee Approval: Since this study is a meta-analysis study, ethical approval is not required.

Informed Consent: Since this study is a meta-analysis study, patient consent is not required.

Footnotes

Author Contributions

Concept: G.D., H.N., Design: B.F., A.G.T., F.N., Data Collection and/or Processing: A.S., M.B., F.N., Analysis and/or Interpretation: H.N., Literature Search: G.D., A.S., M.B., Writing: F.N., H.N.

Conflict of Interest: The authors have no conflict of interest to declare.

Financial Disclosure: The authors declared that this study has received no financial support.

REFERENCES

1. Hakenova K, Mikulecka A, Holubova K, et al. A new two-hit animal model for schizophrenia research: Consequences on social behavior. IBRO Neurosci Reports. 2025;19:38-49.
2. Völker JSD, Micluţia IV. Assessing the quality of life of schizophrenia patients and their family caregivers in a Romanian sample: the role of clinical, sociocultural, and demographic factors. Med Pharm Rep. 2025;98:96-110.
3. Mosquera FEC, Guevara-Montoya MC, Serna-Ramirez V, Liscano Y. Neuroinflammation and schizophrenia: new therapeutic strategies through psychobiotics, nanotechnology, and artificial intelligence (AI). J Pers Med. 2024;14:391.
4. Yu S, Qu Y, Du Z, et al. The expression of immune related genes and potential regulatory mechanisms in schizophrenia. Schizophr Res. 2024;267:507-18.
5. Mikhalitskaya EV, Vyalova NM, Ermakov EA, Levchuk LA, Simutkin GG, Bokhan NA, Ivanova SA. Association of single nucleotide polymorphisms of cytokine genes with depression, schizophrenia and bipolar disorder. Genes (Basel). 2023;14:1460.
6. He S, Zhang L, Yu S, Y et al. Association between tumor necrosis factor-Alpha(TNF-a) polymorphisms and schizophrenia: an updated meta-analysis. Int J Psychiatry Clin Pract. 2022;26:294-302.
7. Ferdosian F, Dastgheib SA, Hosseini-Jangjou SH, et al. Association of TNF-α rs1800629, CASP3 rs72689236 and FCGR2A rs1801274 polymorphisms with susceptibility to kawasaki disease: a comprehensive meta-analysis. Fetal Pediatr Pathol. 2021;40:320-36.
8. Aflatoonian M, Moghimi M, Akbarian-Bafghi MJ, Morovati-Sharifabad M, Jarahzadeh MH, Neamatzadeh H. Association of TNF- α-308G>A polymorphism with susceptibility to celiac disease: a systematic review and meta-analysis. Arq Gastroenterol. 2019;56:88-94.
9. Goldsmith DR, Haroon E, Miller AH, Strauss GP, Buckley PF, Miller BJ. TNF-α and IL-6 are associated with the deficit syndrome and negative symptoms in patients with chronic schizophrenia. Schizophr Res. 2018;199:281-4.
10. Corsi-Zuelli F, Donohoe G, Griffiths SL, et al. Depressive and negative symptoms in the early and established stages of schizophrenia: integrating structural brain alterations, cognitive performance, and plasma interleukin 6 levels. Biol Psychiatry Glob Open Sci. 2024;5:100429.
11. Pantovic-Stefanovic M, Velimirovic M, Jurisic V, et al. Exploring the role of TNF-α, TGF-β, and IL-6 serum levels in categorical and noncategorical models of mood and psychosis. Sci Rep. 2024;14:23117.
12. Miller BJ, Goldsmith DR. Inflammatory biomarkers in schizophrenia: Implications for heterogeneity and neurobiology. Psychiatry and Health Behavior. 2019;1:100006.
13. Bahrami R, Talebi H, Alireza Dastgheib S, et al. Advancements in biomarkers and machine learning for predicting of bronchopulmonary dysplasia and neonatal respiratory distress syndrome in preterm infants. Front Pediatr. 2025;13:1521668.
14. Shams SE, Dastgheib SA, Mousavi-Beni SA, et al. Association of TNF-α genetic variants with neonatal bronchopulmonary dysplasia: consolidated results. Front Pediatr. 2024;12:1511355.
15. HaghighiKian SM, Shirinzadeh-Dastgiri A, Ershadi R, et al. Correlation of TNF-α polymorphisms with susceptibility to lung cancer: evidence from a meta-analysis based on 29 studies. BMC Cancer. 2024;24:1113.
16. Kang N, Shin W, Jung S, Bang M, Lee SH. The effect of TNF-alpha rs1800629 polymorphism on white matter structures and memory function in patients with schizophrenia: a pilot study. Psychiatry Investig. 2022;19:1027-36.
17. Lindbergh CA, Casaletto KB, Staffaroni AM, et al. Systemic tumor necrosis factor-alpha trajectories relate to brain health in typically aging older adults. J Gerontol A Biol Sci Med Sci. 2020;75:1558-65.
18. Qin H, Zhang L, Xu G, Pan X. Lack of association between TNFα rs1800629 polymorphism and schizophrenia risk: a meta-analysis. Psychiatry Res. 2013;209:314-9.
19. Lang X, Trihn TH, Wu HE, Tong Y, Xiu M, Zhang XY. Association between TNF-alpha polymorphism and the age of first suicide attempt in chronic patients with schizophrenia. Aging (Albany NY). 2020;12:1433-45.
20. Padula MC, Padula AA, D'Angelo S, et al. TNFα rs1800629 Polymorphism and response to anti-TNFα treatment in Behçet Syndrome: data from an italian cohort study. J Pers Med. 2023;13:1347.
21. Bahoush G, Vafapour M, Kariminejad R. Detection of new translocation in infant twins with concordant ALL and discordant outcome. Pediatr Rep. 2020;13:9-14.
22. Antikchi MH, Asadian F, Dastgheib SA, et al. Cumulative evidence for association between IL-8 -251T>A and IL-18 -607C>A polymorphisms and colorectal cancer susceptibility: a systematic review and meta-analysis. J Gastrointest Cancer. 2021;52:31-40.
23. HaghighiKian SM, Shirinzadeh-Dastgiri A, Vakili-Ojarood M, et al. A Holistic approach to implementing artificial intelligence in lung cancer. Indian J Surg Oncol. 2025:16;1-22.
24. Ghelmani Y, Asadian F, Antikchi MH, et al. Association between the hOGG1 1245C>G (rs1052133) polymorphism and susceptibility to colorectal cancer: a meta-analysis based on 7010 cases and 10,674 controls. J Gastrointest Cancer. 2021;52:389-98.

25. Neamatzadeh H, Dastgheib SA, Mazaheri M, et al. Hardy-Weinberg Equilibrium in Meta-Analysis Studies and Large-Scale Genomic Sequencing Era. Asian Pac J Cancer Prev. 2024;25:2229-35.
26. Asadian F, Niktabar SM, Ghelmani Y, et al. Association of XPC polymorphisms with cutaneous malignant melanoma risk: evidence from a meta-analysis. Acta Medica (Hradec Kralove). 2020;63:101-12.
27. Sobouti B, Bahrami A, Rahmani F, et al. Wiskott-Aldrich syndrome with possible congenital cytomegalovirus infection: A diagnostic dilemma. Natl Med J India. 2021;34:24-6.
28. Sacchetti E, Bocchio-Chiavetto L, Valsecchi P, et al. -G308A tumor necrosis factor alpha functional polymorphism and schizophrenia risk: meta-analysis plus association study. Brain Behav Immun. 2007;21:450-7.
29. Aytac HM, Ozdilli K, Tuncel FC, Pehlivan M, Pehlivan S. Tumor necrosis factor-alpha (TNF-α) -238 G/A polymorphism is associated with the treatment resistance and attempted suicide in schizophrenia. Immunol Invest. 2022;51:368-80.

DOI: 10.4274/MMJ.galenos.2025.87120
Medeni Med J 2025;40:93-100

Original Article

Clumpy Novel Mitochondrial Signatures in Irradiated Human Diabetic Buccal Cells: A Case Control Study

Işınlanmış İnsan Diyabetik Bukkal Hücrelerinde Kümelenmiş Yeni Mitokondriyal Signatürler: Bir Olgu Kontrol Çalışması

Surraj SUSAI[1], Mrudula CHANDRUPATLA[1], Sumitra SIVAKOTI[2], Govindrao N. KUSNENIWA[3], Anand K. PYATI[4]

[1]All India Institute of Medical Sciences, Department of Anatomy, Bibinagar, India
[2]All India Institute of Medical Sciences, Department of Pathology, Bibinagar, India
[3]All India Institute of Medical Sciences, Department of Community medicine, Bibinagar, India
[4]All India Institute of Medical Sciences, Department of Biochemistry, Bibinagar, India

ABSTRACT

Objective: This study aimed to determine the whole free mitochondria in type-2 diabetic buccal epithelial cells using a supravital stain called "Janus Green B" and assess their behavior after exposure to near infrared light. The researchers observed microscopic mitochondrial load and its intracellular spatial behavior after exposure to near-infrared rays, bridging the gap in understanding mitochondrial orientation in diseases like diabetes. The aim of this research was to find out the quantitative involvement and electrostatic intracellular spatial patterns of whole mitochondria in diabetes.

Methods: Exfoliated buccal cell wet mounts, supravitally stained using Janus green, and excited using infrared rays, were observed using an advanced bright field Axiocam microscope, and the images of whole mitochondria within the cells were photographed and analyzed using the ZEN 2.0 cell sense software. The migration patterns of mitochondria were observed.

Results: A quantitative decrease in mitochondria was noted in diabetic cells. Signatures of clumpy peripheral shifts in mitochondria were observed in diabetic buccal cells post radiation.

Conclusions: Advanced glycation end products of diabetes combined with oxidative stressors influenced the free mitochondria to clump peripherally and produce a characteristic signature. The decreased mitochondrial load contributed additional evidence to the reduced respiratory capacity of cells, which forced mitochondria to emit a detectable signature when irradiated.

Keywords: Peripheral clumps, infra red rays, power houses, intracellular, shift, comets

ÖZ

Amaç: Bu çalışmanın amacı, tip-2 diyabetik bukkal epitel hücrelerindeki tüm serbest mitokondriyi "Janus Green B" adı verilen supravital bir boya kullanarak belirlemek ve yakın kızılötesi ışığa maruz kaldıktan sonraki davranışlarını değerlendirmektir. Araştırmacılar, yakın kızılötesi ışınlara maruz kaldıktan sonra mikroskobik mitokondriyal yükü ve hücre içi uzamsal davranışını gözlemleyerek diyabet gibi hastalıklarda mitokondriyal yönelimin anlaşılmasındaki boşluğu doldurmuşlardır. Bu araştırmanın amacı, diyabette tüm mitokondrinin kantitatif katılımını ve elektrostatik hücre içi uzamsal modellerini bulmaktır.

Yöntemler: Janus yeşili kullanılarak supravital olarak boyanmış ve kızılötesi ışınlar kullanılarak uyarılmış eksfoliye edilmiş bukkal hücre ıslak numuneler, gelişmiş bir parlak alan Axiocam mikroskobu kullanılarak gözlemlendi ve hücrelerdeki tüm mitokondrilerin görüntüleri ZEN 2.0 hücre algılama yazılımı kullanılarak fotoğraflandı ve analiz edildi. Mitokondrilerin göç modelleri gözlemlendi.

Bulgular: Diyabetik hücrelerde mitokondride kantitatif bir azalma kaydedildi. Radyasyon sonrası diyabetik bukkal hücrelerde mitokondride topaklanmış periferik kayma belirtileri gözlendi.

Sonuçlar: Diyabetin ileri glikasyon son ürünleri oksidatif stres faktörleriyle birleşerek serbest mitokondrilerin periferik olarak kümelenmesini ve karakteristik bir signatür üretmesini etkilemiştir. Mitokondriyal yükün azalması, hücrelerin solunum kapasitesinin azaldığına dair ek kanıtlar sunmuş ve bu düşüş mitokondriyi ışınlandığında tespit edilebilir bir signatür yaymaya zorlamıştır.

Anahtar kelimeler: Periferik kümeler, kızıl ötesi ışınlar, güç santrali, hücre içi, kayma, komet

Address for Correspondence: Surraj Susai, All India Institute of Medical Sciences, Department of Anatomy, Bibinagar, India
E-mail: surraj18@gmail.com **ORCID ID:** orcid.org/0000-0001-5472-6841

Received: 17 March 2025
Accepted: 10 June 2025
Published: 26 June 2025

Cite as: Susai S, Chandrupatla M, Sivakoti S, Kusneniwar GN, Pyati AK. Clumpy Novel mitochondrial signatures in irradiated human diabetic buccal cells: a case control study. Medeni Med J. 2025;40:93-100

INTRODUCTION

Though type-2 diabetes is a complex disorder with bio-molecular imbalances, its lab diagnostic investigations to date have focused only on sugar substrates, glycated products, or urinary sediment patterns. This is with the exception of a few studies that have focused on intracellular changes in cellular organelles, such as mitochondrial DNA, without giving impetus to the estimation of whole membrane-bound free mitochondrial count[1,2]. Mitochondria, the energy turbines of cells, are susceptible to glycation in type-2 diabetes, and there is no consensus neither on their intracellular behaviour nor on their count within the diabetic cells due to the paucity of microscopic studies on the same in contrast to the numerous studies that have been done on mitochondrial DNA[3-5]. Hence, this study aimed to quantify whole free mitochondria in type-2 diabetic buccal epithelial cells using the supravital stain "Janus Green B"; it also assessed their spatial behaviour after exposure to near-infrared light. Previous studies had only determined varied expressions of mitochondrial DNA, which may not reflect the disease's severity or prognosis[3-5]. The researchers in this study used supravitally stained wet mount smears of infrared-irradiated inner cheek cells to assess the spatial arrangement of mitochondria, which helped them understand the spatial alignments of these organelles in response to the disease's course[6]. This approach overcame the problem of invasive needle insertion for obtaining blood samples for mitochondrial DNA estimation. This research is the first of its kind to bridge the gap in understanding the intracellular orientation of mitochondria in diseases like diabetes[2,3,6]. This research also opens a new area to study the electrostatic repulsive behaviour of adapted mitochondria within buccal cells in response to infrared rays. This is also the first study to have observed specific whole mitochondrial signatures in human buccal cells in response to oxidative stress and glycosylation, and to determine their mitochondrial number and distribution. Previous similar studies had been done only in the myocytes, neurons, or blood cells of biopsied diabetic-induced rats or other lower mammals, but not in humans[7,8].

Methodology

Study Design

Informed consent was obtained from all patients. This was a case-control study conducted at a tertiary care institute wherein the departments of anatomy, pathology, biochemistry, and community medicine were collaboratively involved. The case subjects for the study were chosen from the population that visited the non-communicable disease clinic at the outpatient department. Cases included only patients with confirmed pure diabetes in the age group of 30 to 60 years, without other co-morbid stressors and having the disease for a minimum duration of at least 3 years. Controls included healthy volunteers who had visited the Out Patient Department for unrelated reasons. This study excluded subjects with history of smoking, betel nut chewing, other oxidative stress illnesses (except diabetes), poor oral hygiene, and oral diseases. Pre-diabetics, diabetics with hypertension, and diabetics with other co-morbid illnesses arising due to oxidative stress were excluded from the study. Forty cases and forty controls were included in this study, which was performed over 18 months. Cases and controls were age and sex matched to avoid bias. Approval was obtained from the Institutional Ethics Committee for this study (reference number: AIIMS/BBN/IEC/OCT/2022/224, date: 08.10.2022).

Sample Size Estimation

The sample size for this study was calculated using the clincalc sample size calculator available free to all online using the website www.clincalc.com/stats/sample. The primary variable for assessing the outcome in both cases and controls was the mitochondrial load per field of microscope, which was expressed as mean±standard deviation for both groups. The means and standard deviations of mitochondrial load volume in case and control groups from a previously done related study on primate choroidal epithelial cells, which were 13+1.9 and 11.5+1.2 respectively, were then fed into the software[5]. It was estimated by the software that 38 patients in each group would be required to detect a mean difference of 12.25 in mitochondrial load between the two groups of cases and controls. The calculations were based on 80% power, α=0.05, and a two-sided 95% confidence interval. Keeping an attrition factor of 2, the total sample size for both groups together in this case-control study was calculated to be 80, that is, 40 cases and 40 controls.

MATERIALS and METHODS

Informed consent was obtained from the patients prior to the start of this study. The study was done only after obtaining approval and clearance from the institute research council, institute scientific advisory committee, and institute ethics committee. The grants and funds that were required for purchasing the reagents and materials for this study were released by the institute where the authors work after ethics approval. This was an intramurally funded research. Two wet mount buccal epithelial cell smears were obtained from each of the cases and controls and smeared onto two clean glass

slides for each subject. The first smeared slide was stained directly with Janus green staining solution without subjecting the slide to infrared rays. It was then observed under the Zeiss Axiocam bright field microscope at 40X with a specialized in-built zoom camera that magnified the image of the buccal cells to 100X with visible mitochondrial dots, and the images were photo-captured with a computer-attached DSLR camera. The second smeared slide, on the other hand, was subjected to near-infrared radiation (600 nm wavelength at 65 cm distance from the central convex point of the infra-red lamp) for 7 seconds and then stained with Janus green and observed under the microscope. The slides were thoroughly examined from one corner of the smear to another corner by three independent researchers, and the number of buccal cells in a smear was counted using the image J software. The buccal cell density per smear was determined by the software and then the area of maximum density was marked for counting the number of dark colored mitochondrial spots within each of the buccal cells and a quantitative measurement of the same was made using the "ZEN BLUE cell sense-cell counting software" that picked up the mitochondria dots and estimated the number of mitochondria. The slide fields under the Axiocam microscope were observed from left to right from top to bottom in a zig-zag fashion by three independent researchers so that no mitochondrial dots were missed and the observer bias would be eliminated. The number of mitochondrial dots per buccal cell in cases was noted before and after radiation and compared with their blood HbA1C levels. The mitochondrial load was expressed as the aggregated mean of the mitochondrial dots per buccal cell for the cases and was then compared with the mitochondrial load of controls.

Statistical Analysis

Descriptive and inferential statistics were used to analyze the data. The baseline characteristics were analyzed by descriptive statistics. The data on the quantity of mitochondria and levels of HbA1C were expressed as the mean with standard deviation, and an attempt was made to find out if an association existed between the mitochondrial load in cases compared with controls. The unpaired Student's t-test was used to compare the means between two groups. In contrast, the one-way analysis of variance (ANOVA) test was used to compare three groups at a time. The mitochondrial levels were correlated separately with the blood HbA1C levels by applying linear regression. All statistical analyses were carried out at a 5% level of significance, and the p-value <0.05 was considered significant. The GraphPad Prism software version 2.0 was used for statistical analysis. The tables were plotted using Microsoft Office Excel 2010.

RESULTS

After staining the buccal smears with Janus green B stain prior to radiation, it was observed that the mean number of mitochondria per buccal cell in cases was fewer than the mean number of mitochondria per buccal cell in controls (Table 1). On subjecting the buccal cells of cases to near-infrared rays and then staining them with Janus green, it was observed that the contours of diabetic buccal cells became enlarged and distorted after radiation (Figure 1). The mitochondria present within the diabetic buccal cells became organized into clumps and shifted towards the periphery of the cell. Also, in those diabetic cells with a mean HbA1C value greater than 8 mg/dL, the mitochondria clusters moved away from the part of the cell that was close to the nucleus and migrated to the periphery of the cell, producing comet-like trails within the cell (Figures 1 and 2). Such a phenomenon was not observed in control cells after radiation, and there was no change in mitochondrial dots except that the cell outlines became distorted and the mitochondrial dots became brighter (Figure 1). It was observed that there was a significant association between the mean number of irradiated mitochondrial clumps per buccal cell of cases and the mean HbA1C values in blood (Table 2). The mean number of mitochondrial dots per buccal cell in cases before radiation, the mean number of irradiated mitochondrial clumps per buccal in cases after radiation, and the mean HbA1C values were compared using the one-way ANOVA test, and a significant association between each of the three groups was obtained (Table 3). Furthermore, the post-hoc Tukey HSD beta test (true post-hoc significant difference test) was applied to the three groups to validate the findings of the one-way ANOVA, and a significant Q-value was obtained between each of the three groups (Table 3). A positive linear correlation was obtained between the mean HbA1C levels and the mean number of irradiated mitochondrial clumps per cell in cases, further adding strength to this study (Table 2).

DISCUSSION

Eldarov et al.[7] found that mitochondria within the rat cells, when subjected to artificially induced diabetes, had fused with each other and then scattered away from the nucleus on subsequent application of stressors such as lipid peroxidation and intense light. A similar observation was noted by Brivio et al.[8] and Raza et al.[9], wherein they had shown that mitochondria within the cells of stress-induced diabetic mice fused with each

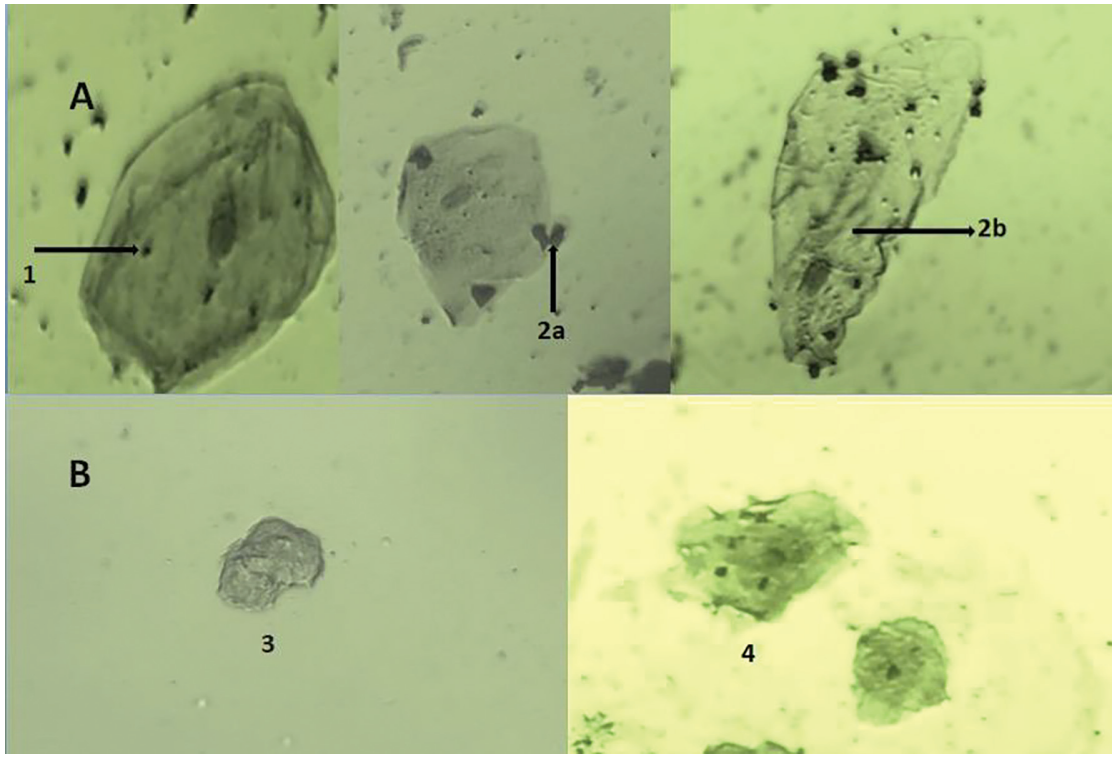

Figure 1. Buccal cell Mitochondria (A-cases, 1-normal before IR, 2a-clumps after IR, 2b-comets after IR, B-controls, 3-before IR, 4-after IR) Janus Green B stain, 100X

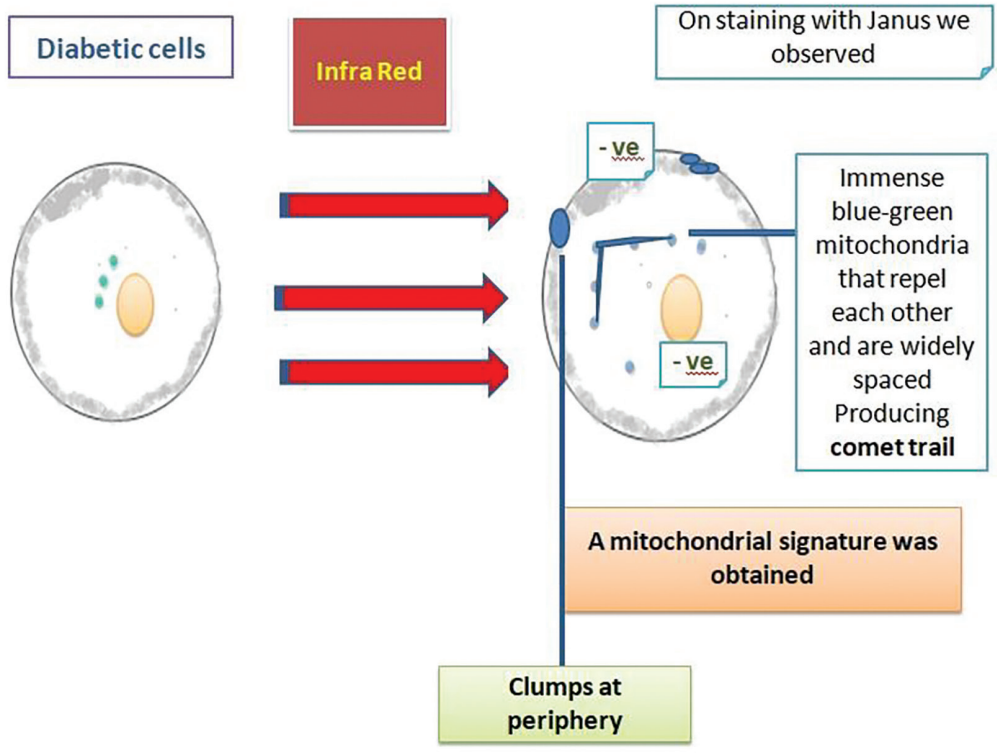

Figure 2. Schema showing the formation of mitochondrial signatures post infra red radiation in diabetic buccal cells

Table 1. Comparison between mean number of mitochondria per buccal cell in cases and controls prior to radiation.

Sl. no	Cases (n=30)		Controls (n=30)		t-test* p-value$
	Mean no.of mitochondria per buccal cell	Standard deviation (SD)	Mean no.of mitochondria per buccal cell	Standard deviation (SD)	
1	10.33	0.47	20.67	0.47	0.00019
2	9.67	0.41	20.67	0.36	
3	9.33	0.41	22	0.35	
4	7.66	0.41	20.67	0.47	
5	8.33	0.41	20.67	0.37	
6	8.67	0.47	20.67	0.45	
7	9	0.47	20.67	0.45	
8	9.33	0.47	20.67	0.45	
9	10	0.49	20.67	0.45	
10	9.33	0.47	20.67	0.45	
11	8	0.47	20.67	0.45	
12	8.67	0.47	22	0.38	
13	9	0.21	22	0.38	
14	8.67	0.29	22	0.38	
15	8.33	0.31	22	0.38	
16	8	0.29	22	0.38	
17	10	0.29	22	0.38	
18	9.67	0.27	22	0.39	
19	10	0.29	22	0.39	
20	10	0.29	19	0.39	
21	11.33	0.27	19	0.39	
22	11.33	0.31	19	0.39	
23	10	0.31	19	0.45	
24	10.67	0.31	19	0.45	
25	10	0.33	19	0.45	
26	10.67	0.31	20.67	0.45	
27	10.33	0.31	20.67	0.45	
28	10.33	0.31	20.67	0.45	
29	10	0.33	20.67	0.45	
30	10.33	0.31	20.67	0.45	
31	10.33	0.47	20.67	0.47	
32	9.67	0.41	20.67	0.36	
33	9.33	0.41	22	0.35	
34	7.66	0.41	20.67	0.47	
35	8.33	0.41	20.67	0.37	
36	8.67	0.47	20.67	0.45	
37	9	0.47	20.67	0.45	
38	9.33	0.47	20.67	0.45	
39	10	0.49	20.67	0.45	
40	9.33	0.47	20.67	0.45	
Aggregated mean±SD	9.47	0.38	20.75	0.42	

*Unpaired t-test was used, $statistically significant, SD: Standard deviation

Table 2. Comparison between the mean number of irradiated mitochondrial clumps per buccal cell in cases with their blood HbA1C levels.

Sl. no	Cases (n=30)					
	Mean no.of mitochondrial clumps per buccal cell	Standard deviation (SD)	Mean HbA1C values of last one year	Standard deviation	t-test* p-value$	Linear regression
1	2.33	0.37	7.1	0.37	0.0031	y=1.53x+3.97 positive@ correlation, p=0.0001,
2	1.33	0.37	6.1	0.31		
3	3	0.37	9.1	0.31		
4	2	0.37	7.1	0.31		
5	1.33	0.37	6.1	0.31		
6	1.33	0.45	6.2	0.31		
7	1.33	0.45	6.2	0.31		
8	1.33	0.45	6.2	0.31		
9	1.33	0.45	6.2	0.29		
10	1.33	0.39	6.2	0.29		
11	1.33	0.33	6.2	0.29		
12	2.33	0.39	7.2	0.29		
13	2.33	0.33	7.2	0.29		
14	2.33	0.33	7.2	0.29		
15	2.33	0.33	7.2	0.29		
16	2.33	0.33	7.2	0.33		
17	2.33	0.33	7.2	0.33		
18	3	0.33	9.2	0.22		
19	3	0.33	8.6	0.22		
20	1	0.33	6.2	0.22		
21	2	0.33	7.4	0.22		
22	2	0.33	7.4	0.22		
23	3	0.33	8.9	0.22		
24	3	0.33	8.9	0.22		
25	2	0.45	6.2	0.22		
26	2	0.45	7	0.22		
27	2	0.45	7	0.44		
28	1	0.45	6.2	0.44		
29	2.33	0.45	7.1	0.44		
30	2	0.45	7.1	0.44		
31	2.33	0.37	7.1	0.37		
32	1.33	0.37	6.1	0.31		
33	3	0.37	9.1	0.31		
34	2	0.37	7.1	0.31		
35	1.33	0.37	6.1	0.31		
36	1.33	0.45	6.2	0.31		
37	1.33	0.45	6.2	0.31		
38	1.33	0.45	6.2	0.31		
39	1.33	0.45	6.2	0.29		
40	1.33	0.39	6.2	0.29		
Aggregated mean and SD	1.92	0.39	6.99	0.31		

*Unpaired t test was used, $statistically significant, @both parameters were deviating positively in one direction with good correlation, SD: Standard deviation

Table 3. Comparison between no. of mitochondria, mitochondrial clumps and blood HbA1C levels in cases.

	Cases (n=30)			
Parameter	**Mean±SD**	**f-ratio value between the group parameters**	**One way ANOVA (p-value)***	**Post-hoc tukey HSD@ (beta) to validate the ANOVA (p-value)***
Aggregated mean no. of mitochondrial dots per buccal cell in cases	9.47±0.38	593.706	0.00011	0.00121
Aggregated mean no. of mitochondrial clumps per buccal cell in cases	1.92±0.39			
Mean blood HbA1C levels in cases (mg/dl)	6.99±0.31			

*Significant ANOVA, @true post-hoc significant differencce, SD: Standart deviation, ANOVA: Analysis of variance

other and exhibited a metabolomic signature by moving slightly away from the nucleus upon the application of external stressors. In this study, we showed that mitochondria within the buccal cells of diabetic humans formed clumps on being subjected to near infrared radiation and shifted towards the periphery of the cell, sometimes even distorting the cell's outline. The authors would like to term this phenomenon "mitochondrial signatures" exhibited by the mitochondria inside the diabetic buccal cells when they receive a radiation boost. Goh et al.[10] and Li et al.[11] observed that guinea pig cells under severe oxidative states such as diabetes, when subjected to laser, formed an oscillatory pattern that shifted away from the center of the cell. Romanova et al.[12] observed similar findings in ovarian cells of diabetic Chinese hamsters when subjected to oxidative stress, wherein the mitochondria underwent a peripheral shift away from the nucleus. In our study, we found that the mitochondria within the buccal cells of those diabetic patients in whom the blood HbA1C levels were more than 8 mg/dL formed comet-like trails along with peripheral clumps during their migration towards the periphery of the cell away from the nucleus. On the other hand, those mitochondria within the diabetic buccal cells of patients whose HbA1C values were less than 8 mg/dL did not show a comet trail; rather, they just formed clumps at the periphery of the squamous cell.

The number of mitochondrial dots that representing whole free mitochondria was found to be reduced in human diabetic buccal cells, as compared to normal cells in this study. Our findings allude to Kwak et al.[1] and Sivitz and Yorek[2] which showed that the mitochondria in the cells of mammals subjected to diabetes would undergo dysfunction due to dysregulation of the genes coding for mitochondrial proteins. The increase in mitochondrial clumps after the infrared stimulation in diabetic buccal cells suggested the massive influx of calcium from the mitochondrial membranes, and the shift of mitochondria to the periphery was possibly due to the release of electrons from their membranes. Latti et al.[13], had theorized the importance of buccal cells as indicator tools in diabetes and this study also proves the same as buccal cells provided a clear image of the free mitochondrial behaviour in diabetes. Ravindran et al.[14] have shown that the mucins between the buccal cells increased in diabetics and postulated that the number of mitochondria in diabetic buccal cells may have an impact due to the mucins and also found an association between salivary glucose and mucins. This study partly alluded to the findings of Ravindran et al.[14], due to the observations which revealed that the number of mitochondria within the buccal cells in this study correlated well with the number of peripheral mitochondrial clumps and the levels of HbA1C seen in diabetic individuals. Hence, it can be said that an association exists between the levels of advanced glycation and the levels of mitochondria and that the end products of glycation could have induced the mitochondria to emit the peripheral clumpy shift signatures, along with comet trails, in response to a sudden flow of negatively charged electrons when bombarded with near infrared rays (Figure 2). The schematic diagram in Figure 2. explains the reason for mitochondrial clumps due to a negative charge boost of electrons, which were observed in response to oxidative stressors such as diabetes. The possible reasons could be the oxygen glucose deprivation, as observed by Yu et al.[15], in the cortical neurons of lower mammals, or could be due to the rapid calcium influx in response to glycation end products excited by infrared rays, as observed by Barrett et al.[16] in lower mammals. The possible explanations behind the formation of clumps and shifts in mitochondria within the diabetic buccal epithelial cells could either be due to dense electron-induced apoptotic

trigger mechanisms that initiated when the mitochondria try to align themselves to the infra-red rays to counter-balance Earth's magnetic field, or due to the triggering of mitochondrial signaling pathways. These pathways are initiated by upstream mitochondrial regulatory proteins in response to glycosylation end products and oxidative stress[17,18]. The findings in our study partly alluded to the excitatory findings of mitochondria in diabetic mammals observed by other researchers. The clumpy peripheral mitochondrial signatures with comet-like trails observed by us in human diabetic cells after radiation were quite unique, and could be used along with HbA1C levels in inspecting the course of type 2 diabetes, as it is non-invasive too.

CONCLUSIONS

Mitochondrial signatures in the form of peripheral clumps were observed in diabetic buccal cells after exposure to infrared rays. Intracellular mitochondrial comet trails were noticed in advanced diabetic cells, post-radiation. There was an overall decrease in free mitochondrial count in diabetic buccal cells as compared to controls. This spatial shift of mitochondrial dots could serve as a guide to indicate the progression of diabetes in collaboration with HbA1C levels.

Ethics

Ethics Committee Approval: Approval was obtained from the Institutional Ethics Committee for this study (reference number: AIIMS/BBN/IEC/OCT/2022/224, date: 08.10.2022).

Informed Consent: Was obtained from patients

Footnotes

Author Contributions

Surgical and Medical Practices: S.S.M.C., S.S., G.N.K., A.K.P., Concept: S.S.M.C., S.S., G.N.K., A.K.P., Design: S.S.M.C., S.S., G.N.K., A.K.P., Data Collection and/or Processing: S.S.M.C., S.S., G.N.K., A.K.P., Analysis and/or Interpretation: S.S.M.C., S.S., G.N.K., A.K.P., Literature Search: S.S.M.C., S.S., G.N.K., A.K.P., Writing: S.S.M.C., S.S., G.N.K., A.K.P.

Conflict of Interest: The authors have no conflict of interest to declare.

Financial Disclosure: The authors declared that this study has received no financial support.

REFERENCES

1. Kwak SH, Park KS, Lee KU, Lee HK. Mitochondrial metabolism and diabetes. J Diabetes Investig. 2010;1:161-9.
2. Sivitz WI, Yorek MA. Mitochondrial dysfunction in diabetes: from molecular mechanisms to functional significance and therapeutic opportunities. Antioxid Redox Signal. 2010;12:537-77.
3. World Health Organization. Use of glycated haemoglobin (HbA1c) in the diagnosis of diabetes mellitus: Abbreviated report of a WHO consultation. 1st ed. Geneva: World Health Organization; 2011. Available from: https://www.ncbi.nlm.nih.gov/books/NBK304271/
4. Saenen ND, Provost EB, Cuypers A, et al. Child's buccal cell mitochondrial DNA content modifies the association between heart rate variability and recent air pollution exposure at school. Environ Int. 2019;123:39-49.
5. Cornford EM, Varesi JB, Hyman S, Damian RT, Raleigh MJ. Mitochondrial content of choroid plexus epithelium. Exp Brain Res. 1997;116:399-405.
6. Indira Gandhi National Open University. Staining and visualisation of mitochondria by Janus Green stain – Experiment 8. 1st ed. New Delhi: Indira Gandhi National Open University; 2020. Available from: https://egyankosh.ac.in/bitstream/123456789/68541/3/Experiment-8pdf
7. Eldarov CM, Vangely IM, Vays VB, et al. Mitochondria in the nuclei of rat myocardial cells. Cells. 2020;9:712.
8. Brivio P, Audano M, Gallo MT, et al. Metabolomic signature and mitochondrial dynamics outline the difference between vulnerability and resilience to chronic stress. Transl Psychiatry. 2022;12:87.
9. Raza H, Prabu SK, John A, Avadhani NG. Impaired mitochondrial respiratory functions and oxidative stress in streptozotocin-induced diabetic rats. Int J Mol Sci. 2011;12:3133-47.
10. Goh KY, Qu J, Hong H, et al. Impaired mitochondrial network excitability in failing guinea-pig cardiomyocytes. Cardiovasc Res. 2016;109:79-89.
11. Li Q, Su D, O'Rourke B, Pogwizd SM, Zhou L. Mitochondria-derived ROS bursts disturb Ca^{2+} cycling and induce abnormal automaticity in guinea pig cardiomyocytes: a theoretical study. Am J Physiol Heart Circ Physiol. 2015;308:H623-36.
12. Romanova N, Schmitz J, Strakeljahn M, Grünberger A, Bahnemann J, Noll T. Single-cell analysis of CHO cells reveals clonal heterogeneity in hyperosmolality-induced stress response. Cells. 2022;11:1763.
13. Latti BR, Birajdar SB, Latti RG. Periodic acid schiff-diastase as a key in exfoliative cytology in diabetics: a pilot study. J Oral Maxillofac Pathol. 2015;19:188-91.
14. Ravindran R, Gopinathan DM, Sukumaran S. Estimation of salivary glucose and glycogen content in exfoliated buccal mucosal cells of patients with type ii diabetes mellitus. J Clin Diagn Res. 2015;9:ZC89-93.
15. Yu Z, Liu N, Zhao J, et al. Near infrared radiation rescues mitochondrial dysfunction in cortical neurons after oxygen-glucose deprivation. Metab Brain Dis. 2015;30:491-6.
16. Barrett JN, Barrett EF, Rajguru SM. Mitochondrial responses to intracellular Ca^{2+} release following infrared stimulation. J Neurophysiol. 2023;129:700-16.
17. Frank S, Oliver L, Lebreton-De Coster C, et al. Infrared radiation affects the mitochondrial pathway of apoptosis in human fibroblasts. J Invest Dermatol. 2004;123:823-31.
18. Nguyen LM, Malamo AG, Larkin-Kaiser KA, Borsa PA, Adhihetty PJ. Effect of near-infrared light exposure on mitochondrial signaling in C2C12 muscle cells. Mitochondrion. 2014;14:42-8.

DOI: 10.4274/MMJ.galenos.2025.40460
Medeni Med J 2025;40:101-109

Review

TMPRSS2: A Key Host Factor in SARS-CoV-2 Infection and Potential Therapeutic Target

TMPRSS2: SARS-CoV-2 Enfeksiyonunda Önemli Bir Konak Faktörü ve Potansiyel Terapötik Hedef

Haily Liduin KOYOU[1], Mohd Nazil SALLEH[2], Caroline Satu JELEMIE[3], Mohd Jaamia Qaadir BADRIN[4], Muhammad Evy PRASTIYANTO[5], Vasudevan RAMACHANDRAN[1]

[1]University College of MAIWP International Faculty of Medicine and Health Sciences, Department of Medical Sciences, Kuala Lumpur, Malaysia
[2]University College of MAIWP International, Centre of Excellence in Advanced Molecular Diagnostics, Kuala Lumpur, Malaysia
[3]Universiti Malaysia Sabah Faculty of Medicine and Health Sciences, Department of Nursing, Sabah, Malaysia
[4]Universiti Selangor Faculty of Health Sciences, Department of Medical Diagnostics, Shah Alam, Malaysia
[5]Universitas Muhhamadiyah Semarang Faculty of Nursing and Health Sciences, Department of Medical Laboratory Technology, Semarang, Indonesia

ABSTRACT

The transmembrane serine protease 2 (*TMPRSS2*) gene plays a crucial role in severe acute respiratory syndrome coronavirus 2 (SARS-CoV-2) infection by priming the viral spike protein for membrane fusion and facilitating viral entry into host cells. This review aims to explore the molecular function of TMPRSS2, its genetic variations, and its potential as a therapeutic target in corona virus disease 2019 (COVID-19) and other respiratory viral infections. TMPRSS2 is highly expressed in lung and prostate tissues and is regulated by androgens, which may contribute to sex-based differences in COVID-19 severity. Genetic polymorphisms in TMPRSS2 have been been associated with variability in disease susceptibility and severity across populations. Several TMPRSS2 inhibitors, including serine protease inhibitors, such as camostat mesylate and nafamostat, have demonstarted promise in blocking viral entry. In addition, RNA based strategies such as siRNA and clustered regularly interspaced short palindromic repeats offer potential approaches for downregulating TMPRSS2 expression. However, the development of selective inhibitors that avoid off target effects remains a challenge. The presence of *TMPRSS2-ERG* gene fusion, commonly found in prostate cancer, has also been linked to altered COVID-19 susceptibility, suggesting a complex interplay between viral infection and cancer biology. This review also discusses future perspectives, including large-scale genomic studies to identify high-risk individuals, the development of next-generation TMPRSS2 inhibitors, and potential broad-spectrum antiviral therapies targeting TMPRSS2.

Keywords: Transmembrane serine protease 2, Severe acute respiratory syndrome coronavirus 2, corona virus disease-2019, viral entry, therapeutic targets

ÖZ

Transmembran serin proteaz 2 (*TMPRSS2*) geni, membran füzyonu için viral spike proteinini hazırlayarak ve konakçı hücrelere viral girişi kolaylaştırarak şiddetli akut solunum yolu sendromu koronavirüs 2 (SARS-CoV-2) enfeksiyonunda önemli bir rol oynar. Bu derleme, *TMPRSS2*'nin moleküler işlevini, genetik varyasyonlarını ve koronavirüs hastalığı 2019 (COVID-19) ve diğer solunum yolu viral enfeksiyonlarında terapötik bir hedef olarak potansiyelini araştırmayı amaçlamaktadır. TMPRSS2 akciğer ve prostat dokularında yüksek oranda eksprese edilir ve androjenler tarafından düzenlenir, bu da COVID-19 şiddetinde cinsiyete dayalı farklılıklara katkıda bulunabilir. TMPRSS2'deki genetik polimorfizmler, popülasyonlar arasında hastalık duyarlılığı ve şiddetindeki değişkenlikle ilişkilendirilmiştir. Camostat mesilat ve nafamostat gibi serin proteaz inhibitörleri de dahil olmak üzere çeşitli TMPRSS2 inhibitörleri, viral girişin bloke edilmesinde umut vaat etmiştir. Buna ek olarak, siRNA ve kümelenmiş düzenli aralıklı kısa palindromik tekrarlar gibi RNA tabanlı stratejiler, TMPRSS2 ekspresyonunun aşağı regülasyonu için potansiyel yaklaşımlar sunmaktadır. Bununla birlikte, hedef dışı etkilerden kaçınan seçici inhibitörlerin geliştirilmesi bir zorluk olmaya devam etmektedir.

Prostat kanserinde yaygın olarak bulunan *TMPRSS2-ERG* gen füzyonunun varlığı da değişmiş COVID-19 duyarlılığı ile bağlantılıdır ve viral enfeksiyon ile kanser biyolojisi arasında karmaşık bir etkileşim olduğunu düşündürmektedir. Bu derlemede ayrıca, yüksek riskli bireyleri belirlemek için büyük ölçekli genomik çalışmalar, yeni nesil TMPRSS2 inhibitörlerinin geliştirilmesi ve TMPRSS2'yi hedefleyen potansiyel geniş spektrumlu antiviral tedaviler de dahil olmak üzere geleceğe yönelik perspektifler tartışılmaktadır.

Anahtar kelimeler: Transmembran serin proteaz 2, şiddetli akut solunum yolu sendromu koronavirüs 2, koronavirüs hastalığı 2019, viral giriş, terapötik hedefler

Address for Correspondence: V. Ramachandran, University College of MAIWP International Faculty of Medicine and Health Sciences, Department of Medical Sciences, Kuala Lumpur, Malaysia
E-mail: drvasu@ucmi.edu.my **ORCID ID:** orcid.org/0000-0003-0044-1626

Received: 02.02.2025
Accepted: 10.05.2025
Published: 26 June 2025

Cite as: Haily Liduin K, Salleh MN, Jelemie CS, Badrin MJQ, Prastiyanto ME, Ramachandran V. TMPRSS2: A key host factor in SARS-CoV-2 infection and potential therapeutic target. Medeni Med J.

INTRODUCTION

The coronavirus disease 2019 (COVID-19) pandemic, caused by the severe acute respiratory syndrome coronavirus 2 (SARS-CoV-2), has led to an unprecedented global health crisis, affecting millions of people worldwide[1,2]. SARS-CoV-2 primarily targets the respiratory system, with clinical manifestations ranging from mild flu-like symptoms to severe pneumonia, acute respiratory distress syndrome (ARDS), and multi-organ failure. Despite extensive research on viral pathogenesis and host-virus interactions, effective antiviral strategies remain limited[3,4]. One of the key factors influencing SARS-CoV-2 infection is the host protease *transmembrane serine protease 2* (*TMPRSS2*) (Figure 1), which plays a critical role in viral entry by facilitating spike (S) protein priming and fusion with host cell membranes[5].

TMPRSS2 is a *TMPRSS2* encoded by the TMPRSS2 gene located on chromosome 21q22.36.

Its role in viral infections was first recognized in influenza and other coronaviruses (e.g., SARS-CoV-1 and MERS-CoV,), where it enhanced viral entry by cleaving hemagglutinin (HA) and spike glycoproteins. In SARS-CoV-2 infection, TMPRSS2 functions in conjunction with *angiotensin-converting enzyme 2* (ACE2), the primary receptor for the virus. Upon binding of the viral S protein to ACE2, TMPRSS2 cleaves the S1/S2 site, triggering membrane fusion and viral entry, thereby bypassing the endosomal pathway[7].

Interestingly, TMPRSS2 is androgen-regulated, which may explain sex-based differences in COVID-19 severity, with males exhibiting higher susceptibility and worse outcomes than females. Furthermore, genetic polymorphisms in TMPRSS2 have been associated with variations in susceptibility to infection and severity across different populations. Additionally, TMPRSS2-*E26 transformation-specific-related gene* (*ERG*) fusion, commonly found in prostate cancer, has raised questions about the potential link between cancer, androgen signalling, and COVID-19 outcomes[8].

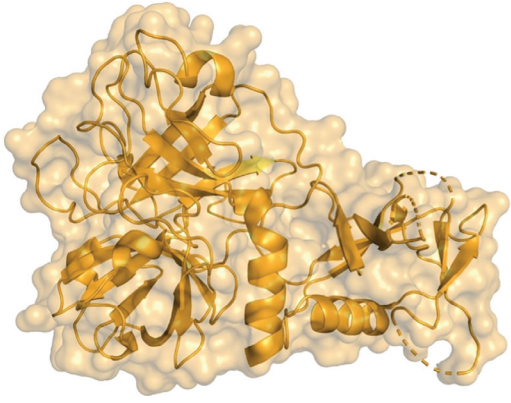

Figure 1. Illustration of TMPRSS2 protein structure from the PDB database.

TMPRSS2: Transmembrane protease serine 2, PDB: Protein Data Bank

The *TMPRSS2* gene plays a critical role in SARS-CoV-2 infection by helping the virus enter human cells. It does so by priming the viral spike protein, allowing it to fuse with the host cell membrane. This process is androgen-regulated, meaning it is influenced by male hormones. As a result, males tend to have higher levels of TMPRSS2 and may experience more severe outcomes from COVID-19 compared to females. Additionally, genetic variations in TMPRSS2 have been linked to differences in how individuals respond to the virus, with some populations being more susceptible to infection or severe disease[8].

An important genetic alteration associated with prostate cancer is the TMPRSS2-ERG fusion, where the TMPRSS2 gene fuses with the *ERG* gene. This fusion leads to overexpression of the ERG protein, which contributes to prostate cancer progression[9]. Since TMPRSS2 is essential for SARS-CoV-2 entry into cells, the *TMPRSS2-ERG* fusion could increase the susceptibility of prostate cancer patients to COVID-19, as they may have higher levels of TMPRSS2 expression. This potential link between prostate cancer, androgen signaling, and COVID-19 severity has raised important questions[10,11]. Prostate cancer therapies, such as androgen deprivation therapy (ADT), may affect the immune system and influence how patients respond to viral infections like SARS-CoV-2. Understanding how the TMPRSS2-ERG fusion impacts both cancer and COVID-19 can help identify high-risk patients and inform potential treatment strategies[12].

Given the critical role of TMPRSS2 in viral entry, it has emerged as a promising therapeutic target for COVID-19. Several pharmacological inhibitors-including serine protease inhibitors such as camostat mesylate and Nafamostat-have demonstrated the ability to block TMPRSS2-mediated SARS-CoV-2 entry[13]. Additionally, RNA-based approaches, such as siRNA and clustered regularly interspaced short palindromic repeats-associated protein 9 (CRISPR)-Cas9, have been explored to downregulate TMPRSS2 expression. However, challenges remain in developing selective inhibitors that minimize off-target effects because TMPRSS2 also plays a physiological role in lung homeostasis.

This review aims to provide a comprehensive overview of TMPRSS2 in the context of SARS-CoV-2 infection, including its molecular function, genetic variability, and potential as a therapeutic target. We discuss emerging research on TMPRSS2 inhibitors, the impact of genetic polymorphisms on COVID-19 susceptibility, and future perspectives on targeting TMPRSS2 for broad-spectrum antiviral therapy. Understanding the interplay between

TMPRSS2 and SARS-CoV-2 may provide new insights into the disease mechanisms and pave the way for effective therapeutic interventions.

Structure and Function of *TMPRSS2*

The *TMPRSS2* gene encodes a *TMPRSS2* that plays a crucial role in various physiological and pathological processes, including viral infections and cancer progression[14]. This gene is highly expressed in epithelial tissues, particularly in the lungs, prostate, gastrointestinal tract, and kidneys, making it a key factor in respiratory viral infections[15].

TMPRSS2 is a membrane-bound serine protease that consists of several structural domains (Figure 2). The cytoplasmic domain (N-terminal region) is responsible for intracellular signalling. The transmembrane domain anchors proteins to the plasma membrane. The low-density lipoprotein receptor class A domain is thought to facilitate protein-protein interactions. The scavenger receptor cysteine-rich domain may be involved in ligand binding. A serine protease catalytic domain (C-terminal region) is responsible for cleaving and activating substrates, including viral glycoproteins[16]. The catalytic activity of TMPRSS2 depends on a conserved histidine (H), aspartic acid (D), and serine (S) catalytic triad, which is characteristic of serine proteases[17].

Beyond its involvement in viral infections, TMPRSS2 plays important roles in normal physiological processes. Particularly in lung homeostasis, TMPRSS2 is expressed in alveolar epithelial cells, where it regulates epithelial sodium channels, which are critical for lung fluid balance[18]. *TMPRSS2* is recognized for its regulation by androgens, particularly in the prostate, where its abnormal activity, such as fusion with the ERG oncogene, has been associated with the progression of prostate cancer. This regulation is mediated by the androgen receptor (AR)[19]. When androgens bind to AR, the complex translocates to the nucleus and enhances TMPRSS2 transcription by interacting with specific androgen-responsive elements within the gene's promoter region[20]. Although TMPRSS2 is clearly androgen-responsive, current evidence does not confirm whether postmenopausal women exhibit increased TMPRSS2 expression in the respiratory tract[21]. Nevertheless, the decline in estrogen levels after menopause may alter immune function, potentially affecting the response to viral infections. Further investigation is required to clarify TMPRSS2 expression patterns and their implications in this population[22,23]. TMPRSS2 expression in the gastrointestinal tract suggests a possible involvement in the regulation of digestive processes, while its presence in endothelial cells points to a potential role in maintaining vascular integrity and homeostasis[24,25].

TMPRSS2 in SARS-CoV-2 Infection

TMPRSS2 plays a crucial role in the early stages of SARS-CoV-2 infection by facilitating viral entry into the host cells (Figure 3). SARS-CoV-2, like other coronaviruses, relies on host proteases to cleave its spike (*S*) glycoprotein, which enables fusion with the host cell membrane. The viral spike protein is composed of two subunits: S1, which is responsible for receptor binding,

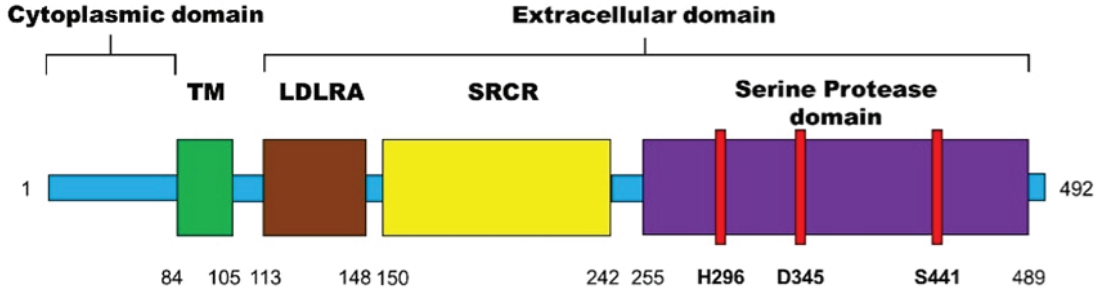

Figure 2. TMPRSS2 structural domains.

TMPRSS2: Transmembrane protease serine 2, LDLRA: Low-density lipoprotein receptor class A, SRCR: Scavenger Receptor Cysteine-Rich

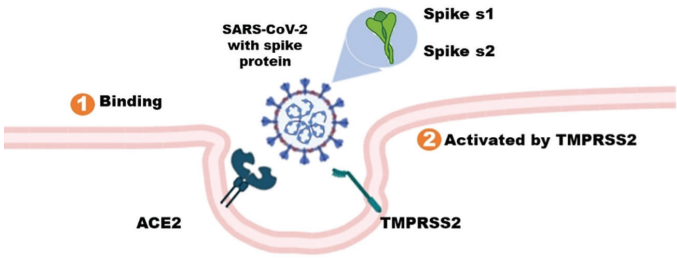

Figure 3. Illustration of TMPRSS2 protein structure from the PDB database.

TMPRSS2: Transmembrane protease serine 2, PDB: Protein Data Bank, ACE2: Angiotensin-converting enzyme 2, SARS-CoV-2: Severe acute respiratory syndrome coronavirus 2

and S2, which mediates membrane fusion. *TMPRSS2* specifically cleaves the S1/S2 junction and the S2′ site of the spike protein, which is essential for viral-host membrane fusion and subsequent viral RNA release into the cytoplasm[16].

SARS-CoV-2 primarily uses the ACE2 receptor for host cell attachment. The interaction between the viral receptor-binding domain of S1 and ACE2 is a prerequisite for infection. However, ACE2 binding alone is not sufficient for viral entry, and proteolytic activation of the spike protein is required to expose the fusion peptide. TMPRSS2 cleaves and activates the spike protein at the cell surface, enabling direct fusion of the viral and host membranes, bypassing the need for endosomal processing[16].

In the absence of *TMPRSS2*, SARS-CoV-2 can enter cells via an alternative endosomal pathway that is mediated by cathepsin L/B. However, this route is generally less efficient and is more dependent on endosomal acidification. Studies have shown that TMPRSS2-expressing cells have significantly higher viral infectivity compared to those relying on cathepsins alone[17]. This explains why inhibitors of *TMPRSS2*, such as Camostat mesylate, effectively block SARS-CoV-2 infection, whereas cathepsin inhibitors have limited efficacy.

Notably, TMPRSS2 expression is regulated by androgens, leading to higher expression levels in males compared to females. This may contribute to the observed sex-based differences in COVID-19 severity, with males experiencing higher rates of severe disease and mortality. Studies suggest that ADT, commonly used in prostate cancer treatment, may reduce TMPRSS2 expression and lower COVID-19 severity in prostate cancer patients[26].

Additionally, *TMPRSS2* expression levels increased with age, particularly in lung tissue. This may partially explain why older individuals are more susceptible to severe SARS-CoV-2 infections, as higher *TMPRSS2* levels can enhance viral entry and replication.

TMPRSS2-Mediated SARS-CoV-2 Pathogenesis

In addition to viral entry, *TMPRSS2* may contribute to COVID-19 severity by promoting viral spread and tissue damage. Infected epithelial cells undergo apoptosis and inflammatory cytokine release, exacerbating lung injury and leading to ARDS in severe cases[27]. *TMPRSS2*'s role in facilitating direct viral entry rather than endosomal processing may also influence immune evasion strategies employed by SARS-CoV-2.

The role of TMPRSS2 is not unique to SARS-CoV-2; it also plays a crucial role in other coronaviruses. Similar to SARS-CoV-2, SARS-CoV-1 utilizes TMPRSS2 for spike protein activation and cell entry. *TMPRSS2* inhibition reduces SARS-CoV-1 infectivity. Unlike SARS-CoV-2, MERS-CoV primarily binds to dipeptidyl peptidase 4 instead of ACE2. However, TMPRSS2 is still involved in spike protein priming, playing a role in viral tropism and pathogenesis[28]. *TMPRSS2* also activates the HA protein of influenza A virus, facilitating viral entry into host cells. This highlights its broad role in respiratory viral infections, making it an attractive antiviral target beyond coronaviruses.

Genetic Variability and Population Susceptibility

Genetic variation in *TMPRSS2* has been implicated in the differential susceptibility to SARS-CoV-2 infection and COVID-19 severity across populations. Polymorphisms in TMPRSS2 can influence its expression levels, enzymatic activity, and interaction with the viral spike protein, affecting viral entry efficiency and disease outcomes (Table 1)[16,29-33].

Several single-nucleotide polymorphisms (SNPs) in *TMPRSS2* have been identified as potential modulators of SARS-CoV-2 infection. Genome-wide association studies have revealed that variants such as rs2070788 and rs383510 are associated with increased expression of TMPRSS2 in lung tissues, potentially enhancing viral entry and increasing disease severity[16]. Conversely, certain loss-of-function mutations may confer partial resistance to SARS-CoV-2 by reducing TMPRSS2-mediated spike protein cleavage[33].

A study by Asselta et al.[29] reported that the rs12329760 (V160M) SNP, a missense variant in TMPRSS2, is associated with reduced proteolytic activity, potentially leading to lower viral entry efficiency and milder COVID-19 symptoms. This variant is more prevalent in

Table 1. Key TMPRSS2 polymorphisms and their association with COVID-19.

Study	SNP (rsID)	Variant type	Effect on TMPRSS2 expression	Population distribution	Impact on COVID-19 susceptibility/severity	c.DNA locus
Hoffmann et al.[16] (2020)	rs464397, rs469390, rs383510 and rs2070788	Upstream variant	Increased TMPRSS2 expression in lungs	High in Europeans and Africans	Higher risk of severe COVID-19 due to increased viral entry efficiency	chromosome 21q22.3,
Asselta et al.[29] (2020)	rs2285666 (c.439+4G>A) and rs35803318 (p.Val749Val)	Upstream variant	Increased TMPRSS2 expression	High in Europeans	Higher susceptibility to SARS-CoV-2 infection	Xp22 in intron 3
Irham et al.[30] (2020)	rs12329760 (p.Val160Met))	Missense mutation	Reduced TMPRSS2 protease activity	Common in East Asians	Potential protective effect, lower viral entry efficiency	chr21:41480570
Adli et al.[31] (2022)	rs75603675 (p.Gly197Ser)	Missense mutation	Alters TMPRSS2 enzymatic activity	Higher in South Asian populations	Possible role in modifying COVID-19 outcomes	chr21:41507982
Zeberg and Pääbo[32] (2020)	rs8134378 (c.585+312T>C)	Intronic variant	Affects TMPRSS2 regulation	High in African populations	Linked to severe COVID-19 cases in some studies	Intron 6, chr21:41521831
Daniloski et al.[33] (2020)	rs35074065 (c.-74+475A>G)	Regulatory variant	Alters TMPRSS2 transcription	Present in multiple ethnic groups	Associated with lung tissue expression variability	chr21:41461593

COVID-19: Corona virus disease 19, TMPRSS2 The transmembrane serine protease 2, SNP: Single-nucleotide polymorphisms

East Asian populations, suggesting potential population-level differences in COVID-19 susceptibility[30]. Studies have shown that *TMPRSS2* expression varies significantly across ethnic groups, which may contribute to disparities in COVID-19 severity. For instance, higher expression levels have been reported in European and African populations compared to East Asians, correlating with the prevalence of high-expression SNPs such as rs207078824. This could partly explain the observed differences in COVID-19 hospitalization and mortality rates among different ethnic groups[31].

Furthermore, variations in *TMPRSS2* expression were influenced by the local genetic landscape and evolutionary pressure. The high prevalence of specific TMPRSS2 SNPs in certain populations may reflect historical adaptation to past pandemics involving coronaviruses or other respiratory pathogens[32].

Androgen Regulation and Sex-Based Differences

Sex-based disparities in COVID-19 outcomes have been widely documented, with males experiencing higher mortality rates than females[35]. One contributing factor is the androgen-regulated expression of *TMPRSS2*, which is significantly upregulated in male tissues, including the lungs and prostate[36]. The androgen response element within the TMPRSS2 promoter region enhances its transcriptional activity in response to circulating testosterone levels, leading to higher expression in males[37].

This regulation may provide a mechanistic explanation for the higher disease severity observed in male subjects. In contrast, female sex hormones such as estrogen have been suggested to downregulate TMPRSS2 expression, potentially offering a protective effect[38]. Clinical trials have explored the use of ADT to reduce TMPRSS2 expression and mitigate COVID-19 severity in high-risk male populations[39].

Cancer-Related Gene Fusions and Their Potential Role in COVID-19 Susceptibility

Gene fusions, such as the *TMPRSS2-ERG* fusion commonly observed in prostate cancer, have been linked to altered TMPRSS2 expression, potentially affecting viral entry and increasing susceptibility to SARS-CoV-2[37]. However, gene fusions are not exclusive to prostate cancer. Similar alterations have been observed in other cancers, including lung, breast, and cholangiocarcinoma, where changes in TMPRSS2 expression could influence

COVID-19 outcomes[40,41]. While cancer-related gene fusions may contribute to altered immune responses, the direct connection between these fusions and COVID-19 severity remains an area of ongoing research[42,43].

Patients with cancers, particularly aggressive or metastatic types, are generally at higher risk for severe COVID-19 outcomes due to factors such as immune dysregulation, tumor microenvironment, and pre-existing comorbidities. However, further studies are needed to clarify whether specific gene fusions in various cancers contribute directly to SARS-CoV-2 susceptibility or severity[44,45].

TMPRSS2 as a Therapeutic Target

Given its critical role in SARS-CoV-2 entry, *TMPRSS2* has emerged as a promising therapeutic target for COVID-19 treatment. Unlike endosomal entry mechanisms that rely on cathepsins, *TMPRSS2*-mediated viral entry occurs at the plasma membrane, facilitating direct fusion of the viral envelope with the host cell membrane. Blocking *TMPRSS2* activity effectively prevents spike protein cleavage, thereby inhibiting viral entry and reducing infection rates. Unlike ACE2, which has essential physiological functions in the renin-angiotensin system, TMPRSS2 is a non-essential protease, making it a safer therapeutic target with fewer systemic side effects[16].

Several serine protease inhibitors have been investigated for their ability to block *TMPRSS2* activity and prevent SARS-CoV-2 infections. Camostat mesylate, a synthetic serine protease inhibitor, was initially developed for the treatment of chronic pancreatitis and postoperative reflux esophagitis. It has been shown to effectively inhibit *TMPRSS2*-mediated spike protein priming and prevent SARS-CoV-2 entry *in vitro*. Early clinical trials suggested that Camostat mesylate might reduce viral load and improve outcomes in COVID-19 patients. However, its short half-life and need for frequent dosing present limitations for clinical use[46].

Nafamostat, a structurally related serine protease inhibitor, exhibited higher potency than camostat in inhibiting *TMPRSS2* activity. Due to its strong anti-coagulant properties, it has been explored as a dual therapy for COVID-19 patients with thrombotic complications. Nafamostat efficiently blocks spike protein processing at nanomolar concentrations, and has demonstrated promising results in preclinical studies. However, intravenous administration and potential bleeding risks limit its widespread use[47].

Bromhexine, an over-the-counter mucolytic drug, has been identified as an indirect *TMPRSS2* inhibitor. It reduces TMPRSS2 expression, and has been shown to be effective in decreasing viral replication in preliminary studies. While promising, further clinical validation is required to establish its role in COVID-19 treatment[48].

Gene-silencing technologies offer an alternative approach to inhibiting TMPRSS2, reducing its expression rather than directly targeting its enzymatic activity; siRNA-based therapeutics can selectively degrade TMPRSS2 mRNA, reducing protein expression and preventing SARS-CoV-2 entry. Several *in vitro* studies have demonstrated that *TMPRSS2*-targeting siRNAs effectively suppress viral infection. However, challenges such as efficient delivery, stability, and potential off-target effects remain significant barriers to clinical application[49].

CRISPR-Cas9 and CRISPR interference (CRISPRi) technologies have been explored for the selective knockdown of *TMPRSS2* expression. These genome-editing approaches could provide long-term resistance against coronaviruses, but face regulatory and ethical challenges before clinical translation[50].

Because *TMPRSS2* is regulated by androgens, hormonal modulation has been proposed as a strategy to reduce its expression and limit SARS-CoV-2 infection. ADT, which is commonly used for prostate cancer, has been suggested as a potential strategy for reducing *TMPRSS2* expression in COVID-19 patients. Drugs, such as bicalutamide and enzalutamide, which inhibit AR signaling, have shown promise in reducing *TMPRSS2* levels in lung tissues. Retrospective studies have suggested that prostate cancer patients receiving ADT have lower rates of severe COVID-19. However, broader clinical trials are needed to validate these findings[51].

Finasteride and dutasteride, used to treat benign prostatic hyperplasia, inhibit 5-alpha reductase, an enzyme that converts testosterone to its more active form, dihydrotestosterone (DHT). By lowering the DHT levels, these drugs may indirectly reduce *TMPRSS2* expression and viral entry. Clinical trials are currently underway to assess their efficacy against COVID-19. Several Food and Drug Administration-approved drugs have been investigated for TMPRSS2 inhibition, and aprotinin has shown efficacy in inhibiting SARS-CoV-2 entry. Aprotinin is a protease inhibitor used in surgeries to reduce bleeding. E-64d, a cathepsin inhibitor, has been explored in combination with *TMPRSS2* inhibitors to block both the membrane fusion and endosomal viral entry pathways. While *TMPRSS2* inhibitors prevent membrane fusion, ACE2-based therapies, such as soluble ACE2 decoys, can block viral attachment. Combining

TMPRSS2 inhibition with ACE2 blockade may enhance antiviral efficacy[52].

Challenges and Future Directions

Despite the promise of *TMPRSS2* inhibitors, several challenges remain to be overcome. Selective inhibition: *TMPRSS2* plays physiological roles in lung function, and complete inhibition may have unintended side effects. The development of highly selective inhibitors that target viral entry while preserving normal lung function is crucial. Delivery mechanisms: RNA-based therapies require efficient delivery systems that target lung epithelial cells. Advances in nanoparticle and lipid-based delivery systems could improve their clinical feasibility[53].

Clinical validation: many *TMPRSS2* inhibitors have shown efficacy in preclinical models, but large-scale clinical trials are required to confirm their safety and effectiveness in COVID-19 patients. Broad-Spectrum Antiviral potential: since *TMPRSS2* also facilitates infection by other coronaviruses (e.g., SARS-CoV-1, MERS-CoV) and influenza viruses, developing *TMPRSS2*-targeting drugs could provide protection against future pandemics[16].

CONCLUSION

TMPRSS2 plays a pivotal role in the pathogenesis of SARS-CoV-2 by facilitating viral entry through the cleavage of the spike protein. Its expression in lung and prostate tissues, combined with androgen regulation, may explain the sex-based differences in COVID-19 severity. Genetic variants of *TMPRSS2* contribute to the variability in disease susceptibility and severity, highlighting the need for personalized therapeutic strategies. Several *TMPRSS2* inhibitors, including serine protease inhibitors such as Camostat mesylate and Nafamostat, show promise in clinical trials for reducing viral entry and infection. Additionally, RNA-based approaches, such as siRNA and CRISPR, offer potential strategies for downregulating *TMPRSS2* expression. The association of *TMPRSS2* with prostate cancer underscores its dual role in viral infection and cancer biology, suggesting broader therapeutic implications. Future research should focus on large-scale genomic studies to identify high-risk populations and develop selective *TMPRSS2* inhibitors. These efforts will be key to advancing antiviral therapies for COVID-19 and preparing for future pandemics involving similar respiratory viruses. Targeting *TMPRSS2* offers a promising approach for managing COVID-19 and other viral infections.

Ethics

Author Contributions

Concept: M.N.S., V.R., Design: H.L.K., V.R., Data Collection and/or Processing: C.S.J., M.J.Q.B., M.E.P., Analysis and/or Interpretation: M.N.S., V.R., Literature Search: H.L.K., C.S.J., M.J.Q.B., Writing: H.L.K., M.E.P.

Conflict of Interest: The authors have no conflict of interest to declare.

Financial Disclosure: The authors declared that this study has received no financial support.

REFERENCES

1. Hussain M, Jabeen N, Amanullah A, Baig AA, Aziz B, Shabbir S, et al. Structural basis of SARS-CoV-2 spike protein priming by TMPRSS2. 2020;6:350-60
2. Reis S, Faske A, Monsef I, et al. Anticoagulation in COVID-19 patients - an updated systematic review and meta-analysis. Thromb Res. 2024;238:141-150
3. Cascella M, Rajnik M, Aleem A, Dulebohn SC, Di Napoli R. Features, evaluation, and treatment of coronavirus (COVID-19). StatPearls. 2025.
4. Amara A, Trabelsi S, Hai A, Zaidi SHH, Siddiqui F, Alsaeed S. Equivocating and deliberating on the probability of covid-19 infection serving as a risk factor for lung cancer and common molecular pathways serving as a link. Pathogens. 2024;13:1070.
5. Fuentes-Prior P. Priming of SARS-CoV-2 S protein by several membrane-bound serine proteinases could explain enhanced viral infectivity and systemic COVID-19 infection. J Biol Chem. 2021;296:100135.
6. Thunders M, Delahunt B. Gene of the month: TMPRSS2 (transmembrane serine protease 2). J Clin Pathol. 2020;73:773-6.
7. Chen JT. Anti-SARS-CoV-2 Activity of Flavonoids. Boca Raton: CRC Press; 2024.
8. Baratchian M, McManus JM, Berk MP, et al. Androgen regulation of pulmonary AR, TMPRSS2 and ACE2 with implications for sex-discordant COVID-19 outcomes. Sci Rep. 2021;11:11130.
9. Raina K, Kant R, Prasad RR, et al. Characterization of stage-specific tumor progression in TMPRSS2-ERG (fusion)-driven and non-fusion-driven prostate cancer in GEM models. Mol Carcinog. 2022;61:717-34.
10. Sari Motlagh R, Abufaraj M, Karakiewicz PI, et al. Association between SARS-CoV-2 infection and disease severity among prostate cancer patients on androgen deprivation therapy: a systematic review and meta-analysis. World J Urol. 2022;40:907-14.
11. Afshari A, Janfeshan S, Yaghobi R, Roozbeh J, Azarpira N. Covid-19 pathogenesis in prostatic cancer and TMPRSS2-ERG regulatory genetic pathway. Infect Genet Evol. 2021;88:104669.
12. Montopoli M, Zumerle S, Vettor R, et al. Androgen-deprivation therapies for prostate cancer and risk of infection by SARS-CoV-2: a population-based study (N = 4532). Ann Oncol. 2020;31:1040-5.
13. Durairajan SSK, Singh AK, Saravanan UB, et al. Gastrointestinal manifestations of SARS-CoV-2: transmission, pathogenesis, immunomodulation, microflora dysbiosis, and clinical implications. Viruses. 2023;15:1231.

14. Bertram S, Heurich A, Lavender H, et al. Influenza and SARS-coronavirus activating proteases TMPRSS2 and HAT are expressed at multiple sites in human respiratory and gastrointestinal tracts. PLoS One. 2012;7:e35876.
15. Vaarala MH, Porvari KS, Kellokumpu S, Kyllönen AP, Vihko PT. Expression of transmembrane serine protease TMPRSS2 in mouse and human tissues. J Pathol. 2001;193:134-40.
16. Hoffmann M, Kleine-Weber H, Schroeder S, et al. SARS-CoV-2 cell entry depends on ACE2 and TMPRSS2 and is blocked by a clinically proven protease inhibitor. Cell. 2020;181:271-80.e8.
17. Matsuyama S, Nao N, Shirato K, et al. Enhanced isolation of SARS-CoV-2 by TMPRSS2-expressing cells. Proc Natl Acad Sci U S A. 2020;117:7001-3.
18. Cheng Z, Zhou J, To KK, et al. Identification of TMPRSS2 as a susceptibility gene for severe 2009 pandemic A(H1N1) influenza and A(H7N9) influenza. J Infect Dis. 2015;212:1214-21.
19. Tomlins SA, Rhodes DR, Perner S, et al. Recurrent fusion of TMPRSS2 and ETS transcription factor genes in prostate cancer. Science. 2005;310:644-8.
20. Deng Q, Rasool RU, Russell RM, Natesan R, Asangani IA. Targeting androgen regulation of TMPRSS2 and ACE2 as a therapeutic strategy to combat COVID-19. iScience. 2021;24:102254.
21. Wang H, Sun X, L VonCannon J, Kon ND, Ferrario CM, Groban L. Estrogen receptors are linked to angiotensin-converting enzyme 2 (ACE2), ADAM metallopeptidase domain 17 (ADAM-17), and transmembrane protease serine 2 (TMPRSS2) expression in the human atrium: insights into COVID-19. Hypertens Res. 2021;44:882-4.
22. Vom Steeg LG, Shen Z, Collins J, et al. Increases in the susceptibility of human endometrial CD4+ T cells to HIV-1 infection post-menopause are not dependent on greater viral receptor expression frequency. Front Immunol. 2025;15:1506653.
23. Patel MV, Shen Z, Hopkins DC, Barr FD, Wira CR. Aging Selectively Alters PRR and ISG expression in endo- and ecto-cervical stromal fibroblasts from the human female reproductive tract. Am J Reprod Immunol. 2025;93:e70031.
24. Wettstein L, Kirchhoff F, Münch J. The Transmembrane Protease TMPRSS2 as a therapeutic target for COVID-19 treatment. Int J Mol Sci. 2022;23:1351.
25. Matarese A, Gambardella J, Sardu C, Santulli G. miR-98 regulates TMPRSS2 expression in human endothelial cells: Key implications for COVID-19. Biomedicines. 2020;8:462.
26. Shirato K, Kawase M, Matsuyama S. Middle east respiratory syndrome coronavirus infection mediated by the transmembrane serine protease TMPRSS2. J Virol. 2013;87:12552-61.
27. Zang R, Gomez Castro MF, et al. TMPRSS2 and TMPRSS4 promote SARS-CoV-2 infection of human small intestinal enterocytes. Sci Immunol. 2020;5:eabc3582.
28. Glowacka I, Bertram S, Müller MA, et al. Evidence that TMPRSS2 activates the severe acute respiratory syndrome coronavirus spike protein for membrane fusion and reduces viral control by the humoral immune response. J Virol. 2011;85:4122-34.
29. Asselta R, Paraboschi EM, Mantovani A, Duga S. ACE2 and TMPRSS2 variants and expression as candidates to sex and country differences in COVID-19 severity in Italy. Aging (Albany NY). 2020;12:10087-98.
30. Irham LM, Chou WH, Calkins MJ, Adikusuma W, Hsieh SL, Chang WC. Genetic variants that influence SARS-CoV-2 receptor TMPRSS2 expression among population cohorts from multiple continents. Biochem Biophys Res Commun. 2020;529:263-9.
31. Adli A, Rahimi M, Khodaie R, Hashemzaei N, Hosseini SM. Role of genetic variants and host polymorphisms on COVID-19: From viral entrance mechanisms to immunological reactions. J Med Virol. 2022;94:1846-65.
32. Zeberg H, Pääbo S. The major genetic risk factor for severe COVID-19 is inherited from Neanderthals. Nature. 2020;587:610-2.
33. Daniloski Z, Jordan TX, Wessels HH, et al. Identification of required host factors for SARS-CoV-2 infection in human cells. Cell. 2021;184:92-105.e16.
34. Elnagdy MH, Magdy A, Eldars W, et al. Genetic association of ACE2 and TMPRSS2 polymorphisms with COVID-19 severity; a single centre study from Egypt. Virol J. 2024;21:27.
35. Peckham H, de Gruijter NM, Raine C, et al. Male sex identified by global COVID-19 meta-analysis as a risk factor for death and ITU admission. Nat Commun. 2020;11:6317.
36. Wambier CG, Goren A, Vaño-Galván S, et al. Androgen sensitivity gateway to COVID-19 disease severity. Drug Dev Res. 2020;81:771-6.
37. Stopsack KH, Mucci LA, Antonarakis ES, Nelson PS, Kantoff PW. TMPRSS2 and COVID-19: serendipity or opportunity for intervention? Cancer Discov. 2020;10:779-82.
38. Scully EP, Haverfield J, Ursin RL, Tannenbaum C, Klein SL. Considering how biological sex impacts immune responses and COVID-19 outcomes. Nat Rev Immunol. 2020;20:442-7.
39. McCoy J, Cadegiani FA, Wambier CG, et al. 5-alpha-reductase inhibitors are associated with reduced frequency of COVID-19 symptoms in males with androgenetic alopecia. J Eur Acad Dermatol Venereol. 2021;35:e243-6.
40. Gupta B, Wu S, Ou S, Darabi S, Mileham K, Gandhi N, et al. NRG1 fusions in solid tumors. Journal of Clinical Oncology. 2023. https://ascopubs.org/doi/pdf/10.1200/JCO.2023.41.16_suppl.3132
41. Argani P, Palsgrove DN, Anders RA, et al. A Novel NIPBL-NACC1 gene fusion is characteristic of the cholangioblastic variant of intrahepatic cholangiocarcinoma. Am J Surg Pathol. 2021;45:1550-60.
42. Claps M, Jachetti E, Badenchini F, et al. Effect of SNPs in TMPRSS2 to severe COVID-19 in patients with prostate cancer. Journal of Clinical Oncology. 2023. https://ascopubs.org/doi/10.1200/JCO.2023.41.16_suppl.e17043
43. Fu J, Liu S, Tan Q, et al. Impact of TMPRSS2 expression, mutation prognostics, and small molecule (CD, AD, TQ, and TQFL12) inhibition on pan-cancer tumors and susceptibility to SARS-CoV-2. Molecules. 2022;27:7413.
44. Ravaioli S, Tebaldi M, Fonzi E, et al. ACE2 and TMPRSS2 potential involvement in genetic susceptibility to SARS-COV-2 in cancer patients. Cell Transplant. 2020;29:963689720968749.
45. Liu X, Wei L, Xu F, et al. SARS-CoV-2 spike protein-induced cell fusion activates the cGAS-STING pathway and the interferon response. Sci Signal. 2022;15:eabg8744.
46. Khan U, Mubariz M, Khlidj Y, et al. Safety and efficacy of camostat mesylate for Covid-19: a systematic review and meta-analysis of randomized controlled trials. BMC Infect Dis. 2024;24:709.
47. Li K, Meyerholz DK, Bartlett JA, McCray PB Jr. The TMPRSS2 inhibitor nafamostat reduces SARS-CoV-2 pulmonary infection in mouse models of COVID-19. mBio. 2021;12:e0097021.

48. Vila Méndez ML, Antón Sanz C, Cárdenas García ADR, et al. Efficacy of bromhexine versus standard of care in reducing viral load in patients with mild-to-moderate COVID-19 disease attended in primary care: a randomized open-label trial. J Clin Med. 2022;12:142.

49. Ou X, Liu Y, Lei X, et al. Characterization of spike glycoprotein of SARS-CoV-2 on virus entry and its immune cross-reactivity with SARS-CoV. Nat Commun. 2020;11:1620.

50. Echaide M, Chocarro de Erauso L, Bocanegra A, Blanco E, Kochan G, Escors D. mRNA vaccines against SARS-CoV-2: advantages and caveats. Int J Mol Sci. 2023;24:5944.

51. Song H, Seddighzadeh B, Cooperberg MR, Huang FW. Expression of ACE2, the SARS-CoV-2 receptor, and TMPRSS2 in prostate epithelial cells. Eur Urol. 2020;78:296-8.

52. Eastman RT, Roth JS, Brimacombe KR, et al. Remdesivir: a review of its discovery and development leading to emergency use authorization for treatment of COVID-19. ACS Cent Sci. 2020;6:672-83.

53. V'kovski P, Kratzel A, Steiner S, Stalder H, Thiel V. Coronavirus biology and replication: implications for SARS-CoV-2. Nat Rev Microbiol. 2021;19:155-70.

DOI: 10.4274/MMJ.galenos.2025.82284
Medeni Med J 2025;40:110-113

Case Report

Refractory Infantyl Chylous Ascites Treatment by Everolimus

Everolimus ile Refrakter İnfantil Şiloz Asit Tedavisi

Masallah BARAN[1], Sinem KAHVECI[2], Betul AKSOY[1], Yeliz CAGAN APPAK[1], Gizem DOGAN[3], Hacer ORSDEMIR HORTU[3], Gokhan KOYLUOGLU[4]

[1]Izmir City Hospital; Izmir Katip Celebi University Faculty of Medicine, Department of Pediatric Gastroenterology, Hepatology and Nutrition, Izmir, Türkiye
[2]Izmir City Hospital, Clinic of Pediatric Gastroenterology, Hepatology and Nutrition, Izmir, Türkiye
[3]Izmir Katip Celebi University Faculty of Medicine, Department of Child Health and Diseases, Izmir, Türkiye
[4]University of Health Sciences Türkiye, Izmir City Hospital; Izmir Katip Celebi University Faculty of Medicine, Department of Pediatric Surgery, Izmir, Türkiye

ABSTRACT

The accumulation of lymphatic fluid in the abdomen is defined as chylous ascites. Different causes play a role in the etiology of the disease. Congenital anomalies are the most common cause in pediatric patients. A high protein, low fat diet rich in medium-chain fatty acids should be planned. The first-line treatment is dietary management and is total parenteral nutrition, and the first preferred medical agent is somatostatin. In patients who do not respond to standard treatments, surgical treatment or new limited alternative medical agents are applied. A six-month-old girl presented with a complaint of abdominal swelling was diagnosed with chylous acid. The patient was put on the standard nutritional therapy and somatostatin treatment but did not respond to these treatments. The chylous ascites was controlled with everolimus treatment.

Keywords: Infantile chylous ascites, everolimus, medical treatment

ÖZ

Karında lenfatik sıvı birikimi şilöz asit olarak tanımlanır. Etiyolojide farklı nedenler rol oynamaktadır. Konjenital anomaliler pediyatrik hastalarda en sık neden olan etiyolojidir. Yüksek proteinli, düşük yağlı ve orta zincirli yağ asitlerinden zengin bir diyet planlanmalıdır. İlk basamak tedavi diyet yönetimi ve toplam parenteral beslenme olup, ilk tercih edilen medikal ajan somatostatindir. Standart tedavilere cevap vermeyen hastalarda cerrahi tedavi veya yeni sınırlı alternatif medikal ajanlar tedavi için uygulanmaktadır. Altı aylık kız hasta karında şişlik şikayeti ile başvurdu ve şilöz asit tanısı konuldu. Hastaya standart beslenme tedavisi ve somatostatin tedavisi başlandı, ancak bu tedavilere yanıt vermedi. Şilöz asit everolimus tedavisi ile kontrol altına alındı.

Anahtar kelimeler: İnfantil şilöz assit, everolimus, tedavi

INTRODUCTION

Ascites is the collection of fluids in the abdominal cavity. It can occur in the intrauterine period and postnatally during childhood. There are many causes of chylous ascites. Chronic liver disease and cirrhosis are known to be the primary causes of liver-related health issues in children[1]. Chylous ascites is a rare type of ascites. Its reported incidence at a large university-based hospital over a 20 year period is approximately 1 in 20,000 admissions[2]. It may develop due to congenital malformations, lymphangiomatosis (LAM), peritoneal bands, tumors, and chronic inflammatory processes in the intestines. Changes in nutritional management, total parenteral nutrition (TPN), and somatostatin therapy are preferred as first-line treatment. In patients refractory to these treatments, surgical treatments and new medical agents are considered. In this case report, the diagnosis and treatment with everolimus of a six-month-old girl with refractory chylous ascites is presented.

CASE REPORT

The parents of patient have signed consent to publication form and the form is held by our institution.

A six month old baby girl was brought in with abdominal swelling for one month. At the time of

Address for Correspondence: M Baran, Izmir City Hospital; Izmir Katip Celebi University Faculty of Medicine, Department of Pediatric Gastroenterology, Hepatology and Nutrition, Izmir, Türkiye
E-mail: mbaran2509@gmail.com **ORCID ID:** orcid.org/0000-0003-3827-2039

Cite as: Baran M, Kahveci S, Aksoy B, et al. Refractory infantyl chylous ascites treatment by everolimus. Medeni Med J.2025;40:110-113

Received: 18 December 2024
Accepted: 23 March 2025
Epub: 22 May 2025
Published: 26 June 2025

her admission, she had a sickly appearance. In the physical examination, her abdomen was observed to be distended. Her body weight was 7,600g (50-75 p); her height was 60 cm (<3 p). Her vital signs were compatible with her age, and she was hemodynamically stable. Her laboratory findings were shown in Table 1. Free fluid was observed in abdominal ultrasonography. No pathology was seen in portal Doppler ultrasonography, abdominal magnetic resonance imaging (MRI), and MRI angiography, except diffuse intraabdominal fluid. After diagnostic paracentesis, the triglyceride level in the fluid was found to be 1.274 mg/dL. Chylous ascites was thus defined. In etiology, conditions such as trauma, surgical conditions, malignancy, infections, and heart diseases were excluded. For etiological investigation, lymphoscintigraphy was performed. With the patient's clinical, laboratory, and paracentesis findings, the intra-abdominal fluid detected was evaluated as chylous by the medical team. However, due to the young age of the patient and technical conditions in lymphoscintigraphy, the focus of lymphatic leakage could not be clearly demonstrated (Figure 1). Malrotation was also not detected in the small intestine passage radiography. The patient's oral nutrition was discontinued and TPN was started. Somatostatin analogs were added to the treatment at 1 mcg/kg/hour intravenously. In the follow-up, nutrition was started with a formula rich in medium-chain fatty acids. As the abdominal distension increased and tachypnea developed in the follow-up period, the chylous fluid was drained with several paracenteses. The chylous acid increase continued intermittently, and the patient developed hypoalbuminemia. Because of acid refractoriness, somatostatin analog therapy was gradually increased to 7 mcg/kg/hour. Intermittently, on the basis of case monitoring, the peritoneal fluid was drained through a catheter, albumin support was provided, and the patient's daily weight and waist circumference were monitored. The TPN support was continued, but the oral nutrition was partially replaced with a special lipid-free formula supported by medium-chain triglyceride oil. As the patient's acid regressed in the 6th week, her oral nutrition was increased and the somatostatin dose was gradually decreased to 4 mcg/kg/h. After the somatostatin dose reduction, the fluid around the abdomen was observed to have increased. Upon re-evaluation through lymphoscintigraphy, the site of lymph leakage into the abdomen was not detected. The patient was thus evaluated as needing pediatric surgery due to the treatment-resistant prognosis and the discovery of the lymph leakage focus. However, surgical intervention was not considered due to surgical difficulties owing to the persistence of intraabdominal diffuse ascites. The somatostatin treatment was increased again, and oral nutrition had to be discontinued intermittently. Since the desired improvement was not achieved with the standard treatments, everolimus was started at week 12. TPN was eventually stopped due to the reduction of the patient's ascites, and the somatostatin infusion was tapared for four weeks following everolimus administration. After the first month of everolimus treatment, the somatostatin dose was reduced to 1 mcg/kg/day, and subcutaneous treatment was started. In the 16th week, the patient was followed up as an outpatient, and ultrasonography was conducted. The somatostatin

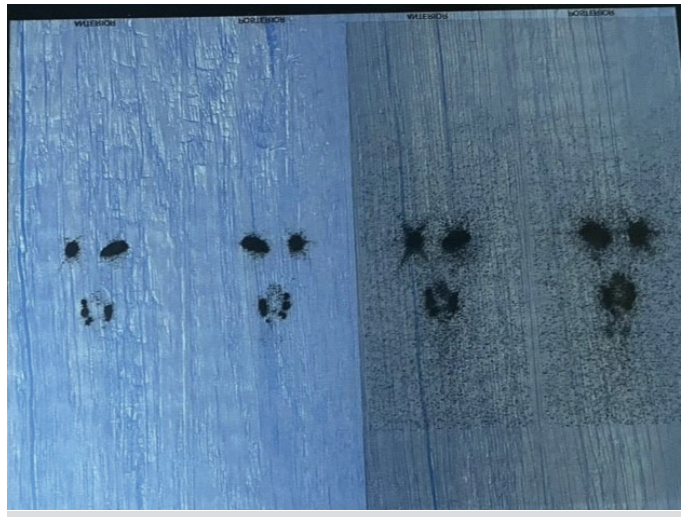

Figure 1. Normal findings in lymphoscintigraphy image of the patient.

Table 1. Laboratory findings of patient.

Hemoglobin	**11.4 gr/dL**	**Triglyceride**	**327 mg/dL**	**GGT**	**24 U/L**	**Creatinine**	**0.4 mg/dL**
Leukocyte	5300/mm^3	**Albumin**	4.1 g/dL	**ALP**	180 U/L	**Sedimentation**	11 mm/h
Platelets	391,000/mm^3	**LDH**	475 U/L	**Total bilirubin**	0.75 mg/dL	**IgG**	0.72 g/L
C-reactive protein	2.8 mg/L	**Sodium**	133 mmol/L	**Direct bilirubin**	0.06 mg/dL	**IgM**	0.33g/L
ALT	57 U/L	**Potassium**	4.6 mmol/L	**EBV**	Negative	**IgE**	111 IU/mL
AST	141 U/L	**Magnesium**	2.6 mg/dL	**CMV**	Negative	**IgA**	0.26 g/L

ALT: Alanine aminotransferase, AST: Aspartate transferase, LDH: Lactate dehydrogenase, GGT: Gamma-glutamyl transferase, ALP: Alkaline phosphatase, EBV: Epstein-Barr virus, CMV: Cytomegalovirus, Ig: Immunoglobulin

treatment was discontinued in the 20th week. Treatment with everolimus was continued for twenty-four-months. No recurrence of acid was observed in the patient. No drug-related adverse events were observed during follow-up. The patient is now 6-years-old, and no recurrence was found (the parents of patient have signed consent to publication form and the form is held by our institution).

DISCUSSION

Chylous ascites, which commonly occurs during the neonatal period but can also be seen in infancy, has many possible etiologies. Congenital etiologies, including lymphatic hypoplasia or dysplasia, such as LAM and intestinal lymphangiectasia, are the most common causes of chylous ascites in the paediatric population[1]. In children, chylous ascites can also be secondary to an operation, blunt trauma, a traffic accident, or child abuse[1]. The etiology, however, is not always evident. Diagnostic paracentesis is essential in identifying the etiology. The presence of a milky, creamy ascitic fluid with a triglyceride content of 200 mg/dL establishes the diagnosis of chylous ascites, although some authors use a threshold of 110 mg/dL[3]. Lymphoscintigraphy, lymphangiogram, or surgical laparotomy can be used as diagnostic methods. The nutritional approach should be the primary agent in chylous ascites management. A high-protein/low fat diet rich in medium-chain fatty acids is essential. In cases where there is no response to enteral feeding, however, feeding with TPN should be started. In the treatment of chylous ascites in children and adults, octreotide, a somatostatin analogue, has been used as an adjunct to TPN. The mechanism of action in chylous acid is not clearly known. Somatostatin reduces fat absorption from the intestine, lowers triglycerides in the thoracic duct, reduces lymph flow in the main ducts, and also decreases gastrointestinal secretions and motor activity[3]. The success rates of nutritional therapy and somatostatin treatment can be found in the literature, mostly in cases of chylothorax and chylous ascites[2,4].

The mammalian target of rapamycin (mTOR) is a serine/threonine kinase regulated by phosphoinositide-3-kinase, and is involved in a number of cellular processes, including cellular catabolism and anabolism, cell motility, angiogenesis, and cell growth. Sirolimus was recently reported to reduce refractory chylothorax and chylous ascites in patients with LAM. This effusion was ameliorated by the administration of octreotide, a somatostatin analog peptide, in addition to sirolimus. Some reports have shown that chylous effusion was ameliorated by sirolimus[5]. Everolimus is also an mTOR inhibitor and is a sirolimus derivative, but has fewer side effects. Its bioavailability is higher than that of sirolimus, and its half life is short. In cases where the focus of lymph leakage had been identified, surgical repair with glubran or cautery was successfully performed. In our patient, the location of the lymph leakage could not be determined by lymphoscintigraphy and no lymphangioma was found but the lymph leakage with lymphatic ascites responded to everolimus treatment. Therefore, we recommend the use of alternative and successful treatments such as everolimus and sirolimus before the surgical approach considering the possible surgical complications in the concerned childhood age group, and particularly in the patient group whose lymph leakage focus has not been found, we recommend the use of alternative and successful treatments such as everolimus and sirolimus before the surgical approach. Cases of chylous ascites and lymphedema due to sirolimus treatment after organ transplantation have been reported in literature[6]. It is remarkable that these side effects related to treatment, are observed especially in patients who underwent surgeries such as organ transplantation. The mechanism of sirolimus action is unclear, but it may be related to the disruption of the proliferative signals that are necessary for sealing the perivascular lymphatics and for promoting wound healing[7]. Its treatment effects are thought to be due to the angiogenic properties of both agents. This treatment was found to be appropriate in our patient with congenital chylous ascites without any previous surgery. After the treatment, the patient was closely monitored for side effects. No drug-related adverse events were observed during follow-up. Somatostatin treatment was stopped after two months of everolimus treatment. The patient's clinical and laboratory parameters were followed up using imaging methods, and no recurrence of the ascites occurred during the twenty-four-month follow-up after the discontinuation of everolimus. The use of everolimus for the treatment of congenital lymphatic disorders such as chylous ascites, which is resistant to diet and somatostatin treatment, should therefore be considered[8].

CONCLUSION

Although dietary management and TPN are the first-line treatments for chylous ascites, there are cases that benefit from somatostatin treatment. In cases of refractory chylous ascites, as in our patient, alternative treatment is needed. Among these treatments, sirolimus has been shown in the literature to be effective. This case has shown, that Everolimus would also be an alternative treatment method in refractory chylous ascites.

Ethics

Informed Consent: The parents of patient have signed consent to publication form and the form is held by our institution.

Footnotes

Author Contributions

Surgical and Medical Practices: M.B., G.K., Concept: S.K., G.D., Design: B.A., Data Collection and/or Processing: M.B., H.O.H., Analysis and/or Interpretation: Y.C.A., Literature Search: S.K., Writing: M.B., S.K.

Conflict of Interest: The authors have no conflict of interest to declare.

Financial Disclosure: The authors declared that this study has received no financial support.

REFERENCES

1. Lane ER, Hsu EK, Murray KF. Management of ascites in children. Expert Rev Gastroenterol Hepatol 2015;9:1281-2.
2. Al-Busafi SA, Ghali P, Deschênes M, et al. Chylous ascites: evaluation and management. ISRN Hepatol 2014;240473.
3. Baran M, Cakir M, Yuksekkaya HA, et al. Chylous ascites after living related liver transplantation treated with somatostatin analog and parenteral nutrition. Transplant Proc. 2008;40:320-1.
4. Kwon Y, Kim ES, Choe YH, et al. Individual approach for treatment of primary intestinal lymphangiectasia in children: single-center experience and review of the literature. BMC Pediatr 2021;21:21.
5. Namba M, Masuda T, Nakamura T, et al. Additional octreotide therapy to sirolimus achieved a decrease in sirolimus-refractory chylous effusion complicated with lymphangioleiomyomatosis. Intern Med 2017;56:3327-31.
6. Saucedo-Crespo H, Roach E, Sakpal SV, et al. Spontaneous chylous ascites after liver transplantation secondary to everolimus: a case report. Transplant Proc 2020;52:638-40.
7. Chen YT, Chen YM. A rare cause of chylous ascites. Clin Kidney J. 2014;7:71-2.
8. Ozeki M, Hori T, Kanda K, et al. Everolimus for primary intestinal lymphangiectasia with protein-losing enteropathy. Pediatrics. 2016;137:e20152562.

DOI: 10.4274/MMJ.galenos.2025.87393
Medeni Med J 2025;40:114-115

Letter to the Editor

Can Pirfenidone and Nintedanib Be Alternative Treatment Options for Radiation Pneumonitis?

Pirfenidon ve Nintedanib Radyasyon Pnömonisi için Alternatif Tedavi Seçenekleri Olabilir mi?

Hikmet COBAN, Mustafa COLAK, Merve YUMRUKUZ ŞENEL, Muzaffer GUNES, Nurhan SARIOGLU, FUAT EREL

Balikesir University Faculty of Medicine, Department of Pulmonology, Balikesir, Türkiye

Keywords: Pirfenidone, nintedanib, radiation pneumonitis, antifibrotic treatment
Anahtar kelimeler: Pirfenidon, nintedanib, radyasyon pnömonisi, antifibrotik tedavi

Dear Editor,

Radiation-induced pneumonitis (RP) is an early event observed in most patients exposed to radiation, typically occurring within 2-4 months after treatment and potentially leading to fibrosis[1]. While clinical observation is recommended for mild symptoms of radiation pneumonitis, systemic steroid therapy is advised for symptomatic patients, provided that lung infection is excluded[2]. In cases where there is no response to systemic steroid therapy, treatments such as azathioprine, cyclosporine, amifostine, and pentoxifylline can be attempted. We achieved near-complete improvement in symptoms, high-resolution computed tomography (HRCT) images, and pulmonary function test parameters, in two patients who developed radiation pneumonitis following radiotherapy (RT) for breast cancer and lung cancer by administering nintedanib and pirfenidone treatments.

Patient 1: A 64-year-old patient with squamous cell carcinoma of the lung had a primary lesion in the upper lobe of the left lung. After six courses of chemotherapy, a complete response was not achieved, so RT was administered for 20 days. Post-RT, the patient complained of cough and dyspnea, and thoracic CT revealed radiation pneumonitis. Despite treatment with a steroid dose of 1 mg/kg/day, there was no regression or improvement in symptoms. By the end of the first month, the prednisolone dose was reduced to 16 mg/day, and additionally, oral nintedanib 150 mg twice daily was initiated. After the commencement of nintedanib therapy, there was a significant improvement in cough and dyspnea. The prednisolone dose was tapered and eventually discontinued. Nintedanib treatment was discontinued after two months. Upon evaluation with control HRCT at the end of the third month, almost complete regression of the parenchymal changes was observed compared to the initial treatment (Figure 1). The improvement in pulmonary function parameters is shown in Table 1.

Patient 2: A 68-year-old female patient diagnosed with left breast cancer had been started on 1 mg/kg/day steroid therapy due to paclitaxel-induced lung injury during chemotherapy. After the symptoms related to

Address for Correspondence: M. Colak, MD, Balikesir University Faculty of Medicine, Department of Pulmonology, Balikesir, Türkiye
E-mail: drmclk@yahoo.com **ORCID ID:** orcid.org/0000-0002-8458-3535

Cite as: Coban H, Colak M, Şenel MY, Gunes M, Sarioglu N, Erel F. Can pirfenidone and nintedanib be alternative treatment options for radiation pneumonitis? Medeni Med J. 2025;40:114-115

Received: 19 March 2025
Accepted: 02 May 2025
Epub: 22 May 2025
Published: 26 June 2025

the drug-induced lung injury regressed, RT was initiated while the patient was on 16 mg/day prednisolone therapy. Upon the detection of an increase in symptoms following RT, HRCT revealed findings of radiation pneumonitis in both lungs, more pronounced on the left side. Pirfenidone at a dose of 4x600 mg was added to the prednisolone therapy. After two months of treatment, control HRCT revealed that the parenchymal lesions had nearly completely resolved, corresponding with a reduction in symptoms (Figure 2). The improvement in pulmonary function parameters is shown in Table 1.

A murine study with the multi-kinase inhibitor nintedanib, described as a treatment to prevent RP and reduce lung fibrosis incidence, nintedanib's efficacy in reducing interstitial edema, interstitial and perivascular fibrosis, inflammation, and vasculitis[3]. As for pirfenidone, there is only one subjective study available in literature, which reports a reduction in symptoms[1]. We did not find any literature data indicating improvements in radiological and pulmonary function parameters with pirfenidone treatment in RP. Based on our review of the literature, we are presenting real-life data for the first time, demonstrating that nintedanib and pirfenidone are effective treatment options in the management of RP.

Table 1. FVC and DLCO parameters of the patients before and after treatment.

	Pre-treatment	Post-treatment
Patient 1		
FVC Liter (%)	1.90 (58)	2.30 (72)
DLCO (%)	72	86
Patient 2		
FVC Liter (%)	1.38 (49)	2.12 (76)
DLCO (%)	80	119

FCV: Forced vital capacity, DLCO: Diffusing lung capacity for carbon monoxide

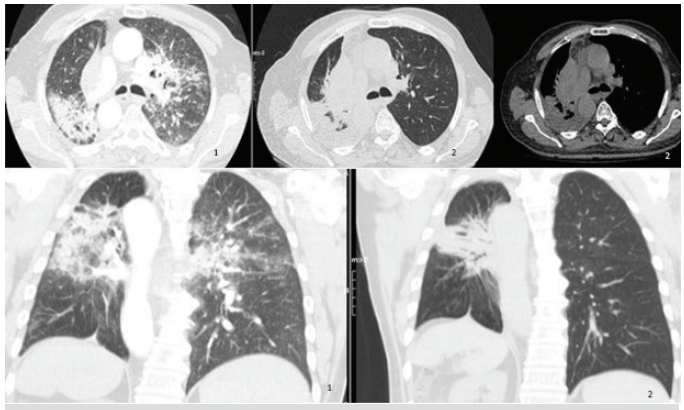

Figure 1. Patient diagnosed with squamous cell carcinoma of the left lung. Significant improvement in the parenchyma is observed following the addition of nintedanib to prednisolone therapy post-RT.

RT: Radiotherapy

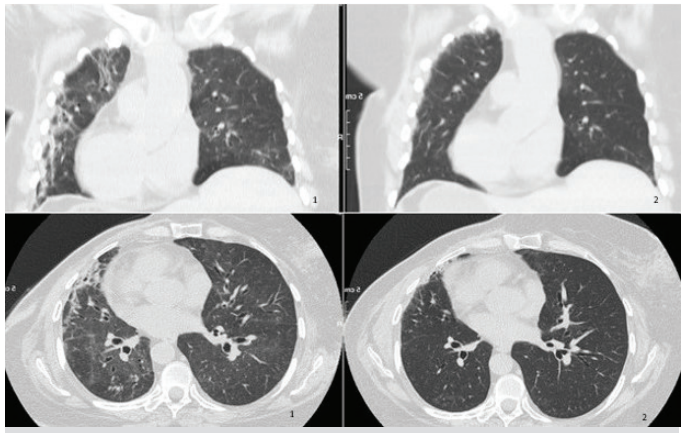

Figure 2. Patient diagnosed with left breast cancer. Improvement in lung parenchyma is observed following pirfenidone therapy in a patient who developed radiation pneumonitis while receiving steroid therapy.

Ethics

Author Contributions

Surgical and Medical Practices: H.C., M.C., Concept: H.C., N.S., Design: H.C., M.C., F.E., Data Collection and/or Processing: H.C., Analysis and/or Interpretation: M.Y.Ş., M.C., Literature Search: H.C., M.Y.Ş., Writing: H.C., M.C.

Conflict of Interest: The authors have no conflict of interest to declare.

Financial Disclosure: The authors declared that this study has received no financial support.

REFERENCES

1. Simone NL, Soule BP, Gerber L, et al. Oral pirfenidone in patients with chronic fibrosis resulting from radiotherapy: a pilot study. Radiat Oncol. 2007;2:19.
2. Bledsoe TJ, Nath SK, Decker RH. Radiation Pneumonitis. Clin Chest Med. 2017;38:201-8.
3. De Ruysscher D, Granton PV, Lieuwes NG, et al. Nintedanib reduces radiation-induced microscopic lung fibrosis but this cannot be monitored by CT imaging: A preclinical study with a high precision image-guided irradiator. Radiother Oncol. 2017;124:482-7.